

Electronic Thesis and Dissertation Repository

8-17-2016 12:00 AM

Evaluation of MERTK evolution and efferocytosis signalling

Amanda L. Evans

The University of Western Ontario

Supervisor

Bryan Heit

The University of Western Ontario

Graduate Program in Microbiology and Immunology

A thesis submitted in partial fulfillment of the requirements for the degree in Master of Science

© Amanda L. Evans 2016

Follow this and additional works at: <https://ir.lib.uwo.ca/etd>



Part of the [Immunity Commons](#)

Recommended Citation

Evans, Amanda L., "Evaluation of MERTK evolution and efferocytosis signalling" (2016). *Electronic Thesis and Dissertation Repository*. 4034.

<https://ir.lib.uwo.ca/etd/4034>

This Dissertation/Thesis is brought to you for free and open access by Scholarship@Western. It has been accepted for inclusion in Electronic Thesis and Dissertation Repository by an authorized administrator of Scholarship@Western. For more information, please contact wlsadmin@uwo.ca.

Abstract

The TAM (TYRO3, AXL, and MERTK) family of receptor tyrosine kinases allow phagocytes to engage in the phagocytic removal of apoptotic cells. Although all three members of the TAM family are structurally homologous and function in a similar fashion, both human genome-wide association studies and knockout mice models have demonstrated that MERTK is the critical member of the TAM family for maintaining homeostasis. In this thesis, an evolutionary analysis was used to provide insight into the function of MERTK. Selection analysis in primates unexpectedly revealed a high degree of recent positive selection in *MERTK*'s signal peptide and transmembrane domain, absent from *TYRO3* and *AXL*. Reconstruction of hominid and primate ancestral signal peptides revealed three nonsynonymous mutations in humans, with a G14C mutation producing a potential non-B DNA cruciform motif, which may regulate MERTK expression. Reconstruction of *MERTK*'s transmembrane domain determined that humans acquired three amino acid substitutions and two insertion/deletion mutations (INDELS) which added four amino acids. These new amino acids were largely leucines and isoleucines, and create a new interaction motif that increased self-clustering of MERTK. Although we found no significant difference among human MERTK and primate- or hominid-ancestral reconstructed signal peptides in expression levels or protein trafficking, recent evolutionary changes in MERTK's transmembrane revealed significantly higher self-clustering with human MERTK, and hominid ancestral, compared to the reconstructed primate-ancestral transmembrane. This project highlights the importance of recent *MERTK* evolution, which has increased self-clustering.

Keywords: TAM receptors, MERTK, Efferocytosis, Evolution, Positive Selection

Acknowledgments

I would like to thank my supervisor Dr. Bryan Heit for his guidance over the past four years, as a work-study student, honours thesis student and now as a Master's student. His encouragement, advice, and scientific knowledge has been invaluable to my project.

I am grateful to the members of my advisory committee, Drs. Jimmy Dikeakos and Lakshman Gunaratnam, for their experimental advice and insightful questions. I would like to especially thank Brennan Dirk and Dr. Dikeakos for their collaboration in the transmembrane analysis.

A special thanks goes to Dr. Ronald Flannagan for his valuable recommendations and aid in experimental design, as well as Peter Szabo and Delfina Mazzuca Siroen for their aid in the flow cytometry experiments. In addition, I would like to thank Ashley Ma for her help in cloning mouse MerTK.

I would also like to thank my parents for their encouragement, and support throughout my studies.

Lastly, I would like to thank my labmate and partner, Jack Blackburn, for his help in conducting the evolutionary analysis and his support throughout this thesis.

Table of contents

Abstract.....	i
Acknowledgments.....	ii
List of figures.....	v
List of tables.....	vi
List of appendices.....	vii
List of abbreviations.....	viii
Chapter 1: Introduction.....	1
1.1 TAM receptor family structure.....	2
1.2 TAM receptor opsonins.....	2
1.3 TAM receptor family evolution.....	6
1.4 Biological roles of TAM receptors.....	7
1.4.1 TAM signalling.....	10
1.4.2 Efferocytosis.....	11
1.5 TAM receptors in infection and disease.....	14
1.5.1 Inflammation and autoimmunity.....	14
1.5.2 TAM receptors as viral targets.....	15
1.5.3 TAM receptor association with cancer.....	16
1.6 Hypothesis and objectives.....	17
Chapter 2: Materials and methods.....	19
2.1 Materials.....	19
2.5 Hydrophobicity and isoelectric point analysis.....	22
2.6 Mouse and human <i>MERTK</i> synthesis and mutagenesis.....	22
2.7 Cell Culture and transfection.....	25
2.8 Primary macrophage preparation.....	25
2.9 Microscopy.....	26
2.10 Immunostaining.....	27
2.11 Immunoblots and coomassie stains.....	27

2.12 Protein trafficking assay	28
2.13 Protein expression analysis	29
2.14 Oligomerization assay	29
2.15 Synthetic efferocytic target preparation	30
2.16 Efferocytosis assays	31
2.17 Statistical analysis	31
Chapter 3: Results	32
3.1 Patterns of recent TAM receptor evolution.....	32
3.2 Recent <i>MERTK</i> evolution	43
3.3 <i>MERTK</i> signal peptide evolution has not altered protein expression or trafficking	47
3.4 <i>MERTK</i> transmembrane evolution has increased self-clustering.....	59
3.6 Development of a model to study <i>MERTK</i> -dependent efferocytosis	64
Chapter 4: Discussion	84
4.1 Rational for thesis.....	84
4.2 Hypothesis and aims.....	84
4.3 <i>MERTK</i> signal peptide evolution	85
4.4 <i>MERTK</i> transmembrane evolution	87
4.5 <i>MERTK</i> -dependent efferocytosis model development.....	89
4.6 <i>MERTK</i> functional domains	91
4.8 Summary and future aims	93
References	95
Appendix.....	111
Curriculum Vitae	123

List of figures

Figure 1: TAM receptor domains and binding interaction.	3
Figure 2: TAM receptor signalling pathway.....	13
Figure 3: Mammalian evolutionary tree for <i>MERTK</i>	33
Figure 4: Full primate trees for evolutionary analysis of <i>TYRO3</i> , <i>AXL</i> and <i>MERTK</i>	34
Figure 5: Recent evolution of <i>TYRO3</i> , <i>AXL</i> and <i>MERTK</i>	36
Figure 6: Per-residue Ka/Ks scores of TAM receptors.....	38
Figure 7: Reconstruction of recent evolution in the <i>MERTK</i> signal peptide and transmembrane domain.....	44
Figure 8: Human HA-MERTK-GFP and modified ancestral signal peptides are ectopically expressed in HeLa cells	48
Figure 9: Evolution in <i>MERTK</i> signal peptide has no significant impact on protein trafficking .	50
Figure 10: Hominid ancestral MERTK signal peptide has augmented expression compared to primate ancestral and human signal peptides.....	53
Figure 11: Flow cytometry shows no significant difference in protein expression between human and ancestral MERTK.....	55
Figure 12: Immunoblots show no significant difference in whole protein expression between human and ancestral MERTK.....	57
Figure 13: Human HA-MERTK-GFP and modified with ancestral transmembrane domains are ectopically expressed in HeLa cells	60
Figure 14: Evolution in <i>MERTK</i> intermolecular interactions driven by transmembrane domain evolution	62
Figure 15: Mouse MERTK is heterologously expressed in COS-7 cells	65
Figure 16: COS-7 <i>MerTK</i> -transfectants uptake antibody-coated beads.	66
Figure 17: Coomassie blue stain of antibodies reveal no opsonin contamination.....	69
Figure 18: COS-7 <i>MerTK</i> -transfectants uptake Fab and full length IgG.....	70
Figure 19: COS-7 <i>MerTK</i> -transfectants do not uptake IgG-coated protein A beads.....	71
Figure 20: COS-7 <i>MerTK</i> -transfectants uptake GAS6 opsonized PtdSer-silica bead.....	73
Figure 21: Human MERTK is heterologously expressed in HEK293T cells.....	76
Figure 22: <i>MERTK</i> transfected HEK293T cells do not internalize opsonin-coated PtdSer-beads	78
Figure 23: Efferocytosis of human serum opsonized PtdSer and PC beads by primary human macrophages	81

List of tables

Table 1: Primers and synthetic DNA elements used for vector construction.	23
Table 2: Biochemical characteristics of the human, hominid-ancestral and primate-ancestral MERTK signal peptide (residues 1-27) and transmembrane domains (residues 499-532).	45

List of appendices

Appendix 1: Codon-optimized MERTK sequence.....	112
Appendix 2: Ethics approval for performing venipuncture on human participants.....	113
Appendix 3: Fisher’s Exact Test of Neutrality for Sequence Pairs for TAM receptors.....	114
Appendix 4: Z-Tests for TAM receptors.	116
Appendix 5: In silico analysis of human and primate- and hominid-ancestral MERTK transmembrane domains.	120
Appendix 6: Letter of permission for inclusion of appendix 5 in thesis.....	122

List of abbreviations

Ab	Antibody
AC	Apoptotic cell
AIC	Akaike Information Criterion
BIC	Bayesian Information Criterion
CblN	Cobalt transport protein
CI	Confidence interval
DMEM	Dulbecco's Modified Eagle's Medium
EGF	Epidermal growth factor
ER	Endoplasmic reticulum
ERK1/2	Extracellular signal regulated kinases 1/2
Fab	Fragment of antigen binding
FAK	Focal adhesion kinase
Fbg	Fibronectin type III domain
FBS	Fetal bovine serum
GAS6	Growth arrest-specific protein 6
GFP	Green fluorescent protein
HEPES	4-(2-hydroxyethyl)piperazine-1-ethanesulfonic acid
Gal-3	Galectin-3
Gla	Gamma-carboxylated glutamic acid
G(r)	Radial distribution function
Grb2	Growth factor receptor-bound protein 2
GSDM	Ground-State Depletion Microscopy
HPMI	HEPES-buffered RPMI
IFN	Interferon
IFNAR	Type I IFN receptor
Ig	Immunoglobulin-like motif
IL	Interleukin
INDELS	Insertion/deletion mutations
JAK	Janus kinase
MFG-E8	Milk fat globule EGF factor 8
MFI	Mean fluorescence intensity
MS	Multiple sclerosis
OS	Outer segments
PBS	Phosphate-buffered saline
PI3K	Phosphoinositide 3 kinase
PIP ₂	Phosphatidylinositol-4,5- <i>bis</i> phosphate
PIP ₃	phosphatidylinositol-3,4,5- <i>tris</i> phosphate
PLC	Phospholipase C γ 2
PK	Protein kinase
PR	Photoreceptor
PROS	Protein S
PtdChol	Phosphatidylcholine
PtdSer	Phosphatidylserine

Rac1	Ras-related C3 botulinum toxin substrate 1
RPE	Retinal pigment epithelium
RPMI	Roswell Park Memorial Institute
RTK	Receptor tyrosine kinase
SHBG	Sex Hormone Binding Globulin
SLE	Systemic lupus erythematosus
SNP	Single nucleotide polymorphism
SOCS1	Suppressor of cytokine signalling-1
SOCS3	Suppressor of cytokine signalling-3
STAT	Signal transducer and activator of transcription
TAM	TYRO3, AXL, and MERTK
TGF β	Transforming growth factor β
TIM	T cell immunoglobulin- and mucin-domain-containing molecule
TIRF	Total internal reflection fluorescence microscopy
TKD	Tyrosine kinase domain
TKO	Triple knockout
TULP-1	Tubby-Like Protein 1
WGD	Whole genome duplication

Chapter 1: Introduction

TYRO3, AXL, and MERTK (TAM) receptors are a family of receptor tyrosine kinases that play essential roles in maintaining homeostasis through the removal of apoptotic cells (ACs). These receptors are found in the nervous, vascular, reproductive, and immune systems¹. The expression of TAM receptors, along with an appropriate integrin co-receptor, imparts an efferocytic capacity on a cell². Like many phagocytic receptors, TAM receptors do not directly bind to their targets, and instead engage soluble protein opsonins which act as bridging molecules between the TAM receptor and cognate ligands on ACs³⁻⁶. Phosphatidylserine (PtdSer) is the primary ligand of TAM receptor opsonins, although some TAM opsonins may recognize other lipids on the surface of ACs⁷. The three TAM receptors arose early in metazoan evolution, with *MERTK* and *TYRO3* evolving as a product of whole genome replication during the divergence of jawed from jawless vertebrates, and *AXL* emerging soon after during the separation of ray-finned and cartilaginous fish⁸. Despite their distant evolutionary origins, all three TAM receptors retain a high degree of structural and functional similarity, as well as a modest degree of sequence homology (40-50% amino acid homology)⁹. Although structurally and functionally similar, in both humans and mice, *MERTK* is the most critical of the three family members. Indeed, mutations resulting in a total loss of *MERTK* cause retinitis pigmentosa, a congenital form of blindness characterized by a failure to clear retinal pigment epithelia (RPE) in the eye, and with less severe single nucleotide polymorphisms (SNPs) in *MERTK* contributing to a range of inflammatory and autoimmune diseases¹⁰⁻¹³. In contrast, few SNPs in *AXL* or *TYRO3* are associated with human diseases^{10,14}, and *AXL* and *TYRO3* knockout mice have a less severe phenotype than *MERTK* knockout mice¹⁵⁻²⁰.

1.1 TAM receptor family structure

The TAM family members are type I transmembrane glycoproteins, with an extracellular domain comprised of tandem immunoglobulin-related domains (Ig) followed by tandem fibronectin type III (Fbg) repeats (Figure 1)^{21,22}. While both of these domains are common in many tyrosine kinases (TKs), TAM receptors uniquely contain two of each domain. TYRO3 and AXL are comparable in size, both around 120 kDa and 890 and 894 amino acids respectively. In contrast, MERTK is significantly larger, at ~150-170 kDa and 999 amino acids, mainly due to a larger ectodomain^{1,9}. All three TAM receptors, like all receptor tyrosine kinases (RTKs), contain a predicted single-pass alpha-helical transmembrane domain. Following the transmembrane domains is a highly conserved (>70% identity) intracellular tyrosine kinase belonging to the PKC-like superfamily of tyrosine kinases^{1,23}. TAM receptors also contain a unique sequence KW(I/L)A(I/L)ES in the catalytic kinase domain of the tyrosine kinase that differs from other RTKs^{21,22}. In MERTK a YSGDY Y motif has been identified as a major autophosphorylation site, where single tyrosine mutations reduce kinase activity from 10 to 100%²⁴. TAM receptors interact with their cognate opsonins as dimers, with the carboxy-terminal sex hormone-binding globulin (SHBG) domains on dimerized opsonins acting to stabilize the TAM dimer and thus initiating signalling²⁵⁻²⁸.

1.2 TAM receptor opsonins

TAM receptors bind to ACs indirectly through use of opsonins such as GAS6 and Protein S (PROS). These paralogs are about 80 kDa in size and share 44% amino acid similarity²⁹. Each contain a carboxy-terminal SHBG domain with two laminin G domains that bind the Ig domains

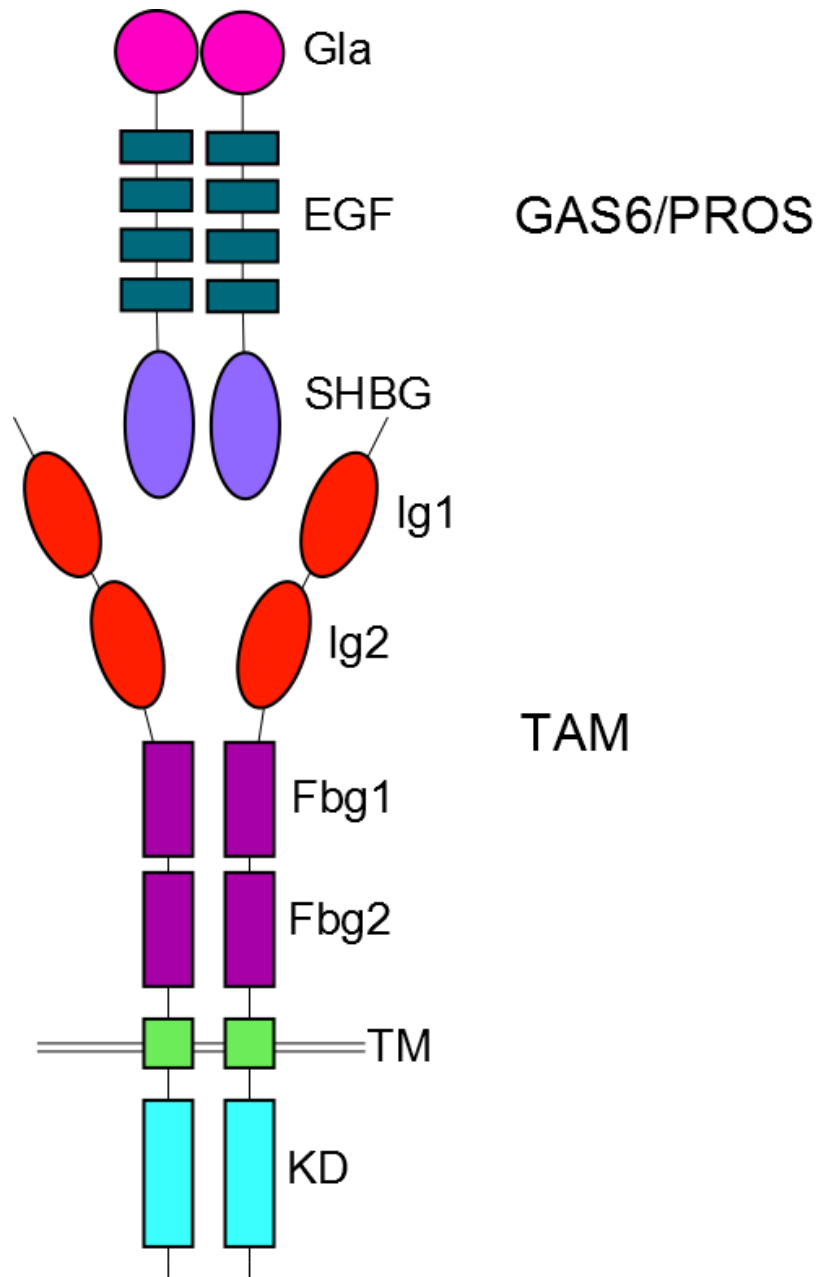


Figure 1: TAM receptor domains and binding interaction. Homodimers of opsonins GAS6 and PROS bind to PtdSer through their Gla domain, while their SHBG domains bind to TAM receptor homodimers through their Ig domains. GAS6/PROS and TAM receptors also contain EGF-like domains and Fbg domains respectively. TAM receptors contain a predicted single pass alpha helix transmembrane domain (TM) and signal through their highly conserved internal kinase domain (KD).

of TAM receptors, thereby inducing TAM dimerization and kinase activation (Figure 1)²⁵⁻²⁸. Following the SHBG domain are four EGF-related domains and the Gamma-carboxylated glutamic acid (Gla) domain on the amino terminus. The Gla domain is rich in glutamic acid residues which undergo a vitamin-K dependent post-translation gamma-carboxylation, allowing for Ca²⁺-dependent binding of PtdSer on the AC²⁵⁻²⁸. Interestingly, the Gla domains also function independent of TAM receptors as an anticoagulant in the blood coagulation cascade. Indeed, *Pros*^{-/-} mice possess an embryotic lethal phenotype due to exuberant blood coagulation³⁰. However, *Gas6* knockout mice appear normal, but have delayed coagulation, indicative of a negative coregulatory role of GAS6³¹.

PROS and GAS6 function as dimers to bind TAM receptors, and they activate TAM receptor signalling following multimerization²⁵⁻²⁸. Although homodimers of both opsonins have been studied, it remains unclear whether the opsonins are capable of heterodimerization, and if so, how this affects receptor binding affinities and signalling. Homodimers of GAS6 and PROS display different affinities among TAM receptors; GAS6 has been shown to bind all three TAM receptors, while PROS only activates TYRO3 and MERTK³². Although GAS6 binds all three TAM members, it has a much higher affinity for AXL ($K_d = 0.4$ nM), then TYRO3 ($K_d = 2.7$ nM) and its lowest affinity is for MERTK ($K_d = 29.0$ nM)³. Interestingly, while AXL has the strongest affinity for GAS6, MERTK is more readily activated when exposed to GAS6 in the presence of PtdSer, highlighting its predominant role in AC clearance³³.

PROS is abundant in human plasma (300 nM), while GAS6 is present at significantly lower concentrations (0.02-0.2 nM)³⁰. Both ligands are produced through autocrine/paracrine signalling

from TAM-positive cells including endothelial cells and hepatocytes³⁴⁻³⁶. Interestingly, GAS6 is believed to be entirely bound to a soluble form of AXL, which is cleaved following activation, in circulation³⁰. GAS6 and AXL share a unique relationship, as GAS6 is AXL's sole opsonin and binds it with a significantly higher affinity than the other TAM receptors³². In addition, expression of GAS6 appears to be dependent on AXL signalling, as GAS6 expression is entirely lost in major organs like the spleen, liver and lungs in *Axl*^{-/-} mice, but not *Tyro3*^{-/-} and *MerTK*^{-/-} mice³³.

GAS6 and PROS are well characterized opsonins for TAM receptors, but new evidence is emerging for three other opsonins: TUBBY, TUBBY-like protein 1 (TULP-1), and Galectin-3 (Gal-3)^{5,6,37}. These three putative opsonins are unusual in that they are normally restricted to the cytosol, with both TUBBY and TULP-1 having known roles as intracellular PtdSer sensors³⁸. TUBBY and TULP-1 are normally retained on the cytosolic face of the plasma membrane through their interactions with phosphatidylinositol 4,5-bisphosphate (PIP₂)³⁸. Following phosphoinositide hydrolysis, TUBBY functions by translocating to the nucleus, likely to function as a transcription factor for lipid synthesis genes through its NH₂-terminal regions³⁹. Secretion of these opsonins does not require cell death, and instead appears to occur via an uncharacterized, ER-independent secretion pathway similar to that used by IL-1β⁴⁰.

TUBBY and TULP-1 are expressed in neural and retinal tissues, but it remains unclear whether they are also present in the circulatory system or released at sites of inflammation^{5,39}. Mutations in both opsonins have shown their importance in RPE phagocytosis, where deficiencies in either opsonin leads to a partial loss of RPE phagocytosis⁴¹. TULP-1 activates all three TAM receptors,

whereas TUBBY solely activates MERTK. Both bind the receptor(s) with their N-terminal region and interact through an unknown ligand on ACs through their C-terminal domain. TULP-1 also possesses an essential sequence (K/R(X)₁₋₂KKK) for activation of MERTK on its N-terminus⁵. Gal-3 is the most recently discovered MERTK-specific opsonin. It is unclear how it binds to MERTK, but it does possess a C-terminal carbohydrate binding domain which binds glycoproteins. This binding is critical for Gal-3's function as an effective MERTK bridging molecule, as saturation of its lectin domain through addition of lactose reduces its ability to facilitate efferocytosis⁶. Like TUBBY and TULP-1, Gal-3 plays a role in RPE phagocytosis, as light exposure causes increased photoreceptor degeneration and a concomitant increase in Gal-3 expression⁴². In addition, Gal-3 is a known binding molecule for advanced glycation end products – found in Alzheimer's disease, diabetes, cardiovascular disease, and in aging retinas – indicating that it may opsonize ACs and lipoproteins independent of PtdSer^{43,44}.

1.3 TAM receptor family evolution

TAM receptors are a subfamily within the PK superfamily. As TAM receptors are transmembrane proteins that specifically phosphorylate the tyrosine residues, they belong to the subdivision of PKs known as receptor tyrosine kinases (RTKs). RTKs all share a common internal C-terminal tyrosine kinase domain (TKD), contain a single pass alpha helical transmembrane domain, and their signalling cascades are involved in an array of critical processes including embryonic development, growth factor signalling, apoptosis, and cell activation and cell differentiation. The main difference between the 20 RTK subfamilies lies in their distinct N-terminal domain exposed to the cell surface. These domains allow RTK-ligand binding, which in turn produces homo- or hetero-receptor dimerization, thus initiating a signalling cascade^{8,45}.

The diversity of human and vertebrate RTK's is due to four whole genome duplications (WGDs) that occurred early in vertebrate evolution⁸. Following these WGDs, genomes returned to a diploid state, but retained many of the duplicated genes, resulting in a vast expansion of many gene families⁴⁶. As gene duplications allow for rapidly increased evolutionary change compared to singletons, retained RTK duplicates created diverse subfamilies with greatly expanded functions^{47,48}. The TAM family members first formed through WGDs, with both *MERTK* and *TYRO3* evolving as jawed and jawless vertebrates diverged, and with *AXL* diverging from *TYRO3* during the separation of ray-finned and cartilaginous fish⁸. The evidence of TAM receptor emergence from WGD is highlighted by their distinct chromosome locations: *TYRO3* on chromosome 15 (at 15q15), *AXL* on chromosome 19 (at 19q13.1), and *MERTK* on chromosome 2 (at 2q14.1)⁹. This distribution is consistent with duplication of whole chromosomes, whereas gene duplication by errors in homologous repair generate gene copies on the same chromosome, and retrotransposition create duplicates lacking introns. Pre-dating TAM receptors, proteins resembling TAM receptor opsonins first appeared in genomes of pre-vertebrate urochordates. Interestingly, urochordate genomes also contain a TAM-like tyrosine kinase which is linked through its transmembrane domain to a TAM-opsonin-like domain, and therefore is likely able to directly recognize apoptotic cell PtdSer⁴⁹. This ancestral gene may represent the ancestor to all TAM receptors, although this relationship has not been thoroughly examined.

1.4 Biological roles of TAM receptors

The biological role of TAM receptors was largely delineated following the creation of TAM KO mice. PTK KO mice are often nonviable as many PTKs function in embryonic development, thus

successful development of single TAM KO mice, as well as double and triple TAM KO, was notable³⁵. TAM KO mice have been invaluable in TAM receptor research, with many studies using these mice or bone marrow-derived macrophages from these mice, for study. TAM triple knockout (TKO) mice appear phenotypically normal for the first three weeks following birth, but thereafter develop a degenerative phenotype that is lethal after approximately one year^{15,16,35,36,50,51}. Generation of these mice has enabled the elucidation of the biological importance of TAM receptors in the male reproductive system, RPE cells, the blood-brain barrier, and in macrophages and dendritic cells.

Adult male TAM TKO mice become infertile after five weeks, one week after the onset of sperm production, due to the failure to remove apoptotic germ cells produced during spermatogenesis in the seminiferous tubules of the testes³⁵. Without removal through efferocytosis, these ACs build-up and lead to the death of all germ cells in the male reproductive system. Sertoli cells – which express all three TAM receptors – are responsible for this function, and without TAM receptor expression, efferocytosis is nearly non-existent^{32,35,52,53}. MERTK plays a critical role in germ cell removal, as *MerTK*^{-/-} mice are the only single KO TAM mice to display AC germ cell build-up. However, AC germ cell build-up levels are exacerbated with dual *MerTK* and *Tyro3* KO mice, resulting in accelerated sterility compared to *MerTK* single knockouts³².

Similar to male germ cells, TAM receptors play a critical role in RPE phagocytosis. In the retina, photoreceptors (PRs) continually grow through the addition of membrane-based segments at the base of their multi-segment bodies. As the segments age they are displaced from the cell body,

becoming outer segments (OS). During this aging process photodamage accumulates, eventually requiring the removal of the OS by RPE cells – expressing TYRO3 and MERTK – which engulf damaged distal OS tips that are no longer capable of light detection. Diurnally, the distal OS tip displays PtdSer on the surface to allow specific engulfment of this section by RPE cells. This is a process unique from efferocytosis as the engulfment is restricted to a portion of the cell, and the cell is still viable^{54,55}. TKO TAM and *MerTK*^{-/-} mice are born with normal retinæ, but are blind two months after birth due to extensive death of their PRs, a phenotype not observed in *Tyro3* and *Axl* knockouts^{36,56}. In humans, mutations in *MERTK*, but not *TYRO3* or *AXL*, have also been shown to lead to retinitis pigmentosa, further highlighting the importance of MERTK compared to other TAM receptors¹³.

TAM receptors are critical for phagocyte-induced efferocytosis in tissues outside of the eyes and testes. In other tissues, TAMs are predominantly expressed by macrophages and dendritic cells, and are required to clear the over 100 billion ACs produced daily in a healthy human³³. In macrophages, MERTK signalling is required for AC clearance, as mice expressing MERTK with a truncated kinase domain show a near abolishment of efferocytosis. Interestingly, *Axl*^{-/-}, *Tyro3*^{-/-}, and *Axl*^{-/-}*Tyro3*^{-/-} mice show a 50% reduction in macrophage AC clearance, indicating that they play a cooperative role with MERTK⁵⁷. Although these studies showed a heavy reliance on MERTK for AC clearance, recent studies have shown differential expression patterns and efferocytosis specialization in macrophages dependent on environmental signals. In tolerogenic and anti-inflammatory settings MERTK expression predominates, while inflammatory environments induce upregulation of AXL and a concomitant downregulation of MERTK; Anti-inflammatory macrophage subtype M2c display high levels of MERTK expression, while

inflammatory macrophage subtype M1 display high AXL expression³³. Bone marrow-derived dendritic cells isolated from wild-type mice show high levels of AXL expression, with low levels of other TAM receptors. However, setting specific TAM receptor expression is also seen in DCs with the same patterns as macrophages. TYRO3 expression is not required for either DC or macrophage efferocytosis⁵⁷. Differential TAM receptor expression highlights the potential differential functions for TAM receptors.

1.4.1 TAM signalling

While incompletely understood, TAM receptor activation drives a RTK signalling cascade involving dimerization-induced TKD autophosphorylation and downstream activation of the phosphoinositide 3 kinase (PI3K)/AKT pathway⁵⁸⁻⁶¹. TAM receptor autophosphorylation occurs at two sites, within the TKD and in the C-terminal tail. TKD phosphorylation activates the kinase domain allowing for phosphorylation of both the C-terminal tail and downstream proteins⁶¹. Phosphorylation of the C-terminal tail creates a binding site for growth factor receptor-bound protein 2 (Grb2), which in turn recruits the p85 adaptor subunit of PI3K, followed by the p110 kinase subunit which phosphorylates PIP₂ to form phosphatidylinositol-3,4,5-triphosphate (PIP₃)^{9,62,63}. The production of PIP₃ induces the canonical PIP₃ signalling cascade, including the activation of AKT and downstream activation of AKT substrates such as mTOR, leading to numerous downstream processes including proliferation, cell survival, growth and angiogenesis⁶⁴.

TAM receptors also function as negative regulators of innate immune responses through the JAK/STAT pathway^{34,65}. Many cytokines and growth factor receptors lack an intrinsic kinase, and instead engage Janus kinases (JAKs) upon receptor dimerization. JAKs autophosphorylate when

dimerized, leading to the recruitment and activation of STATs which then dimerize and translocate to the nucleus, where they act as transcription factors⁶⁶. TAMs function as negative regulators in this pathway by coupling with INFAR, which in turn induces the expression of suppressor of cytokine signalling-1 (SOCS1) and -3 (SOCS3). These inhibitors suppress JAK/STAT signalling by binding phosphotyrosines on JAK kinases, or by acting as a pseudo JAK substrate through their N-terminal domains, thereby reducing STAT activation by JAKs, leading to decreased production of type I IFN⁶⁷.

1.4.2 Efferocytosis

Cell turnover is an essential physiological process constantly occurring in the body, with the removal of old, damaged, senescent or otherwise unneeded cells mediated via the dual processes of apoptosis – programmed cell death – and efferocytosis, the phagocytic removal of ACs. These two processes are responsible for removing more than 100 billion cells daily from the human body, but without timely efferocytosis these ACs accumulate, become necrotic and release inflammatory molecules with danger associated molecular patterns such as heat-shock proteins and ATP⁹. Efferocytosis, however, is an anti-inflammatory and tolerogenic process which induces the secretion of IL-10 and TGF β ⁶⁸. Defects in efferocytosis have many pathological outcomes, including developmental malformations, chronic inflammatory diseases and autoimmunity. The primary signal for AC recognition is the exposure of PtdSer on the cell surface. In healthy cells, flippases maintain membrane asymmetry, confining PtdSer to the inner leaflet of the plasma membrane. However, under apoptotic conditions, scramblases are activated, and flippases inactivated, thereby distributing PtdSer to both leaflets of the plasma membrane, thus allowing for binding by efferocytic opsonins and receptors^{69–71}.

There are an array of efferocytic receptors, which can bind ACs directly or via opsonins. The T cell immunoglobulin- and mucin-domain-containing molecule (TIM) family (TIM-1, TIM-3 and TIM-4) recognize PtdSer directly, whereas integrins recognize PtdSer indirectly through milk fat globule EGF factor 8 (MFG-E8)⁷²⁻⁷⁶. Scavenger receptors such as CD36 can also recognize ACs, but through oxidized lipids and glycoproteins on AC surfaces^{77,78}. Often, multiple receptors cooperate to induce efferocytosis⁷⁹⁻⁸¹. As an example, in macrophages the scavenger receptor CD204 signals through MERTK⁸¹; MERTK in-turn depends on integrins such as $\alpha_v\beta_5$ to complete efferocytosis^{2,79,82}. The integrin plays an active role in AC binding, and engages ACs through the PtdSer binding opsonin MFG-E8. It should be noted that the requirement for integrins in MERTK-induced efferocytosis has been shown in HEK293T cells and CS-1 melanoma cells², but this association has yet to be demonstrated in macrophages, and moreover, some *in vitro* studies have observed MERTK-mediated efferocytosis in the absence of MFG-E8/integrin binding of the AC⁸³. Whether the dependence of MERTK-mediated efferocytosis on integrins represents a cell-type specific phenomenon, or one dependent on the particular efferocytic receptors expressed alongside MERTK, has yet to be elucidated.

Although a detailed mechanism for TAM receptor efferocytotic signalling has yet to be established, several molecules involved in this mechanism have been identified. As discussed above, TAM receptors indirectly bind ACs through opsonins, leading to receptor dimerization and autophosphorylation of tyrosine kinases (Figure 2). The co-activation of integrins by MERTK has been proposed to involve autophosphorylation of Tyr-867 in MERTK, leading to Src recruitment,

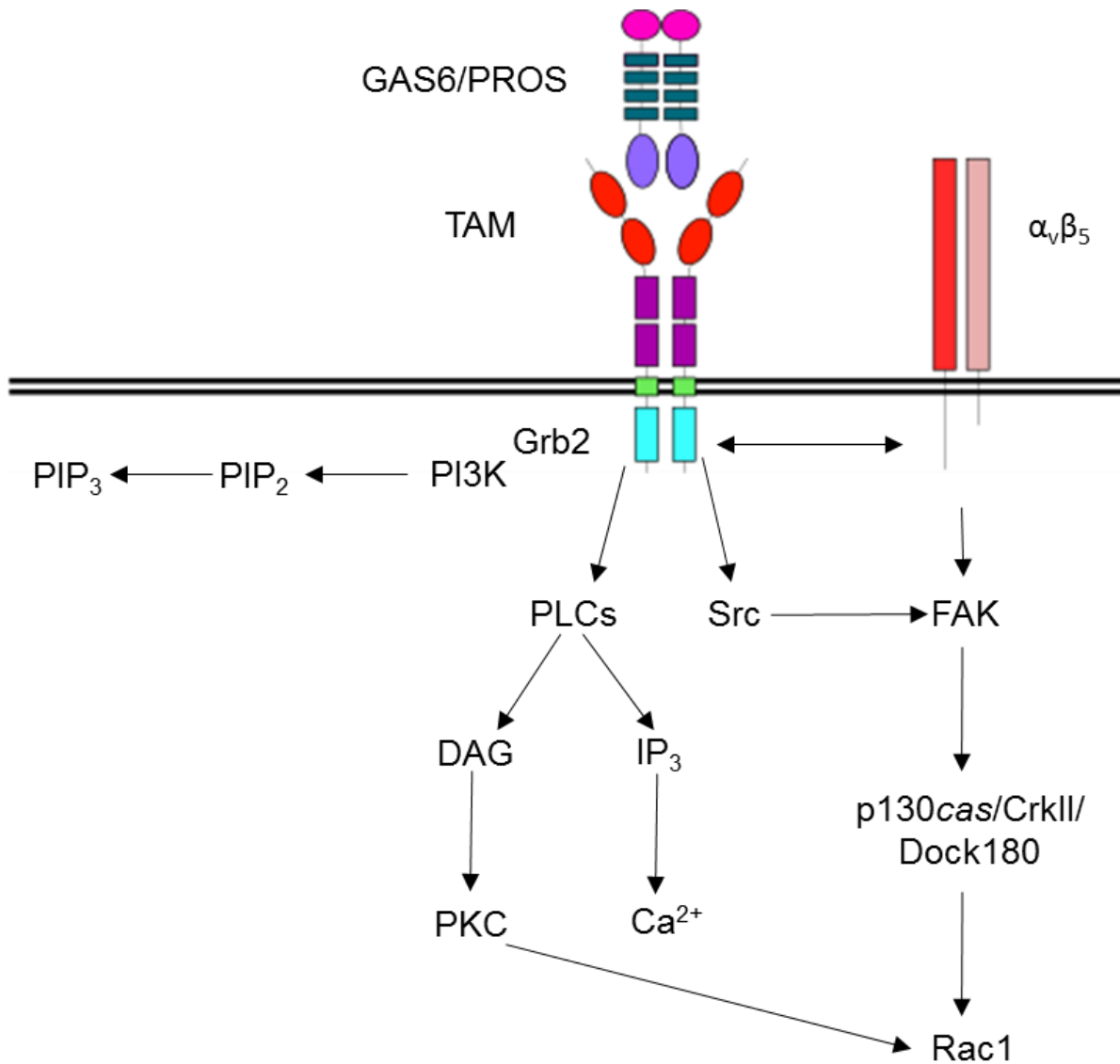


Figure 2: TAM receptor signalling pathway. TAM receptor homodimers bind to opsonins GAS6 and PROS homodimers to activate signalling through the kinase domain. The kinase domains activate when the receptor is bound to its opsonin through autophosphorylation of tyrosine kinases, which are recognized by Grb2. Grb2 recruits PI3K which in turn phosphorylates PIP₂ to promote efferocytosis. Upon TAM activation, phospholipase C_γ2 (PLCs) is stimulated, which leads to enhanced PKC activity. TAMs may be able to solely activate efferocytosis through PKC activation of Rac1, or Rac1 can be activated following Src activation, and cross-talking with α_vβ₅ through FAK. Adapted from ref 84.

activation, and Src-mediated phosphorylation of focal adhesion kinase (FAK)⁶¹. Phosphorylated FAK is recruited to the integrin where it increases the formation of p130cas/CrKII/Dock180 complex which in turn leads to actin cytoskeleton rearrangement through Ras-related C3 botulinum toxin substrate 1 (Rac1) to phagocytose ACs^{2,61}. TAM receptors may also signal directly to Rac1 through activation of PLC potentially allowing TAM receptors to bypass integrin-mediated cytoskeletal modeling⁶¹. Furthermore, the aforementioned PI3K activation is essential for MERTK-dependent phagocytosis, where it likely acts to enhance cytoskeletal rearrangements such that large particulates can be engulfed⁸⁵.

1.5 TAM receptors in infection and disease

1.5.1 Inflammation and autoimmunity

Efferocytosis is a tolerogenic and anti-inflammatory process that removes potential AC-derived autoantigens, thus, TAM receptor deficiencies are unsurprisingly linked to numerous chronic inflammatory and autoimmune diseases^{86,87}. TAM TKO and *MerTK*^{-/-} mice display the most severe phenotypes due to increased levels of autoantibodies, accumulation of ACs and secondary necrotic cells, and elevated levels of inflammatory cytokines such as TNF- α and IL-1^{15,16,20}. These defects are more severe in TAM TKO mice, in part because *MerTK*^{-/-} mice have increased levels of DC maturation and antigen cross-presentation, which augments activation of lymphocytes¹⁵. Even with these defects, both TAM TKO and *MerTK*^{-/-} mice spontaneously develop clinical symptoms similar to systemic lupus erythematosus (SLE)¹⁵. Moreover, TAM receptors – mainly MERTK – have been linked to rheumatoid arthritis, type II diabetes, atherosclerosis, multiple sclerosis (MS) and inflammatory bowel disease in corresponding murine disease models^{15,17–19,23,88,89}. In humans,

genome wide association studies have linked *MERTK* SNPs to MS, and SLE^{11,90}, while polymorphisms in both *MERTK* and *TYRO3* have been linked to atherosclerosis¹⁰. In addition, *AXL* SNPs have been linked to insulin resistance, obesity and high level of C-reactive protein (correlates with risk of developing cardiovascular disease)¹⁴. TAM receptor associations with inflammatory and autoimmune diseases highlight their role, as well as the predominant role of *MERTK*, in maintaining homeostasis.

1.5.2 TAM receptors as viral targets

Enveloped viruses – including viruses from the poxviridae, flaviridae, filoviridae and retroviridae families – exploit TAM receptors for immunosuppressive signalling and cell entry^{34,91}. They use a form of viral mimicry termed “apoptotic mimicry”, where PtdSer asymmetry is lost in their envelopes, leading to PtdSer exposure on the virion surface⁹². Opsonins then bridge these viruses to TAM receptors and signalling is induced. A major innate immune response to viruses is toll-like receptor-signalling which produces a type I IFN-response; however, TAM receptors can inhibit production of type I IFNs through IFNAR-mediated expression of SOCS1 and SOCS3³⁴. Indeed, studies have shown that SOCS1 and SOCS3 mRNA is lower in Ebola-, Marburg virus-, and Murine Leukemia virus-infected TAM TKO DCs, and antiviral type I IFN mRNAs are augmented, compared to wild-type mice⁹³. Furthermore, TAM kinase signalling is critical for viral infections, as mice bearing TAM receptors with non-functional kinase domains have significantly reduced levels of infection, although the mechanism resulting in reduced infection remains to be elucidated³⁴. Infecting viruses also preferentially interact with specific members of the TAM family. TAM TKO DCs have been shown to be highly resistant to West Nile virus and HIV-1

infection, with *MerTK*^{-/-} DCs displaying similar resistance to infection⁹³. Interestingly, expression of AXL has been shown to be increased in patients infected with hepatitis C virus⁹⁴, and patients possessing a favourable SNP in *IFNL3* had lower levels of AXL expression in the liver and stronger induction following IFN treatment⁹⁵. The ability to facilitate viral entry and induce anti-viral immune responses make TAM receptors ideal targets for anti-viral therapeutics.

1.5.3 TAM receptor association with cancer

Overexpression of all three TAM receptors, as well as GAS6, have been linked to cancer – both in regards to tumour development, and to metastasis. Interestingly, although all three receptors have been shown to be upregulated in cancer, it is usually never more than one of the TAM receptors that is upregulated in a given tumour. TAM receptors increase cell motility and cell-to-cell interactions, factors which likely contribute to the association between TAM receptor expression and metastasis^{21,96}. The kinase domain is required for these actin-dependent mechanisms, and provides additional signalling through AKT and ERK1/2 pathways which in addition to inducing motility also promote cell survival^{60,62,97}. Indeed, in studies using an AXL lacking a TKD, cancer cell proliferation was decreased and the cancer cells were less invasive. In addition, studies with inhibited AXL documented decreased levels of angiogenesis – likely due to decreased AKT signalling. Furthermore, some cancers develop mutations within the TAM kinase domain, resulting in a constitutively active kinase. This enhances cell survival and proliferation through activation of the AKT pathway – indeed, MERTK was initially identified as a proto-oncogene^{98,99}. Finally, the upregulation of TAM receptors, and other efferocytic receptors, may act to limit the immunogenicity of tumour cells through enabling the uptake of dying cancer cells by neighbouring

cells within the tumour, thereby avoiding subsequent uptake by professional antigen presenting cells.

As TAM receptor expression increases rates of metastasis, and is associated with poor cancer prognoses, it is unsurprising that many research groups are seeking to inhibit TAM receptor activation in cancers. TAM receptor research in cancer has mainly focused on AXL, and has led to the generation of multiple small molecule inhibitors and anti-AXL monoclonal antibodies, such as R428 which are currently in Phase Ib trials and have been shown to reduce cancer metastasis and enhance survival in breast cancer models¹⁰⁰. MERTK-selective inhibitors – such as UN2025 – are also being tested¹⁰¹. However, as AXL and MERTK have been shown to be alternately expressed in some cancers¹⁰², dual AXL and MERTK inhibitors (6g and GSK2606141) may prove the more effective cancer drugs^{103,104}. While these inhibitors have been designed to inhibit TAM receptor function in cancer, in the future they will be invaluable tools for the study of TAM activity in efferocytosis.

1.6 Hypothesis and objectives

Although TAM receptors are important regulators of homeostasis, as evidenced by their association with numerous autoimmune and chronic inflammatory diseases, little work has been conducted on their evolution. Thus, we conducted an evolutionary analysis on the TAM receptors, and interestingly, noticed two areas in *MERTK*, but not other TAM receptors, dominated by positive selection – the signal peptide and transmembrane domain – as well as a large number of conserved regions. Positive selection indicates evolutionary changes, and while rare, it is observed most often in immune-related genes, likely indicative of compensatory evolution^{105–107}. In general,

signal peptides evolve more slowly than other coding regions in the same gene, but usually display an evolutionary pattern consistent with drift. In contrast, transmembrane domains tend to undergo strong conservation^{106,108}. While positive selection of signal peptides has been observed in some immune-related genes, the biological impact of these changes remains to be elucidated. Thus, the identification of positive selection in *MERTK*'s signal peptide and transmembrane domain led us to evaluate the impacts of these changes in *MERTK* dimerization, expression, protein trafficking, and with the intention of evaluating the impact on *MERTK*-dependent efferocytosis through functional assays. Given these evolutionary patterns, and the predominant use of *MERTK* as a source for viral entry and viral induced anti-inflammatory signalling, **we hypothesized that the positive selection in *MERTK*'s signal peptide would lead to reduced surface expression, and this lower surface *MERTK* expression would be compensated for by the co-evolution of avidity-enhancing self-clustering.**

To evaluate this hypothesis, I established three objectives. **1)** Reconstruct primate- and hominid-ancestral signal peptide and transmembrane domains to identify the specific nucleotide and amino acid changes which occurred during recent *MERTK* evolution. **2)** Use chimeric *MERTK* comprised of the reconstructed primate and hominid-ancestral signal peptide or transmembrane domain inserted into human *MERTK* to evaluate the biological impact of these changes on *MERTK* trafficking, expression, and self-clustering. **3)** Create a heterologous model system to study the impact of evolutionary changes in *MERTK*'s transmembrane domain on efferocytic efficiency and receptor signalling.

Chapter 2: Materials and methods

2.1 Materials

HeLa, COS-7 and HEK293T cells were kind gifts from Dr. Jimmy Dikeakos (University of Western Ontario), Dr. Sergio Grinstein (Hospital for Sick Children, Toronto), and Dr. Eric Arts (University of Western Ontario) respectively. DH5a *Esherichia coli*. were a generous gift from Dr. John McCormick (University of Western Ontario). FcγRIIA-GFP and Tim4-mCherry constructs were kind gifts from Dr. Ronald Flannagan, and cobalt transport protein (CbiN)-GFP and mRas-RFP were previously cloned in the lab. Roswell Park Memorial Institute (RPMI), Hepes-buffered RPMI (HPMI), Dulbecco's Modified Eagle Medium (DMEM), and Fetal Bovine Serum (FBS) were purchased from Wisent (Saint-Jean-Baptiste, Canada), while Trypsin-EDTA and antibiotic/antimycotic were purchased from Corning (Manassas, Virginia). #1.5 thickness round cover slips and 16% paraformaldehyde (PFA) were purchased from Electron Microscopy Supplies (Hatfield, Pennsylvania). Cycloheximide, dexamethasone and rat anti-HA (3F10) were purchased from Sigma-Aldrich (Oakville, Canada). GenJet Plus was purchased from Frogga Bio (North York, New York). Lympholyte-Poly was purchased from Cedarlane (Burlington, Ontario) and all cytokines were purchased from Peprotech (Rocky Hill, New Jersey). Hoechst, permafluor, T4 DNA ligase, Phusion DNA polymerase were purchased from Thermo Scientific. Protein A/G beads, polystyrene beads, and silica beads were purchased from Bangs Laboratories, Inc. (Fishers, Indiana) and lipids from Avanti Polar Lipids, Inc. (Alabaster, Alabama). All opsonins, restriction enzymes, goat isotype control and goat anti-mouse MERTK antibody (AF591) were purchased from R&D (Minneapolis, MN), while the rabbit anti-human MERTK antibody (D21F11), anti-β₁ integrin (P5D2), and fluorescent secondary antibodies were purchased from Cell Signalling Technology (Danvers, Massachusetts), Developmental Studies Hybridoma Bank (Iowa City,

Iowa), and Jackson ImmunoResearch Laboratories, Inc. (West Grove, Pennsylvania) respectively. Mouse anti-HA (12CA5) was purchased from Santa Cruz (Dallas, Texas). All other chemicals were purchased from Canada BioShop (Mississauga, Canada). Matlab software was purchased from MathWorks (Natick, Massachusetts). Prism software was purchased from Graphad (La Jolla, California). Mega6 Software and ImageJ were downloaded from www.megasoftware.net¹⁰⁹ and www.imagej.nih.gov/ij/ respectively.

2.2 Generation of phylogenetic trees

Mammalian *MERTK* sequences were retrieved from the NCBI database and coding sequence alignments for mammals and primates were generated with *Muscle* using default parameters¹¹⁰. For phylogenetic analysis, Bayesian (BIC) and Akaike information criterion (AIC) scores for each nucleotide substitution model were compared to determine the model used for mammal and primate alignments. Phylogenetic analysis of aligned sequences were performed across all reading frames using maximum-likelihood with bootstrapping using the GTR and K2 substitution models for primate and mammalian *MERTK* sequence analysis respectively with gamma distribution, as determined by BIC and AIC scores. While *AXL* and *TYRO3* phylogenetic analyses used the T92 and TN93 selection models respectively, both with gamma distribution. The generated mammalian phylogenetic tree was annotated in EvoView. All phylogenetic and molecular evolutionary analyses were conducted using MEGA6¹⁰⁹.

2.3 Selection analysis

Unaligned TAM primate sequences were imported into the Selecton online server (<http://selecton.tau.ac.il/>)¹¹¹, and the *Homo sapiens* sequence was used as a reference sequence for

data output. The constructed phylogenetic trees were used to guide alignments. Selection analysis was first performed using the Mechanistic Empirical Combination Model (MEC) with 8 distribution categories and the JTT amino-acid matrix. As a test of significance, MEC likelihood and AIC scores were compared against the M8a model (neutral evolution), with lower MEC AIC scores indicating significance. Further selection analysis used the M5 model (positive selection), comparing AIC scores with the M7 model (neutral evolution). A comparison between the MEC/M8a and M5/M7 AIC scores confirmed MEC as the model of best fit by maximum-likelihood. Ka/Ks values were used to score amino acid positions for significance, with confidence intervals (CI) generated through Selecton. Strong evidence for positive selection was indicated by scores of $Ka/Ks > 1.5$ with CI lower bounds greater than 1, while probable positive selection was indicated by CI lower bounds below 1. Strong evidence for purifying selection was indicated by $Ka/Ks < 0.5$ with CI upper bound below 1, while probable purifying selection indicated by CI upper bounds greater than 1. Neutral evolution was defined as amino acid positions with Ka/Ks values between 0.5 and 1.5, or with large CIs. Selecton data was then imported into MATLAB and a custom-written script used to calculate Ka/Ks values averaged over 10 neighboring residues.

2.4 Prediction of ancestral MERTK sequences

Reconstruction of the ancestral Hominidae and primate *MERTK* sequence was performed using MEGA6¹⁰⁹. Nucleotide alignments and phylogenetic trees of the Hominidae and Primate *MERTK* sequences, generated above, were imported into MEGA6 and the ancestral sequences predicted a maximum-likelihood approach and the K2 evolutionary model.

2.5 Hydrophobicity and isoelectric point analysis

To analyze any biochemical changes in the reconstructed primate and hominid-ancestral MERTK signal peptides and transmembrane domains were imported into ExPASy ProtScale and Compute PI/Mw and hydrophobicity and isoelectric points calculated.

2.6 Mouse and human *MERTK* synthesis and mutagenesis

Due to failure to detect heterologous mouse MERTK expression using the pIRES-EGFP Mer (Addgene), we cloned mouse MERTK-GFP was cloned into pEGFP-N1 by digesting mouse MERTK from pIRES-EGFP Mer and pEGFP-N1 using BamHI and BglII for 1 h at 37°C, gel purifying using a 1% TAE/agarose gel and PCR purification kit, and ligating using T4 DNA ligase. The endogenous MERTK stop codon was removed to create a MERTK-GFP fusion protein by amplifying the vector using Mouse-FWD and Mouse-REV 5' phosphorylated primers using Phusion DNA polymerase, 36 cycles with an annealing temperature of 60°C and 8 min elongation at 72°C (Table 1). The PCR product was DpnI treated for 1 h at 37°C to degrade template DNA and gel purified. The purified construct was ligated using T4 DNA ligase, transformed into DH5α *E. coli*, and plated onto 100 µg/mL kanamycin containing LB plates. Clones were sequenced to ensure removal of stop codon.

As conventional cloning of human *MERTK* is not possible due to the presence of multiple motifs recognized by bacteria as recombination and phage integration sites, combined with an unusually high G/C content (63%), we used the OptimumGene codon-optimization algorithm (GenScript) to remove secondary DNA structure, reduce GC content and optimize codon usage (Appendix 1) and had the gene synthesized and subcloned into pcDNA3.1(+) (GenScript). An extracellular HA tag

Table 1: Primers and synthetic DNA elements used for vector construction.

Primer/DNA	Sequence
Mouse-FWD	5' Phos-ACGGATCCACCGGTCG
Mouse-REV	5' Phos-TGAGGAACCTTCTGAGACTTCAAGACTAC
HA-FWD	5' Phos- GGCGTAGTCAGGCACGTCGTAAGGATAGTCGGTCTGCAGGCTTCCG
HA-REV	5' Phos-CACACACCACTGCTGTCACTG
SigPep-FWD	GAGGAGGCTAAGCCATACCCCCTGTTTCCT
SigPep-REV	GGTGGCAAGCTTAAGTTTAAACGCTAGCCA
TM-FWD	AAATTTGGGAATGCTTTCCTGAGGAAGAC
TM-REV	GTTTCCTGGTGCAGGTGTGCTTGAAGGGC
SC-GFP-FWD	GCGTTTAACTTAAGCTTGCCACCATG
SC-GFP-REV	CATGGTGGCGACCGGTCTCATCAGCACCTCGGACCCCT
CD8 α -SigPep*	TGGCTAGCGTTTAACTTAAGCTTGCCACCATGGCCTTACCAGTGACC GCCTTGCTCCTGCCGCTAGCCTTGCTGCTCCACGCCGCCAGGCCGGAG GCAAGGGAAGAGGAGGCTAAGCCATACCCCCTGTTTCCT
Human-SigPep*	TGGCTAGCGTTTAACTTAAGCTTGCCACCATGGGGCCGGCCCCGCTG CCGCTGCTGCTGGGCCTTTCCTCCCCGCGCTCTGGCGTAGAGCTATCA CTGAGGCAAGGGAAGAGGAGGCTAAGCCATACCCCCTGTTTCCT
Hominid-SigPep*	TGGCTAGCGTTTAACTTAAGCTTGCCACCATGGGGCCGGCCCCGCTG CCGCTGCTGCTGGGCCTTTCCTCCCCGCGCTCTGGAGTAGAGCTATC ACTGAGGCAAGGGAAGAGGAGGCTAAGCCATACCCCCTGTTTCCT
Primate-SigPep*	TGGCTAGCGTTTAACTTAAGCTTGCCACCATGGGGCCGGCCCCGCTG CCGCTGCTGCTGGGCCTTTCCTCCCCGCGCTCTGGAGTAGAGCTATC ACCGAGGCAAGGGAAGAGGAGGCTAAGCCATACCCCCTGTTTCCT
Hominid-TM*	GCCCCTCAAGCACACCTGCACCAGGAAACGCAGATCCTGTGCTCATC ATCTTTGGCTGCTTTTGTGGATTTATTTTGATTGGGTTGTTTTATACAT CTCCTTGGCCATCAGAAAAAGAGTCCAGGAGACAAAATTTGGGAATG CTTTCCTGAGGAAGAC
Primate-TM*	GCCCCTCAAGCACACCTGCACCAGGAAACACAGATCCTGTGCTCATC ATCTTTGGCTGCTTTTGTGGATTTATTTTGTTTTATATATCTTGGCCAT CAGAAAAAGAGTCCAGGAGACAAAATTTGGGAATGCTTTCCTGAGG AAGAC

5' Phos = 5' phosphorylated PCR primer

* = double-stranded synthesized DNA

was added by linearizing the codon-optimized *MERTK* vector using the HA-FWD/HA-REV 5' phosphorylated primers for PCR (Table 1). PCR was conducted using Phusion DNA polymerase, 36 cycles with an annealing temperature of 63°C and 8 minutes elongation at 72°C. The PCR product was treated with DpnI at 37°C for 1 h to degrade the template and gel purified using a 1% TAE/agarose gel and PCR purification kit. The purified linearized construct was then recircularized with T4 DNA ligase, transformed into DH5 α *E. coli*, and clones were selected on LB agar plates containing 100 μ g/mL ampicillin. Successful insertion of the HA tag was confirmed by DNA sequencing. This HA-tagged vector and Gibson assembly was used for assembly of all subsequent *MERTK* constructs¹¹⁷. Briefly, the signal peptide and transmembrane domains were replaced by linearizing the *HA-MERTK* construct with PCR using primers flanking the signal peptide (SigPep-FWD/ SigPep-FWD) or transmembrane domain (TM-FWD/TM-REV, Table 1), using the same PCR cycle and purification protocol as above. The linearized vector was then mixed at a 1:5 molar ratio of vector:insert in Gibson assembly¹¹⁷ master mix with synthesized double-stranded DNA constructs containing 20 bp regions of homology flanking the signal peptide (CD8 α -SigPep, Human-SigPep, Hominid-SigPep, Primate-SigPep, Table 1) or transmembrane domain (Hominid-TM or Primate-TM, Table 1) sequence. The reaction was incubated at 50°C for 30 min, then transformed into DH5 α *E. coli* and positive clones identified as described above. Where GFP tagged version of the vector were required, the constructs generated above were subcloned into pEGFP-N1 by PCR amplifying the modified *MERTK* gene with the SC-GFP-FWD/SC-GFP-REV primers (Table 1) using Phusion polymerase, 35 cycles, 63°C annealing temperature and a 3 min elongation at 72°C. The resulting PCR product was gel purified, and inserted into pEGFP-N1 by digesting the PCR product and vector with HindIII and AgeI and ligating the fragments together using T4 DNA ligase.

2.7 Cell Culture and transfection

HeLa cells were maintained in RPMI plus 10% FBS and COS-7 and HEK293T cells were maintained in DMEM plus 10% FBS. Cells were split upon reaching 80% confluency by washing once with phosphate buffered saline (PBS: 0.9% NaCl, 10mM Na₂HPO₄, 2 mM KH₂PO₄, pH 7.4) followed by a 5 min incubation in trypsin-EDTA and resuspension in either RPMI or DMEM plus 10% FBS. For imaging, #1.5 thickness 18 mm diameter coverslips were first rinsed in 100% ethanol, deprotonated for ~12 h in 1M HCl at 50–60°C with intermittent agitation, rinsed with 100% ethanol and dried. The coverslips were then placed into the wells of a 12-well tissue culture plate, 1 ml of RPMI or DMEM + 10% FBS added, and 100 µL of the cell suspension added dropwise to each well. For immunoblot experiments, 300 µL of the cell suspension was added dropwise to wells without coverslips. 12- 24 h later the cells were transfected with the desired construct following manufacturer's protocol. Briefly, for each well two tubes of 38 µl serum-free DMEM were prepared and 1 µg of DNA added to one tube and 2 µl of GenJet Plus added to the second tube. Both tubes were vortexed briefly, the contents combined, and the mixture incubated for 15 min. The DNA:GenJet Plus complexes were then added drop-wise to the well and incubated 18-24 h.

2.8 Primary macrophage preparation

Human blood was collected into heparin, in approval of Western University's Health Sciences Research Ethic Board and in compliance with the Tri-Council Policy Statement on human research (Ethics approval attached as Appendix 2), from healthy adult donors and monocytes isolated using Lympholyte-poly according to manufacturer's protocol. Briefly, 5 mL of human blood was layered over 5 mL of Lympholyte-poly and centrifuged for 35 min at 300 x g. The monocyte layer was

removed using a transfer pipette and the cells washed using 50 mL of PBS and then centrifuged for 8 min at 300 x g. The pellet was resuspended in 300 μ L of 37°C serum-free RPMI per desired well of a 12-well plate. The cell suspension was then pipetted onto sterile 18 mm glass coverslips previously placed into the wells of a 12-well plates. Cells were incubated for 1 h at 37°C with 5% CO₂ to allow monocytes to adhere to glass coverslips and non-adherent cells removed with three gentle washes with PBS, 1 mL of RPMI + 10% FBS and 1:100 antibiotic/antimycotic (10,000 U/mL penicillin, 10 mg/mL streptomycin and 25 μ g/mL Amphotericin B) was then added, supplemented with cytokines for macrophage sub-type differentiation (M0, M2 and M2c: 10 ng/mL M-CSF; M1: 20 ng/mL GM-CSF). Following a 5 day incubation at 37°C with 5% CO₂, cells were washed three times with PBS and media replaced with RPMI + 10% FBS with antibiotic/antimycotic along with the appropriate cytokines to complete macrophage differentiation (M0: 10 ng/mL M-CSF, M1: 20 ng/mL GM-CSF, 100 ng/mL IFN- γ , and 250 μ g/mL LPS, M2: 10 ng/mL MCS-F and 10 ng/mL IL-4, M2c: 10 ng/mL M-CSF + 100 nM dexamethasone). Macrophages were incubated for another 2 days at 37°C with 5% CO₂ prior to use.

2.9 Microscopy

All experiments, save the oligomerization assays, used a Leica DMI6000B microscope equipped with a 100 \times /1.40NA objective, photometrics Evolve-512 delta EM-CCD camera and Chroma Sedat Quad filter set running Leica LAX software, with samples prepared as described below. The oligomerization assays were imaged using a Leica SR Ground-State Depletion microscope equipped with a 100 \times /1.43 NA TIRF objective, plus an addition 1.6 \times optical magnifier for a total of 160 \times magnification, 125 mw–250 mW imaging lasers (488, 555 and 647 nm) and a 30 mW

backpumping laser (405 nm) running Leica Ground-State Depletion Microscopy (GSDM) software. Experiment-specific microscopy procedures are described below.

2.10 Immunostaining

Transfected cells or primary macrophages were washed with PBS and fixed for 15 min with 4% PFA in PBS at room temperature. Cells were washed three times with PBS and 1 mL of 0.1% triton-x-100 in PBS added for 10 min for internal epitope detections only. Cells were blocked for 1 h using 5% skim milk in PBS and stained for 1 h using 1:100 primary antibody (anti-human MERTK, anti-mouse MERTK, anti- β_1 integrin or mouse anti-HA) in blocking buffer. Cells were washed with PBS three times and stained using 1:1000 fluorescently tagged secondary Fab fragment antibodies. Lastly, cells were washed with PBS three times and if required, incubated in 1:20,000 Hoechst in PBS for 5 min where applicable. After a final PBS wash, coverslips were mounted on glass microscope slides using permafluor and imaged using a Leica DMI6000B microscope described.

2.11 Immunoblots and coomassie stains

Cells were seeded onto 6-well plates, and transfected as previously described for 12-well plates. 18 h after transfection cells were lysed using Lammelli buffer (0.1% 2-Mercaptoethanol, 0.0005% Bromophenol blue, 10% glycerol, 2% SDS, 63 mM Tris-HCl, pH 6.8) plus protease inhibitor cocktail. Samples were boiled for 5 min, cooled, and separated using a 10% SDS-PAGE gel at 150V for 2 h. For coomassie stains, gels were fixed (50% methanol, 10% glacial acetic acid, 40% ddH₂O) for 30 min, stained with coomassie blue staining solution (0.1% Coomassie Brilliant Blue, 50% methanol, 10% glacial acetic acid, 40% ddH₂O) for 2 h, and destained for 24 h (5% methanol,

7.5% glacial acetic acid, 87.5% ddH₂O). Lastly, coomassie gels were imaged using a BioRad GelDoc EZ imager. For immunoblots, samples were transferred to nitrocellulose membranes at 4°C for 2 h at 80V, and the membrane blocked with TBST (137 mM NaCl, 2.7 mM KCl, 19 mM Tris-HCl, 0.1% Tween-20, pH 7.4) plus 5% skim milk powder for 2 h at room temperature. The blots were then incubated with 1:100 rat-anti-HA in TBST + 5% skim milk powder for 2 h, washed 3 × 10 min with TBST, incubated with 1:1,000 Alexa800-labeled donkey-anti-rat (in TBST + 5% skim milk powder) and washed a final 3 × 10 min with TBST. Blots were imaged using a LI-COR Odyssey Model 9120.

2.12 Protein trafficking assay

HeLas were seeded onto μ -Slide 8 wells with a glass bottom and transfected at 80% confluency using Fugene HD at 2:0.75 transfection reagent to DNA (μ L: μ g) according to manufacturer's protocol. Transfected cells were washed three times using 10°C PBS and incubated with 1:100 mouse anti-HA in serum-free RPMI for 20 min at 10°C to label surface MERTK. Cells were washed three times using 10°C PBS and incubated with 50 μ g/mL cycloheximide in serum-free RPMI with 1:500 donkey anti-mouse 647 for 20 min at 10°C. Cells were washed 3 times in 10°C PBS and subsequently imaged in 37°C serum-free RPMI with 50 μ g/mL cycloheximide. The wells were placed onto a heated/CO₂ perfused live-cell piezoelectric stage of a Leica DMI6000B microscope described. The position of 10-15 cells were marked using the stage controller and time-lapse videos of MERTK membrane trafficking captured (5 min/frame, 60 min duration). The plasmamella of each cell was identified by the 647 staining (e.g. cell-surface MERTK). This mask was then applied to the GFP channel (total MERTK) and trafficking quantified as the rate of increase in GFP intensity within the 647 mask relative to the initial time point.

2.13 Protein expression analysis

HeLa cells were transfected at a 1:3 ratio of mRas-RFP (internal transfection control) and HA-MERTK-GFP codon-optimized, human or primate or hominid ancestral hybrid constructs. Samples were analyzed using widefield microscopy or flow cytometry (using a BD FACS Canto II Flow Cytometer) and expression quantified using mean fluorescence intensity (MFI) relative to internal control mRas-RFP using ImageJ or FlowJo respectively. For the immunoblot analysis of protein expression, HeLa cells were transfected with 1 µg of a 1:30 ratio mixture of the desired *MERTK* construct and HA-tagged *CD93*. Lysates were obtained and immunoblot conducted as described above. MERTK expression was quantified as integrated density ratio between the HA-CD93 and MERTK bands using ImageJ software. For flow cytometry, cells were trypsinized for 5 min at 37°C for 5 min, and trypsin was inactivated by RPMI + 10% FBS. Cells were centrifuged for 1 min at 6,500 x g, washed three times with PBS, fixed for 10 min using 4% PFA in PBS and washed in PBS prior to analysis.

2.14 Oligomerization assay

Super-resolution GSDM was used to assess oligomerization of GFP-tagged MERTK. HeLa cells were transfected with GFP-tagged MERTK and fixed for 20 min at room temperature using 4% paraformaldehyde in PBS. The cells were washed 3 times in PBS and then permeabilized using PBS + 5% BSA and 0.01% saponin. The fixed and permeabilized samples were then mounted on depression slides with the depressions filled with imaging buffer (PFA + 100 mM Cysteamine). Once mounted the coverslips were sealed using Twinsil and imaged. The GFP color channel was subjected to a depletion period where the sample was excited at maximum intensity until less than 120 active fluorophores were present in each image. The laser intensity was then reduced to 20%

of maximum and the sample imaged at 100 fps for 20,000 to 30,000 frames with the backpumping laser intensity increased over time to maintain 50-120 active fluorophores/frame. The resulting molecule position files were exported, filtered to remove any molecules detected with a precision >20 nm, and to ensure equal sampling of all images, reconstructed using our previously published method such that reconstruction ceased when image autocorrelation reached 0.990¹¹². 4 cells per condition were imaged in each experiment. Self-clustering was assessed using both spatial apposition assays and the radial distribution function, using our custom-written MliSR software for analysis^{112,113}.

2.15 Synthetic efferocytic target preparation

For antibody-coated bead assays, 2 µg of antibody (goat anti-MERTK, goat IgG, human IgG, Fab antibodies) were rotated in 100 µL of PBS with 10 µL of polystyrene beads or protein A/G beads for 30 min at room temperature. PtdSer and phosphatidylcholine (PtdChol) beads were prepared by combining 10 µL of silica beads with 145 µL or 114 µL of phosphatidylcholine respectively with 84 µL of phosphatidylserine for apoptotic mimics only and 4 µL of biotinylated-phosphatidylethanolamine (biotin-PE)¹¹⁴. Coated silica beads were then dried by nitrogen gas. Antibody coated beads and PtdSer/PtdChol beads were washed twice in 500 µL PBS. Beads were centrifuged at 4,500 x g for 1 min and resuspended in 200 µL of serum-free RPMI. Opsonized PtdSer/PC beads were prepared for each well by rotating 3 µL of bead solution with 5 µL of recombinant GAS6 and/or 10 µL of MFG-E8 in a total of 50 µL PBS or 50 µL of human serum overnight at 4°C under constant rotation and washed in PBS.

2.16 Efferocytosis assays

1 mL of 37°C serum-free RPMI with 5 µL antibody-coated beads, 3 µL PtdSer/PC beads or whole mix of opsonized PtdSer/PC bead solution was added to each well of a 12-well plate containing primary human macrophages or transfected cells. Samples were spun down at 300 x g for 1 min and incubated for 20 min at 37°C with 5% CO₂. Cells were washed three times with PBS and 1 mL of 37°C serum-free RPMI added per well. Samples were incubated for 40 min at 37°C with 5% CO₂ and then washed three times with PBS. External beads were labelled using 1:500 streptavidin-Alexa647 in PBS with 1:20,000 Hoechst for 5 min and washed three times with PBS prior to fixing for 15 min with 4% PFA, mounting on microscope slides and imaging using widefield microscopy. Images were exported to ImageJ and efferocytic index quantified by counting the total number of internalized beads (unstained) and dividing by total number of transfected cells.

2.17 Statistical analysis

Unless otherwise noted one-way ANOVAs with Tukey correction was used for analysis. All statistical analyses were conducted using GraphPad Prism software.

Chapter 3: Results

3.1 Patterns of recent TAM receptor evolution

The three members of the TAM family – *TYRO3*, *AXL* and *MERTK* – share a common secondary structure consisting of an amino-terminal signal peptide followed by tandem Ig, tandem Fbg, a transmembrane domain and terminating in an intracellular tyrosine kinase^{21,22}. By analyzing the rates of non-synonymous (K_a) versus synonymous (K_s) codon replacement, residues under purifying ($K_a/K_s < 0.5$) and positive ($K_a/K_s > 1.5$) selection can be detected and compared to their position in the shared TAM structure in order to identify conserved functional regions versus non-critical regions undergoing unconstrained amino acid substitutions ($0.5 < K_a/K_s < 1.5$, neutral evolution/drift). K_a/K_s analysis was performed using evolutionary trees constructed using all available primate *TYRO3*, *AXL* and *MERTK* sequences (Figure 3-5). The evolution of *TYRO3* in primates has been dominated by neutral evolution, with some conservation present in the kinase domain (Figure 5A, 6A). *AXL* is largely conserved, with only ~10% of the gene displaying non-conservative evolution (Figure 5A, 6B). In marked contrast, *MERTK* displays regions of strong conservation with two large islands of positive selection and minimal drift (Figure 5A, 6C). At the level of whole gene evolution, Z-tests and Fisher's Exact Tests demonstrated that both *AXL* and *TYRO3* have undergone a pattern of evolution consistent with drift (neutral evolution) between most tested species (Appendix 3AB & 5AB), whereas, *MERTK* displays a pattern of whole-gene conservation (negative selection) (Appendix 3AB & 4AB). Consistent with these observations, during primate evolution *AXL* and *TYRO3* have undergone a smaller degree of evolutionary divergence than *MERTK* (Figure 5B-D); indeed, negligible divergence has occurred in *AXL* and

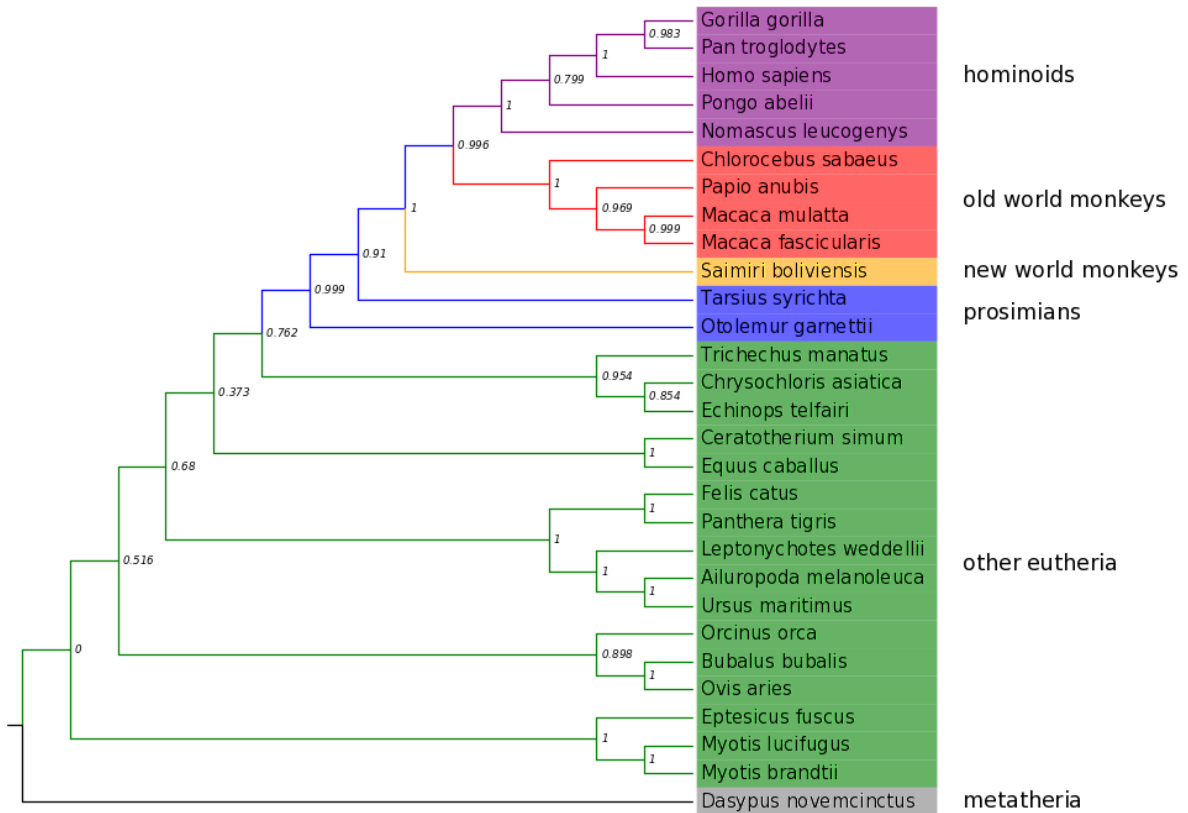


Figure 3: Mammalian evolutionary tree for *MERTK*. Maximum-likelihood evolutionary tree of *MERTK*, produced using all available mammalian *MERTK* sequences in the NCBI database. Branches indicate the degree of evolutionary divergence, numbers at branch-points indicate bootstrap values.

Figure 4: Full primate trees for evolutionary analysis of *TYRO3*, *AXL* and *MERTK*. Maximum-likelihood evolutionary trees of *TYRO3* (A), *AXL* (B) and *MERTK* (C), produced using all available primate *MERTK* sequences in the NCBI database. Scales indicate the degree of evolutionary divergence, numbers at branch-points indicate bootstrap values.

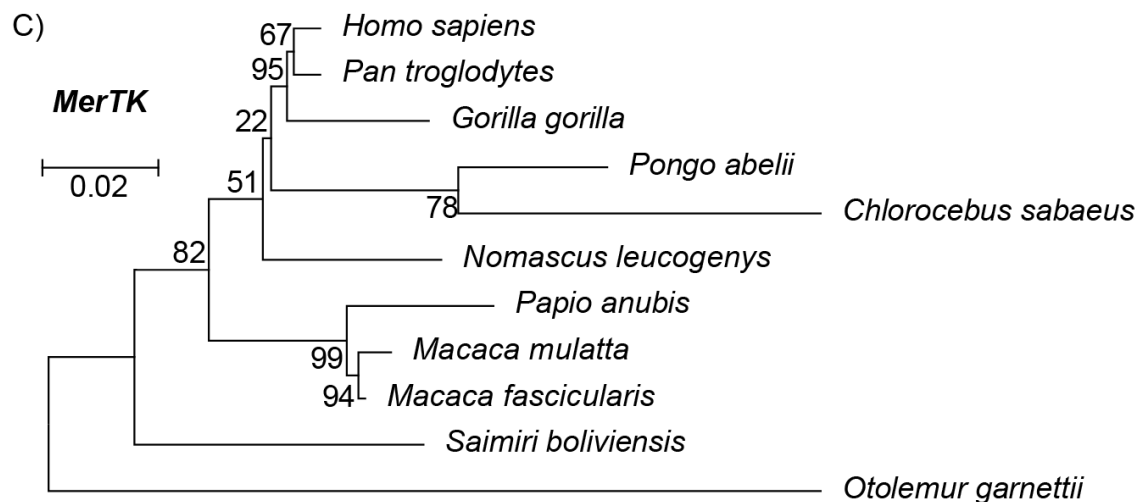
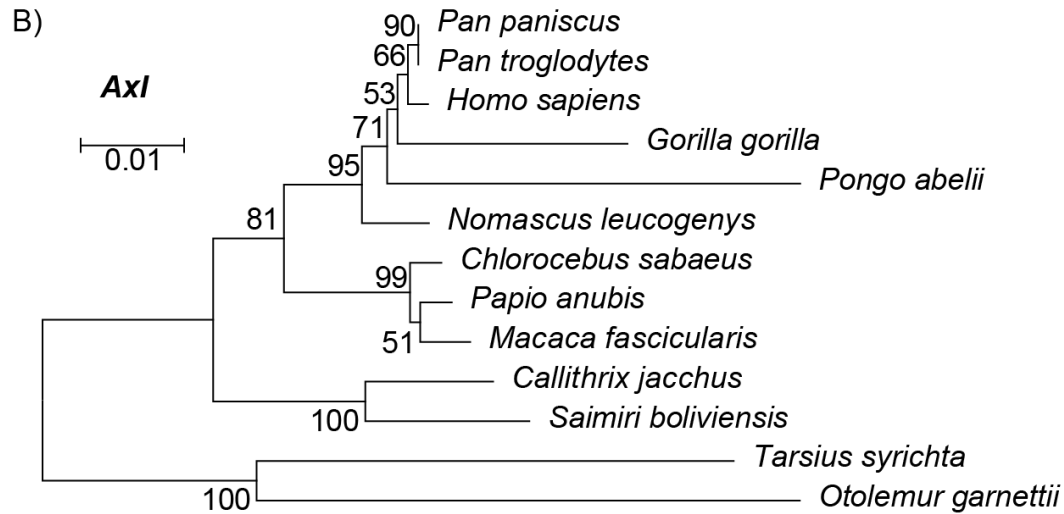
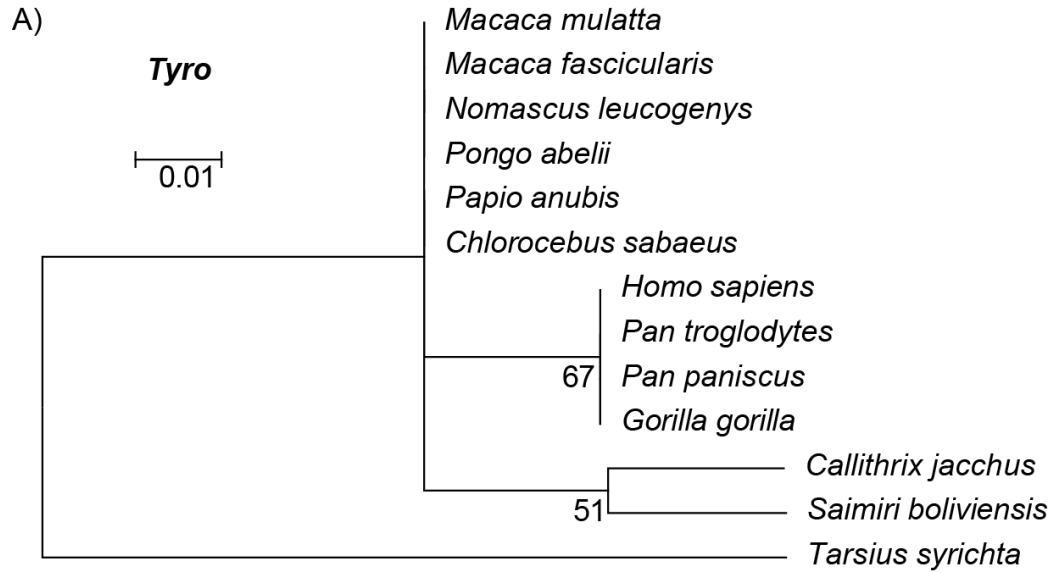


Figure 5: Recent evolution of *TYRO3*, *AXL* and *MERTK*. **A)** Identification of regions of positive and purifying selection by Ka/Ks analysis. Ka/Ks values, averaged over 10 neighboring amino acids, are plotted. Ka/Ks > 1.5 indicate positive selection, Ka/Ks < 0.5 indicate purifying selection (horizontal dotted lines). Major structural domains are indicated by colored shading, a generalized domain diagram is illustrated at the bottom of the figure. SP = signal peptide, Ig = immunoglobulin domain, Fbg = fibrinogen-like domain, TM = transmembrane domain, Kinase = tyrosine kinase domain. **B-D)** Maximum-likelihood evolutionary trees of *TYRO3* (B), *AXL*(C) and *MERTK* (D) containing representative members of the hominini (*H. sapiens*, *P. troglodytes* and *P. paniscus*, orange), the apes (hominini plus *G. gorilla* and *P. abelii*, green), old-world monkeys (*P. Anubis* and *C. sabaesus*, blue) and new-world monkeys (*C. jaccus* and *S. boliviensis*, red). Scales indicate the degree of evolutionary divergence, numbers at branch-points indicate bootstrap values.

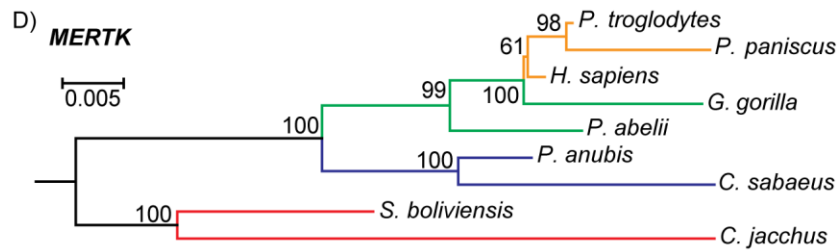
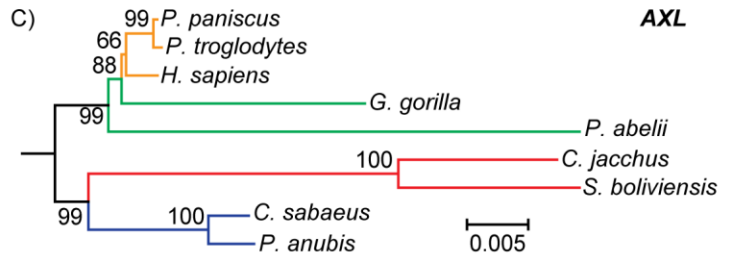
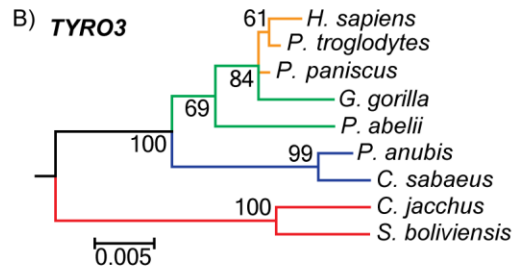
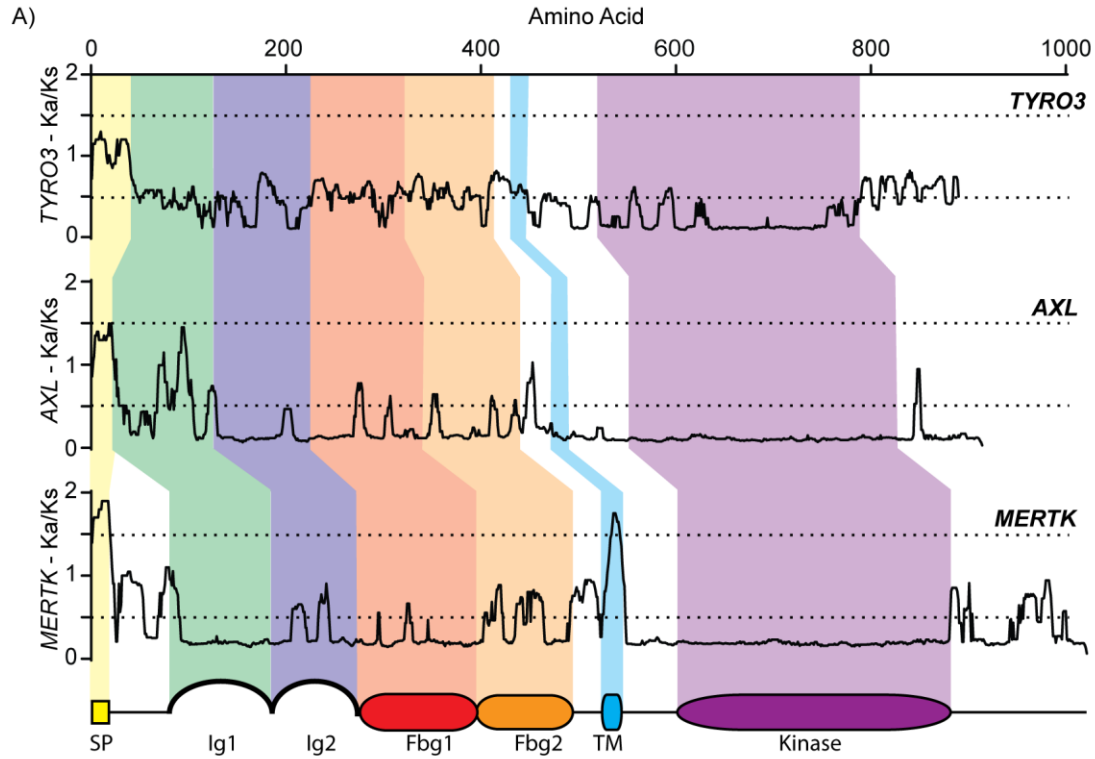


Figure 6: Per-residue Ka/Ks scores of TAM receptors. Ka/Ks values, mapped against the human TYRO3 (A), AXL (B) and MERTK (C) protein sequences. Scores of 1-2 (yellow) indicate positive selection with Ka/Ks values above 1.5, and purifying selection is represented by scores of 6-7 (purple) with Ka/Ks values below 0.5.

A)

```

1          11          21          31          41
MALRRSMGRP GLPPLPLPPP PRLGLLLAAL ASLLLPESAA AGLKLGAPV
51          61          71          81          91
KLTVSOQOPV KLNCSVEGME EPIIQWVKDG AVQNLQLY IPVSEQHWIG
101         111        121        131        141
FLSLKSVERS DAGRYWCQVE DGGETEHSQP WLTVEGV PF FTVEPKDLAV
151         161        171        181        191
PENAPFQLSC SAVGEPEPVT IVWWRGTTKI GGAESPSPVL NVTGV TQSTM
201         211        221        231        241
FSCEAANNLKG LASSRTATV LQALPAAPPN ITVTKLSSSN ASVAWPGAD
251         261        271        281        291
GRALLQSCVT QTQAPGGWE VLAVVVPVPP FTCLLRDLVP ATNYSLRVRC
301         311        321        331        341
ANALEPSPYA DWVPFQTKGL APASAPQNLH AIRTDSGLIL WEEVTPAP
351         361        371        381        391
LEGFLGFEYKL SWVQNGTQD ELTVESTRAN LTGWDPQKEL AVRVCVSNV
401         411        421        431        441
GCGEWSQPLV VSSHIRAGQQ GPPHSRTSWV PVVLGVL TALA VTAALALIL
451         461        471        481        491
LRKRRKTRF QAFTSVMAR GEPAVFERAA RSENRERPER IATLSLGE
501         511        521        531        541
SDELKEKLED VLIPEQOFTL GRMLGKGEFG SVREAQLKQE DGSFVKVAVK
551         561        571        581        591
ALKADTIASS DIEELREAA CKKFFHPEV AKLVVSLRS RAKGRLEPPE
601         611        621        631        641
VILPFMKHSD LHAFLLASRI GENPFNLPLQ TLIRFMVIA CGMEYLSSRN
651         661        671        681        691
FIRRLAARN CLAEHNTVC VAEFGLSRKI YSGDYRQGC ASKLPVKWLA
701         711        721        731        741
LESLADNLYT VQSDVWAFGV TWRIMTRGQ TPYAGLENAE IYNYLIGGNR
751         761        771        781        791
LKQPEECHEE VYDINYOQWS AEPKORPSFT CLRMELENIL GOLSVLSASQ
801         811        821        831        841
EPLYINIERA EEP TAGGSLE LPGRDQFYSG A DGSGMGA VGGTPEFCRYI
851         861        871        881
LTPGELAEQP GQAEHQPESP LNETQRLLLL QQELLP HSSC

```

The selection scale:

1 2 3 4 5 6 7

Positive selection

Purifying selection

B)

```

1           11           21           31           41
MAWRCPRMGR VPLAWCLALC GWACMAPRGT QAEESPFVGN PGNITGARGL
51          61          71          81          91
TGTLRCQLQV QGEPPEVHWL RDGQILELAD STQTQVPLGE DEQDDWIVVS
101         111        121        131        141
QLRITSLQLS DTGQYQCLVF LGHQTFVSQP GYVGLEGLPY FLEEPEDRTV
151        161        171        181        191
AANTPFNLSC QAQGPEPVD LLWLQDAVPL ATAPGHGPR SLHVPGLNKT
201        211        221        231        241
SSFSCEAHNA KGVITSRTAT ITVLPQQPRN LHLVSRQPTE LEVAWTPGLS
251        261        271        281        291
GIYPLHCL QAVLSDDGMG IQAGEPDPPE EPLTSQASVP PHQLRLGSLH
301        311        321        331        341
PHTPYHIRVA CTSSQGPSSW THWLPVETPE GVPLGPPENI SATRNGSQAF
351        361        371        381        391
VHWQEPRAPL QGLLGYRLA YQGQDEPEVL MDIGLRQEVI LELQGDGSVS
401        411        421        431        441
NLTVCVAAYT AAGDGPWSLP VPLEAWRPGQ AQPVHQLVKE PSTPAFSWPW
451        461        471        481        491
WYVLLGAVVA AACVLILALF LVHRRKKER YGEVFEPTVE RGELVVRYRV
501        511        521        531        541
RKSYSRRTE ATLNSLGISE ELHEKLRDVM VDREKVALGK TLGEGEFGAV
551        561        571        581        591
MEGQLNQDDS ILNVAVKTMK IAICTRSELE DFLSEAVCMK EFDHPNVMRL
601        611        621        631        641
IGVCFQGSER ESFPAPVVIL PFMKHGDLS FLLYSRLGDQ PVYLPTQMLV
651        661        671        681        691
KFMADIASGM EYLSTKRFIH RDLAARNCML NENMSVCVAD FGLSKKIYNG
701        711        721        731        741
DYYRQGRIAK MPVKWIAIES LADRVYISKS DVWSFGVTW EIATRGQTPY
751        761        771        781        791
PGVENSEIYD YLRQGNRLKQ PADCLDGLYA LMSRCWELNP QDRPSFTELR
801        811        821        831        841
EDLENTLKAL PPAQEPDEIL YVNMDEGGY PEPPGAAGGA DPPTQPDPND
851        861        871        881        891
SCSCLTAAEV HPAGRYVLCP STTPSPAQPA DEGSPAAPGQ EDGA

```

1 2 3 4 5 6 7
 Positive selection Purifying selection

C)

```

1      11      21      31      41
MGPAPLEPLL GLFLPALWRR AITEAREEAK PYPLFPGFPP GSLQTDHTPL
51     61     71     81     91
LSLPHASGYQ PALMFSPTQP GRPHTGNVAI PQVSVESKP LPPLFKHTV
101    111    121    131    141
GHI LSEHKG VKNCSISVP NIYQDTTISW WKDGKELLGA HHAI TQFYFD
151    161    171    181    191
DEVTAAHASF SNTSVQRSDN GSYICKKI NEEVSDPIY IEVQGLPHFE
201    211    221    231    241
KQPESMNVTR TAFNLTCQ VGPPEFVN F WVQNSSRVNE QPEKSPSVLT
251    261    271    281    291
VPGLTEMAVF SCENHNDKGL TVSKGVQIN KATPSPPEV SIRNSTAHHI
301    311    321    331    341
LSWYPGFDG YSPFRNCISIQ VKEADPLSNG SYMIENTSAL PHL YQKQLQ
351    361    371    381    391
LLNYIGYS CMEEGWSAV SPWILASTE GAPSVAPLV VFL ESSDN
401    411    421    431    441
VDIRWMKPPT KQQDGELVGY RISHVWQSAG ISKELLEEVG QNGSRARSV
451    461    471    481    491
QVHATCTVE IAAVTRGGV GPFDPVKLFI PAHG WVDYAP SSTPAPGNAD
501    511    521    531    541
PVLIEGCFE GFILIGLILY ISLAIRKRVO ETKFGNAFTE EDSELV VNYI
551    561    571    581    591
AKKSFERRA ELHLHSLGVS EELQNKLEDV VIDRNL L LGK LGEGEFGS
601    611    621    631    641
VREG LKQED GSLKVAVKT AKLDN SSQRE EEF LSEAAC MKDF SHPNVI
651    661    671    681    691
RLLGVCHEMS SQGIPKPMVI LPFKKYGD LH YLLYSRLET GPKH PLQTL
701    711    721    731    741
LKFVDIALG EYLSNNFL HRDLNARC LRDDNTVCV DFGLSKKYS
751    761    771    781    791
GDYRQGRRA KPFVKWIAE SLADRYTSK SDVWAFGVW WEATRGMFP
801    811    821    831    841
YPGQNHMY DYLLHGH LK QPEDCLDELY EYSCWR TD PLDRP FSVL
851    861    871    881    891
LQLEKLES LPDVRNQADV YVNTQLLES SEGLQGSTL APLDLNIDPD
901    911    921    931    941
SILASCTPRA ASVVTAEVH DSKPHEGRYI LNGGSEEWED LTSAPSAAVT
951    961    971    981    991
AEKNSVLPGE RLVRGVSW HSMLPLGSS LPDELLFADD SSEGSEVL

```

The selection scale:

1 2 3 4 5 6 7

Positive selection Purifying selection

TYRO3 in the hominini lineage (humans and chimpanzees), and only modest divergence occurred between the Hominini, Gorillini and Ponginae lineages (Figure 5BC). In marked contrast, *MERTK* has undergone continued divergence in Hominini, with the degree of divergence observed between the *Pan* and *Homo* branches of the Hominini equal to or greater than that observed in *TYRO3* and *AXL* between the Hominini and Gorillini/Ponginae lineages (Figure 5D). The presence of adaptive evolution and whole-gene selection in *MERTK* led us to further investigate the impact of *MERTK* evolution on its function.

3.2 Recent *MERTK* evolution

The higher degree of divergence in *MERTK*, combined with the presence of two regions of intense adaptive (positive) selection, led us to characterize the impact of the recent evolution on *MERTK* function. The first positively-selected region, comprised of amino acids 1 to 21, contains the *MERTK* signal peptide plus an additional residue to include the signal peptide cleavage site (Figure 5A, 6C). The second positively selected region contained the transmembrane domain bordered by 7 extracellular and 5 intracellular membrane-proximal residues. Using *MERTK* sequences from all available primate species (Figure 4C) and a maximum likelihood approach, the hominid-ancestral and primate-ancestral sequences for the signal peptide were reconstructed (Figure 7). While all residues of the signal peptide, as well as some proximal residues, have undergone positive selection within the primate clade, two mutations have become fixed during the differentiation of hominids from primates; the first (G14C) resulting in an arginine-to-proline substitution (R5P), and the second (C69T) resulting in a synonymous threonine mutation in a neutrally evolving region following the signal peptide cleavage site (T23T, Figures 7AB). The G14C mutation resulted in a decrease in the polarity of the hominid signal peptide (Table 2), potentially altering the efficacy of signal peptide recognition or rate of *MERTK* trafficking through the ER/Golgi (Figure 7B). A third mutation became fixed as humans differentiated from the other hominids (A55C), substituting an arginine for a serine (S20R, Figures 7AB), restoring the polarity of the human signal peptide to that observed in the primate ancestral sequence (Table 2). In humans, the signal peptide regions of the *MERTK* mRNA is highly GC-rich (75% GC), which can be indicative of the presence of non-B DNA motifs, structures which can create genetic instability and regulate gene expression through altering supercoiling or binding of regulatory proteins such as transcription factors^{115,116}.

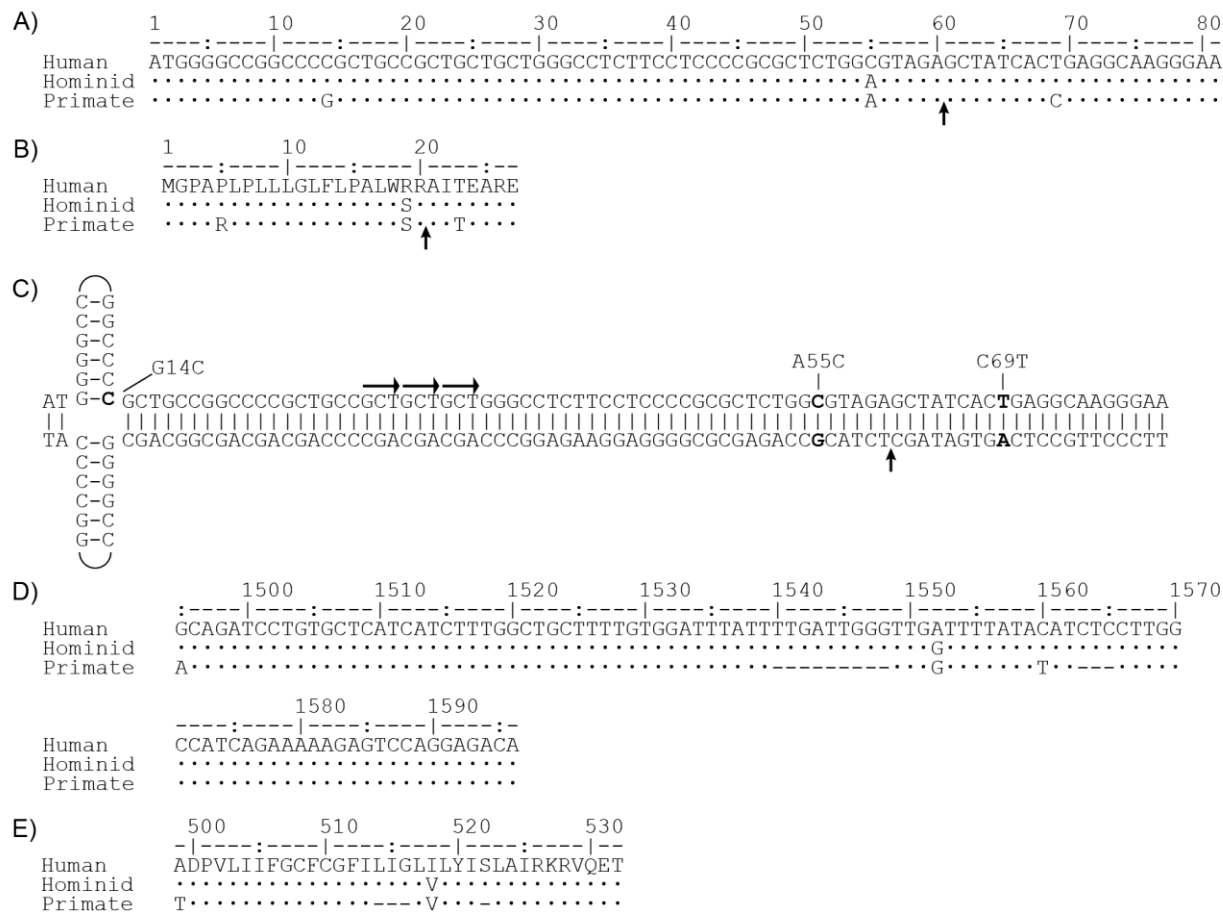


Figure 7: Reconstruction of recent evolution in the *MERTK* signal peptide and transmembrane domain. **A)** Alignments of the human, hominid-ancestral and primate-ancestral signal peptide DNA sequence. The signal peptide cleavage point is indicated by the vertical arrow. **B)** Alignments of the human, hominid-ancestral and primate-ancestral signal peptide protein sequences. The signal peptide cleavage point is indicated by the vertical arrow. **C)** Location of non-B DNA motifs and SNP's in the *MERTK* signal peptide. Tandem GCT repeats are indicated by horizontal arrows, the signal peptide cleavage point is indicated by the vertical arrow. **D)** DNA alignments of the human, hominid-ancestral and primate-ancestral transmembrane domain and membrane-proximal regions. **E)** Amino acid alignments of the human, hominid-ancestral and primate-ancestral transmembrane domain and membrane-proximal regions. Horizontal line indicates the transmembrane domain. Sequences were reconstructed from four hominids (*Homo sapiens*, *Pan troglodytes*, *Gorilla gorilla*, and *Pongo abelii*), four old world monkeys (*Chlorocebus sabaues*, *Macaca mulatta*, *Macaca fascicularis*, and *Papio anubis*), and two new world monkeys (*Saimiri bolviensis*, and *Nomascus leucogenys*) using a maximum-likelihood approach.

Table 2: Biochemical characteristics of the human, hominid-ancestral and primate-ancestral MERTK signal peptide (residues 1-27) and transmembrane domains (residues 499-532).

Clade	Domain	pI*	Hydrophobicity**
Human	Signal Peptide	10.61	0.51
	Transmembrane	8.92	1.38
Hominid	Signal Peptide	7.07	0.64
	Transmembrane	8.92	1.37
Primate	Signal Peptide	10.61	0.54
	Transmembrane	7.72	1.23

*Mono-isotopic isoelectric point

**Hydrophobicity index¹¹⁷

Analysis of the reconstructed *MERTK* signal peptide sequences revealed that the human, hominid and primate signal peptides contain a triplet GCT direct repeat (base pairs 20-29, Figure 7C); sequences which can form slipped hairpin motifs. The G14C mutation that arose as hominids diverged from primates produced a cruciform motif spanning base pairs 3-14, a structure found in both hominids and humans (Figure 7C).

Similar to *MERTK*'s signal peptide evolution, *MERTK*'s transmembrane domain has undergone positive selection leading to amino acid changes. Additionally, small INDELS in the transmembrane domain have occurred throughout the primate tree, with two insertions occurring during the divergence of hominids from primates (Figure 7D). These insertions lengthened the *MERTK* transmembrane domain from a 17 residue domain in the ancestral primate to a 21 residue domain in hominids. In addition, three mutations have become fixed in the human lineage. The first (A1495G) occurred during the divergence of hominids from primates, resulting in a threonine to alanine substitution (T499A, Figure 7DE). The second mutation also occurred during primate/hominid divergence, resulting in a silent mutation to the I521 residue (T1560C, Figure 5DE). The final mutation (G1552A) became fixed during the divergence of humans from hominids and substituted isoleucine for valine (V518I, Figure 7DE). The mutations occurring during the divergence of humans from hominids did not significantly affect the isoelectric point or hydrophobicity of the *MERTK* transmembrane domain (Table 2); however, the insertions which occurred during the divergence of hominids from primates significantly increased the hydrophobicity of the transmembrane domain (Figure 7E). No non-B motifs were found in the transmembrane region of *MERTK*.

3.3 *MERTK* signal peptide evolution has not altered protein expression or trafficking

To determine if the evolution of the *MERTK* signal peptide altered the efficacy of *MERTK* trafficking from the Endoplasmic Reticulum (ER) and Golgi to the cell surface, we synthesized a codon-optimized version of *MERTK* lacking any regulatory motifs, thus minimizing any effects non-B motifs and tRNA availability on our analyses (See Appendix 1 for the DNA sequence). Next, Gibson assembly¹¹⁸ was used to replace amino acids 1-26 of the optimized *MERTK* with the equivalent portion of the human, reconstructed hominid or reconstructed primate *MERTK*. Constructs were transfected into HeLa cells and expression confirmed by immunostain and immunoblot (Figure 8). These constructs enabled us to test the effect signal peptide variation on protein expression and trafficking through the ER/Golgi, independent of any effects incurred by evolution elsewhere in *MERTK*. Using cycloheximide to block further *MERTK* translation, and fluorescence microscopy, *MERTK* trafficking from the ER/Golgi to the cell surface was quantified, with no significant difference in protein trafficking rate among the human, primate and hominid hybrid-ancestral *MERTK* observed, suggesting that recent evolution in *MERTK*'s signal peptide has not affected protein trafficking efficiency (Figure 9).

In addition to altering ER/Golgi trafficking, the evolution of a cruciform motif containing the start codon of the hominid and human signal peptide may alter the expression level of *MERTK*. In addition to the hominid- and primate-ancestral constructs, the codon-optimized *MERTK* was used for analysis where all non-B DNA motifs are removed to specifically evaluate any non-B DNA effects on expression. Protein expression in HeLa cells co-transfected with *MERTK*-constructs

Figure 8: Human HA-MERTK-GFP and modified ancestral signal peptides are ectopically expressed in HeLa cells. HeLa cells were transfected with constructs containing human *MERTK-GFP* or modified human *MERTK* with reconstructed hominid or primate ancestral signal peptides. **A)** Transfected HeLa cells were immunostained using mouse anti-HA and donkey anti-mouse 647 with a Hoechst counterstain. Scale bars represent 10 μm . **B)** *MERTK* expression was further detected through immunoblots using rat anti-HA and donkey anti-rat IR800 antibodies. CbiN was used as a negative control. Data re representative of three independent experiments.

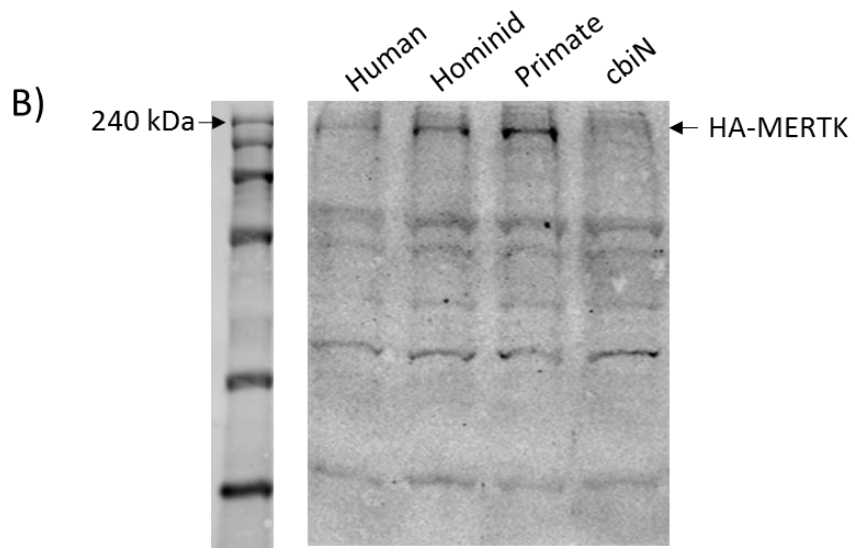
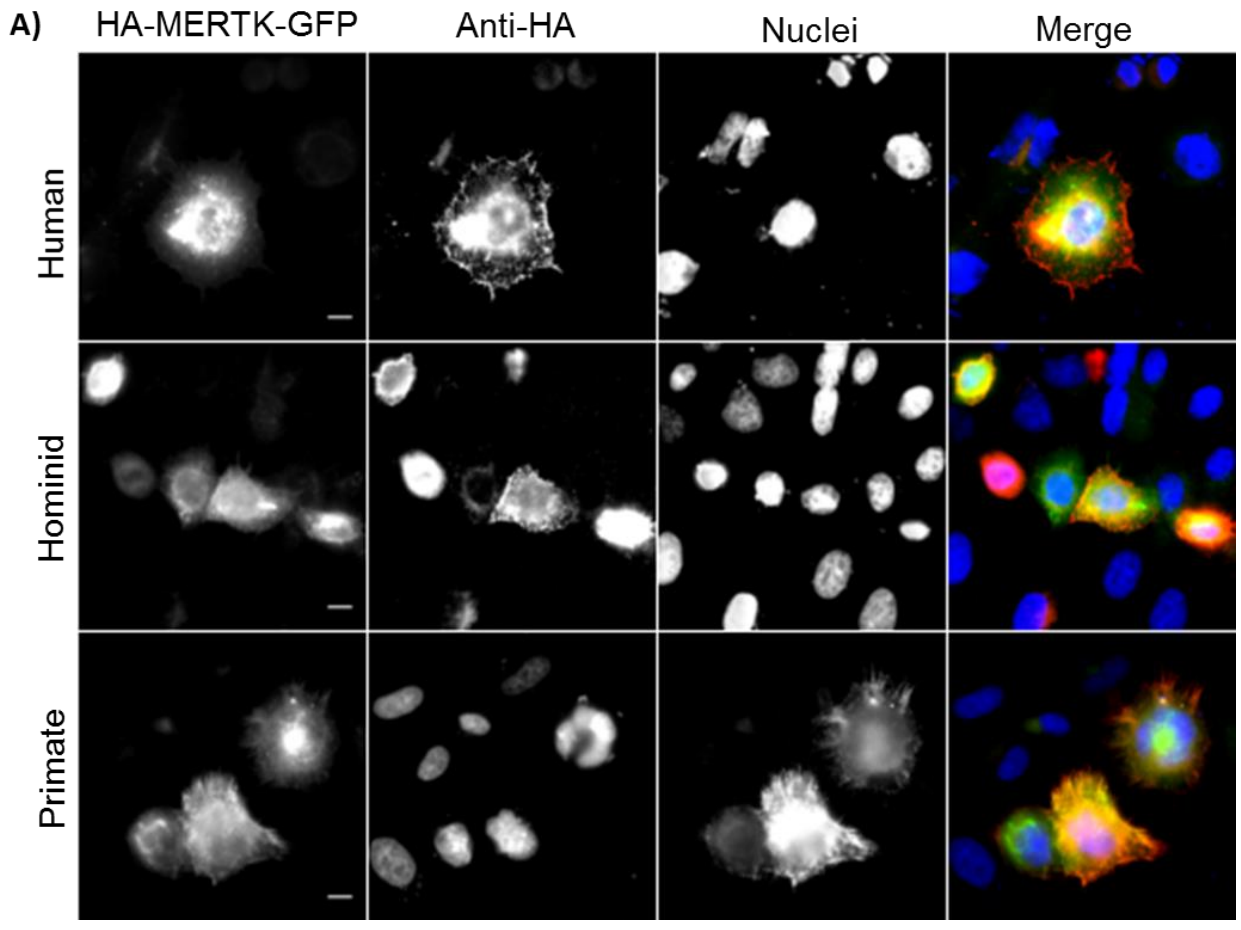
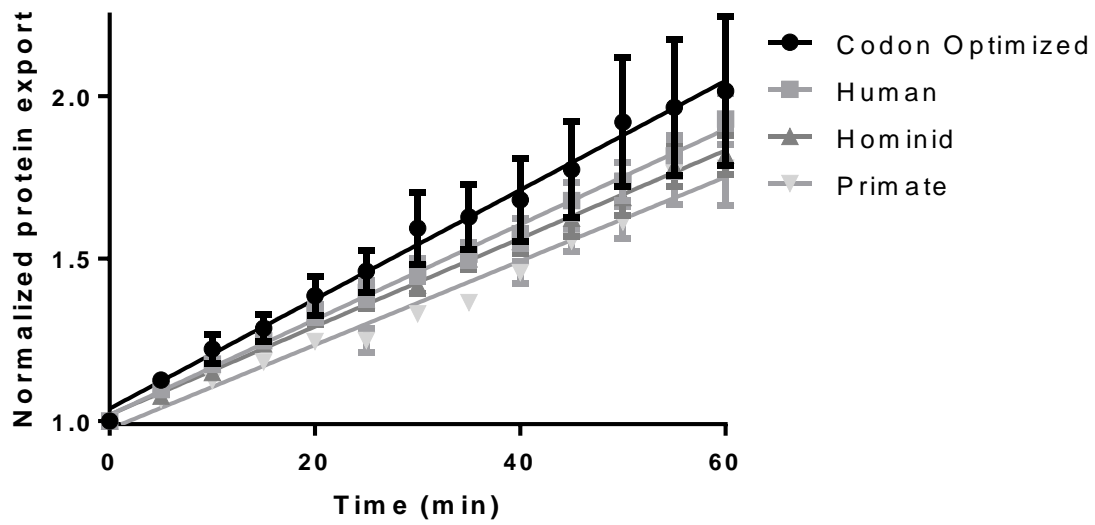
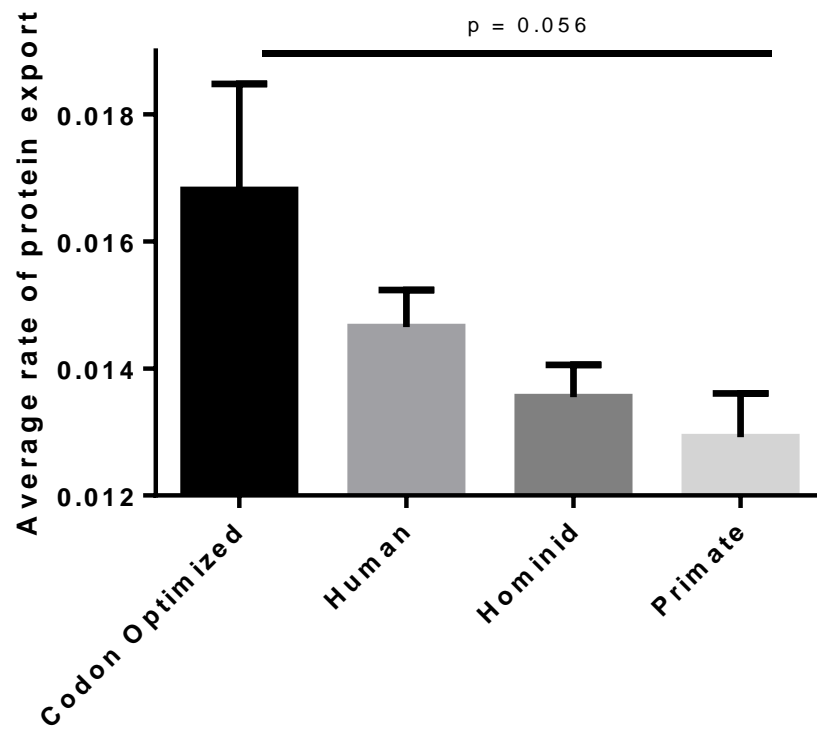


Figure 9: Evolution in *MERTK* signal peptide has no significant impact on protein trafficking. HeLa cells transfected with constructs containing human *HA-MERTK-GFP* modified to remove potential non-B DNA (codon-optimized) or to contain reconstructed hominid or primate ancestral signal peptide domains were surface labelled with anti-HA antibody fluorescently labelled secondary antibody. Cells were treated with cycloheximide to halt protein transport and protein trafficking measured from time-lapse micrographs as the MFI of total *MERTK* expression divided by surface *MERTK* expression, and normalized to $t = 0$. Results are presented as normalized MFI over time (**A**) and as the slope of the protein trafficking plots as quantified by linear regressions (**B**). Data are expressed as \pm SEM, ANOVA with Tukey Correction. Data are representative of four independent experiments.

A)



B)



and mRas-RFP (internal transfection/expression control) was analyzed using widefield microscopy. Hominid-ancestral, but not primate-ancestral, signal peptide MERTK was expressed at significantly higher levels than human MERTK (Figure 10). The difference between human and hominid-ancestral signal peptides is an A55C transversion leading to an alanine to arginine change in the amino acid sequence, which appears to significantly reduce expression. As this expression assay is highly dependent on the plane in which the image is captured and is prone to CCD-camera noise artefacts when quantifying poorly expressing proteins such as *MERTK* from our vectors, we used flow cytometry to validate these results using the same vectors expressed in the same cell type. The flow cytometry analysis showed no significant difference among constructs (Figure 11). Because these two fluorescence-dependent assays did not agree, I analyzed whole cell expression of the *MERTK* constructs using immunoblotting. This would bypass all issues regarding labelling efficiency and detector noise. Moreover, the low level of MERTK expression observed in all constructs, despite the use of a high-expression CMV promoter, suggested that MERTK may be readily turned over; perhaps more quickly than the maturation time of the GFP tag (~30 min), precluding its detection by fluorescent, but not immunological, techniques. In place of mRas-RFP, HA-tagged human CD93 (a transmembrane protein) was used as a transfection/expression control, as both the *MERTK* and *HA-CD93* constructs are expressed off of the same vector (pEGFP-N1) via a CMV promoter, and thus this mixture should provide equal transcription initiation of both constructs. Immunoblot analyses revealed no significant difference in protein expression among the *MERTK* constructs, indicating that the recent evolution in the signal peptide had no impact on MERTK expression and processing in the ER/Golgi (Figure 12). A limitation of these methods is that MERTK expression is driven by the CMV promoter, and as such, any impacts of these promoter-proximal mutations to endogenous MERTK promoter cannot be measured.

Figure 10: Hominid ancestral MERTK signal peptide has augmented expression compared to primate ancestral and human signal peptides. HeLa cells co-transfected with constructs containing human *MERTK-GFP* or modified human *MERTK* with reconstructed hominid or primate ancestral signal peptide domains and *mRas-RFP* as an internal transfection control. Expression of both markers was imaged with epifluorescence microscopy (**A**) and quantified as the MFI of MERTK-GFP normalized to mRas-RFP (**B**). Images are representative of a minimum of 60 cells imaged per condition. Scale bars represent 10 μm . Data are expressed as +/- SEM from three independent experiments, ANOVA with Tukey Correction.

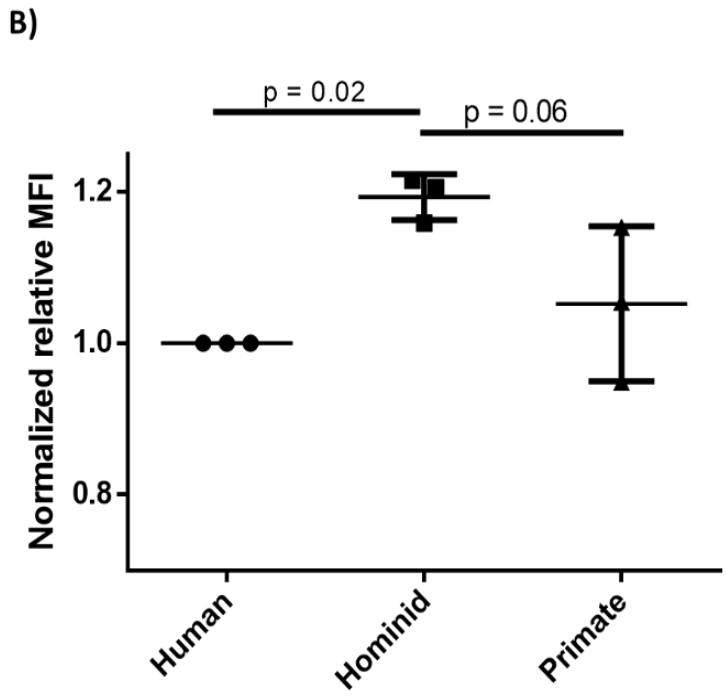
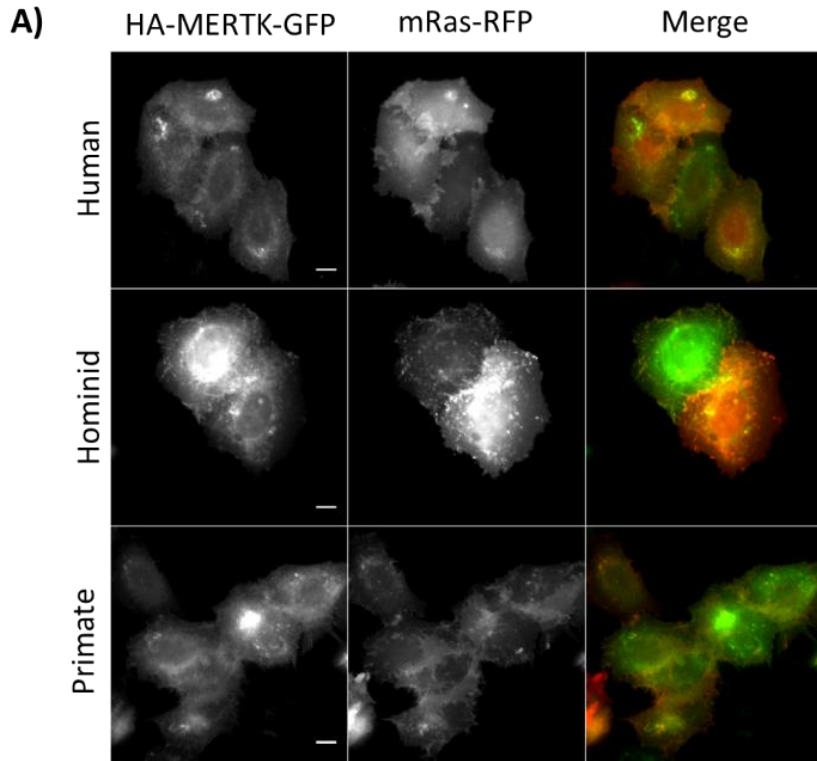
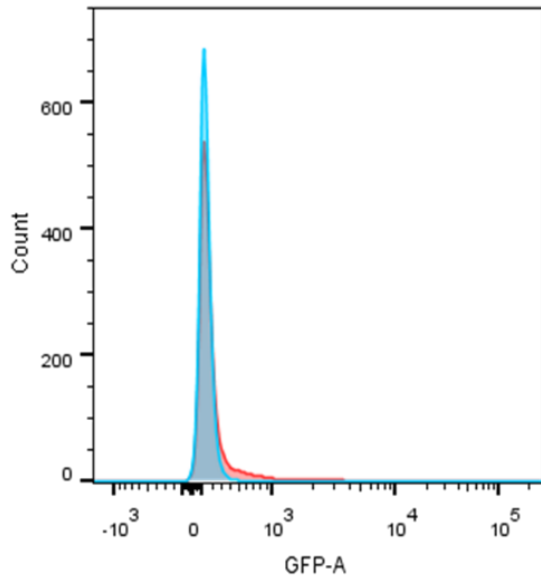


Figure 11: Flow cytometry shows no significant difference in protein expression between human and ancestral MERTK. HeLa cells co-transfected with constructs containing human MERTK-GFP or modified human *MERTK* with reconstructed hominid or primate ancestral signal peptide domains and *mRas-RFP* as an internal transfection control. **A)** Representative GFP histogram of control cells (blue) and MERTK-GFP cells (red). **B)** Expression of both markers was quantified by flow cytometry and normalized to mRas-RFP and normalized to human MERTK. Data are expressed as +/- SEM from three independent experiments with 5,000 cells counted per condition, ANOVA with Tukey Correction.

A)



	Sample Name	Count
■	Compensation Controls_Unstained Control.fcs	5000
■	Compensation Controls_GFP Stained Control.fcs	5000

B)

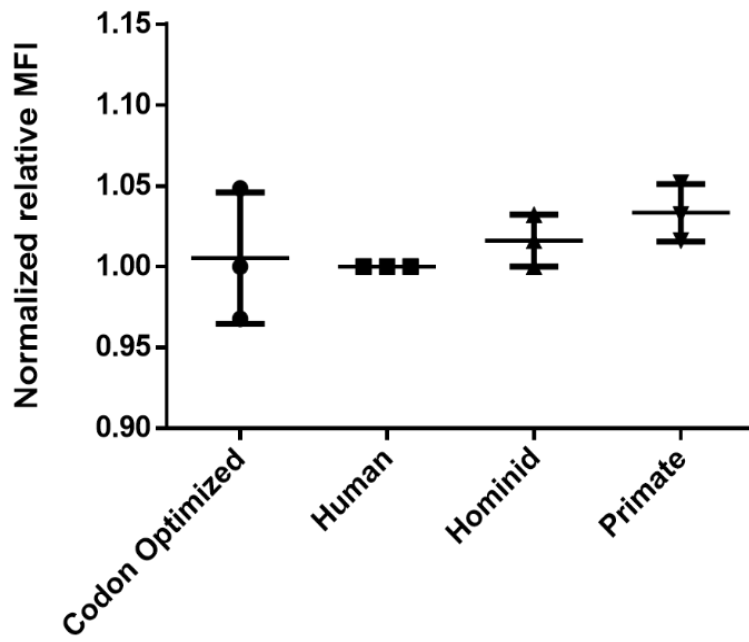
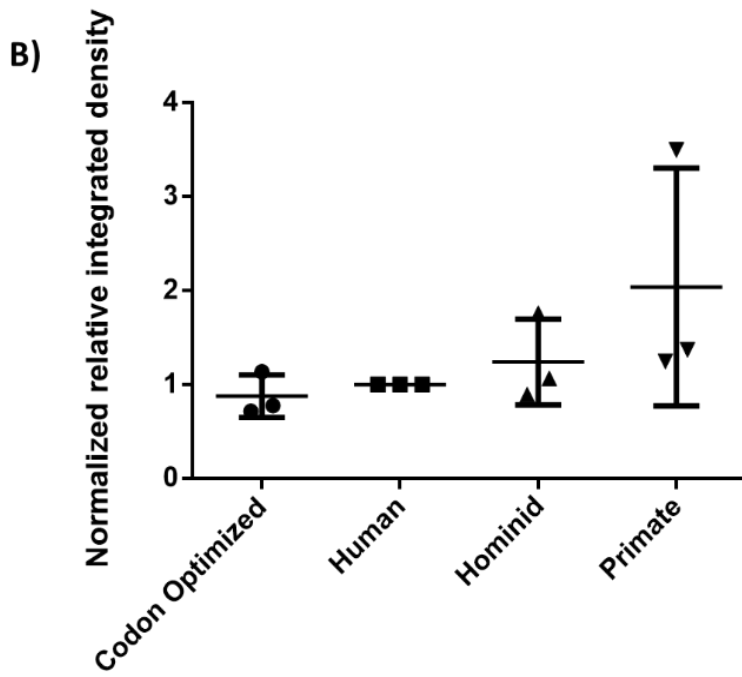
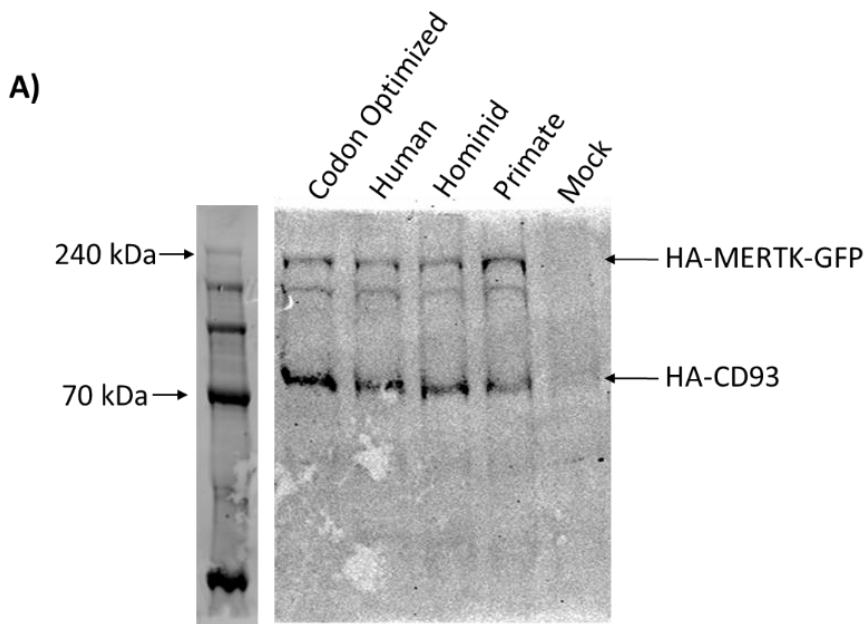


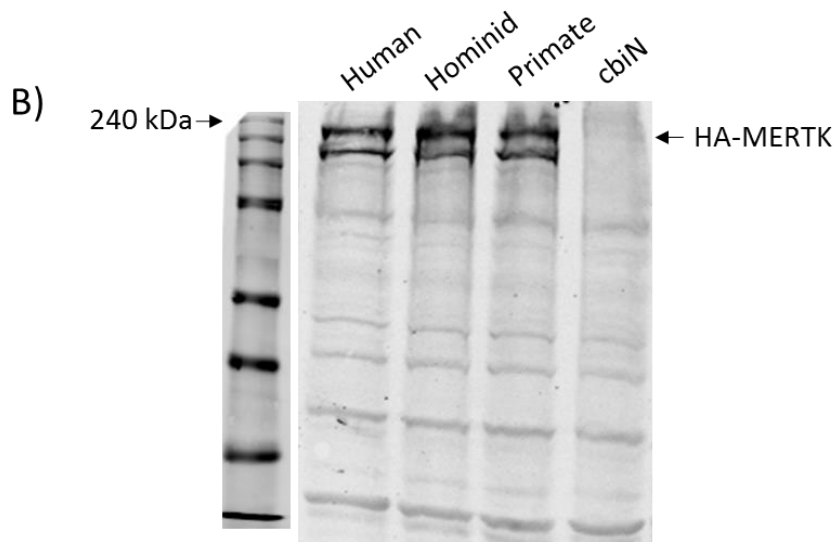
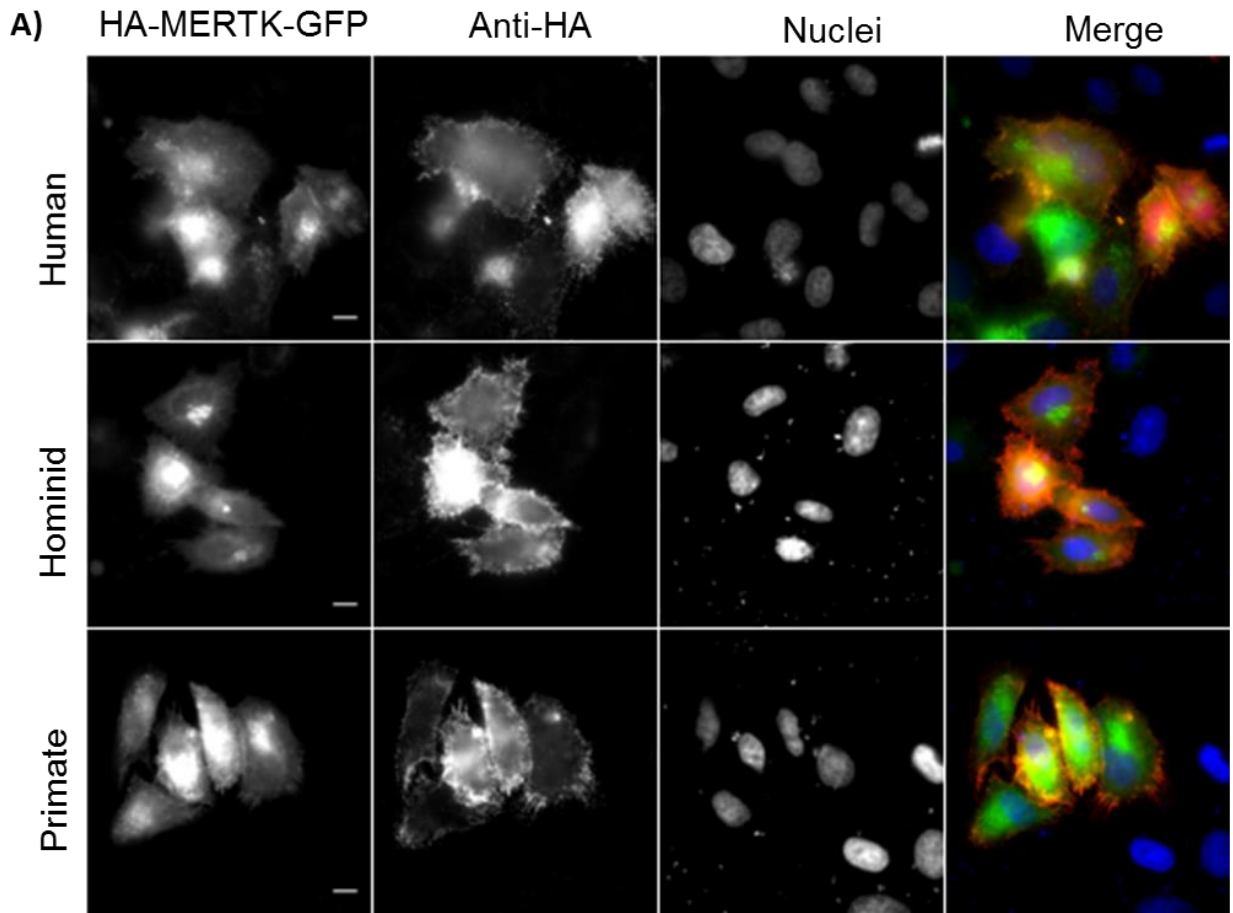
Figure 12: Immunoblots show no significant difference in whole protein expression between human and ancestral MERTK. HeLa cells co-transfected with constructs containing human *MERTK-GFP* or modified human *MERTK* with reconstructed hominid or primate ancestral signal peptide domains and *HA-CD93* as an internal transfection control. **(A)** Representative immunoblot from three independent experiments. Data are presented as integrated fluorescent intensities of the 240 kDa *MERTK-GFP* band normalized to *HA-CD93* **(B)**. Data are expressed as +/- SEM, ANOVA with Tukey Correction.



3.4 *MERTK* transmembrane evolution has increased self-clustering

While no apparent phenotype was observed for the signal peptide, the addition of leucines to the transmembrane domain during the divergence of hominids from primates (Figure 7E) may indicate the development of protein-protein interaction motifs which can act to enhance protein dimerization¹¹⁹, and therefore we assessed the possibility that *MERTK* evolution may have altered *MERTK* self-clustering or interactions with other transmembrane proteins. To determine the impact of evolution on the *MERTK* transmembrane domain, the transmembrane region of the codon-optimized *MERTK* described above was replaced with the equivalent portion of the human, reconstructed hominid or reconstructed primate *MERTK* transmembrane domain. The resulting GFP fusion proteins were expressed in HeLa cells, with expression and trafficking to the cell surface verified by immunoblotting and immunostaining respectively (Figure 13). Next, cells were imaged using super-resolution GSDM microscopy at a resolution of 20 nm, and self-clustering assessed by radial distribution function analysis (Figure 14). Primate, hominid and human *MERTK* all formed micro-clusters on the plasmalammella; however, the proportion of *MERTK* undergoing clustering and cluster size was dramatically increased in humans and hominids compared to primates. Indeed, primate *MERTK* clusters averaged <40 nm in diameter, whereas human and hominid *MERTK* formed clusters averaging 100 nm in diameter, with humans trending towards a larger portion of clustered *MERTK* than hominids (Figure 14BC). The size of the primate clusters is consistent with homodimers, while the larger hominid and human clusters indicate multimeric complexes. Furthermore, *in silico* analysis of human and reconstructed hominid- and primate-ancestral transmembrane domains, conducted by our collaborators Dr. Jimmy Dikeakos and Brennan Dirk, revealed that while all three transmembranes are predicted to be helical, the human and hominid transmembrane domains became slightly elongated as they diverged from the shared

Figure 13: Human HA-MERTK-GFP and modified with ancestral transmembrane domains are ectopically expressed in HeLa cells. HeLa cells were transfected with constructs containing human *HA-MERTK-GFP* or modified human *HA-MERTK-GFP* bearing reconstructed hominid or primate ancestral transmembrane. **A)** Confirmation of MERTK surface expression in transfected HeLa cells. Total MERTK was detected by the MERTK-intrinsic GFP, while cell-surface MERTK was immunostained using an anti-HA antibody. Scale bars represent 10 μm . **B)** Immunoblots confirming MERTK expression, with approximately equal express of all three constructs observed. CbiN was used as a negative control. Data are representative of three independent experiments.



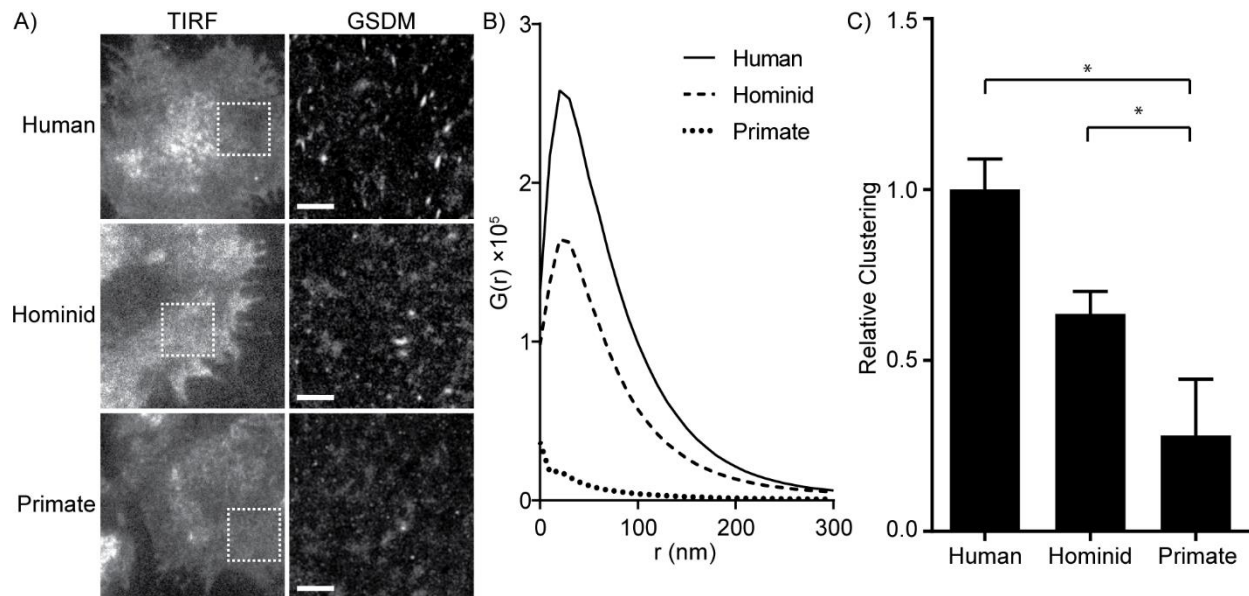


Figure 14: Evolution in MERTK intermolecular interactions driven by transmembrane domain evolution. HeLa cells transfected with constructs containing human MERTK-GFP modified to contain the hominid or primate ancestral transmembrane domain were quantified for self-clustering. **A)** TIRF and super-resolution GSDM images of MERTK transmembrane domain constructs in the basolateral membrane. Boxes in the TIRF image indicate the $5\mu\text{m} \times 5\mu\text{m}$ region shown in the GSDM image, scale bars are $1\mu\text{m}$. **B)** Quantification of MERTK clustering by the radial distribution function ($G(r)$). **C)** Clustering of MERTK transmembrane domain constructs, expressed as the area under the $G(r)$ curve, normalized to the degree of clustering observed in the human construct. A is representative of, and B-C quantify data from three independent experiments, four replicates per experiment. Data are expressed as mean (B) or mean \pm SEM (C), * = $p < 0.05$, ANOVA with Tukey Correction.

primate ancestor, and moreover, the leucines and isoleucines added to the transmembrane domain during this divergence are positioned largely on one facet of the transmembrane domain, potentially creating a new protein interaction site (Appendix 5 and 6). Taken together, these results suggest that recent *MERTK* transmembrane evolution has increased MERTK clustering, via the evolution of a new hydrophobic interaction facet within the MERTK transmembrane helix. The role of this increased clustering remains to be elucidated, but may be indicative of new protein-protein interactions, or of increased avidity-enhancing MERTK self-clustering.

3.6 Development of a model to study MERTK-dependent efferocytosis

To evaluate the impact of MERTK clustering and the necessity of integrins as co-receptors in MERTK-mediated efferocytosis, we required a robust and reproducible efferocytosis assay which would allow quantification of MERTK-specific efferocytosis. To avoid confounding factors such as other efferocytic receptors, non-macrophage cell lines and ligand-specific opsonins or ligands were used. To this effect, a mammalian expression vector containing GFP-tagged mouse *MerTK* was created and ectopically expressed in COS-7 cells (Figure 15). MERTK-specific antibody coated polystyrene beads were fed to *MerTK*-transfected COS-7 cells to induce efferocytosis. We found that *MerTK*-transfected, but not CbiN-GFP transfected control cells, internalized polystyrene beads coated with MerTK-activating antibodies (Figure 16). However, this uptake was nonspecific, as beads coated with isotype control antibodies were also internalized by *MerTK* transfected cells (Figure 16). This non-specific uptake of isotype control beads suggested that the antibody preparation may be contaminated by MERTK opsonins. As such, we tested antibodies for purity using a commassie stain but found no evidence of opsonin contaminants that may explain activation of MERTK (Figure 17). Upon further testing we found that while MERTK internalizes both Fab and full length antibodies (Figure 18), internalization was not detected with protein A beads coated with anti-MERTK or isotype control antibodies (Figure 19). It is unclear whether this was due to non-specific interactions, or if MERTK binds antibodies via a region in the Fab portion that is masked by protein A binding. As we could not determine what was inducing MERTK internalization with antibody-coated beads, an alternate approach using beads coated in purified MERTK-opsonins was assessed.

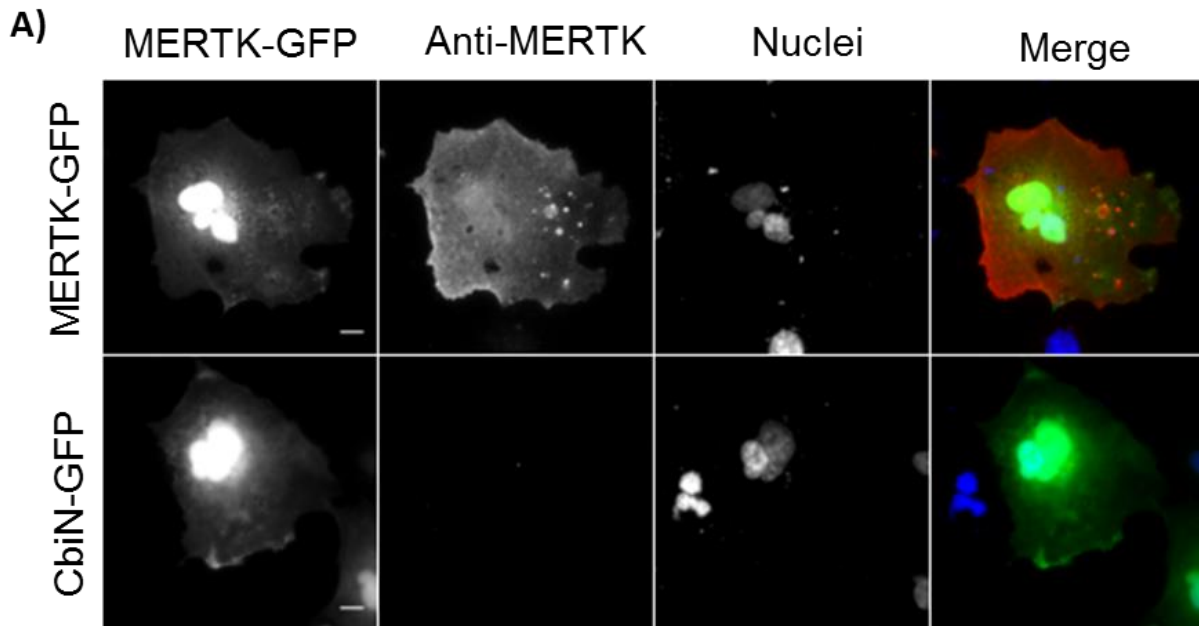
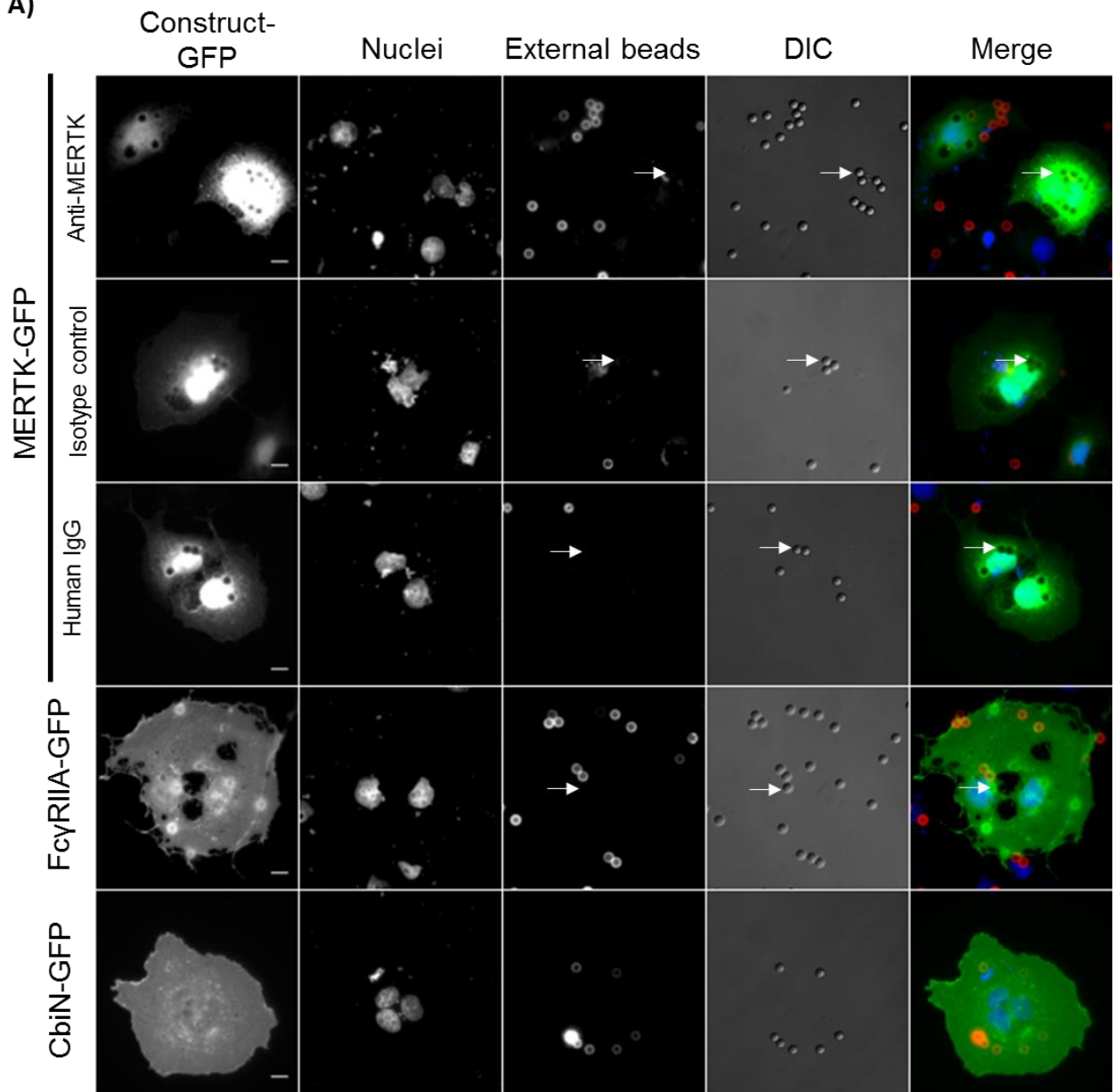


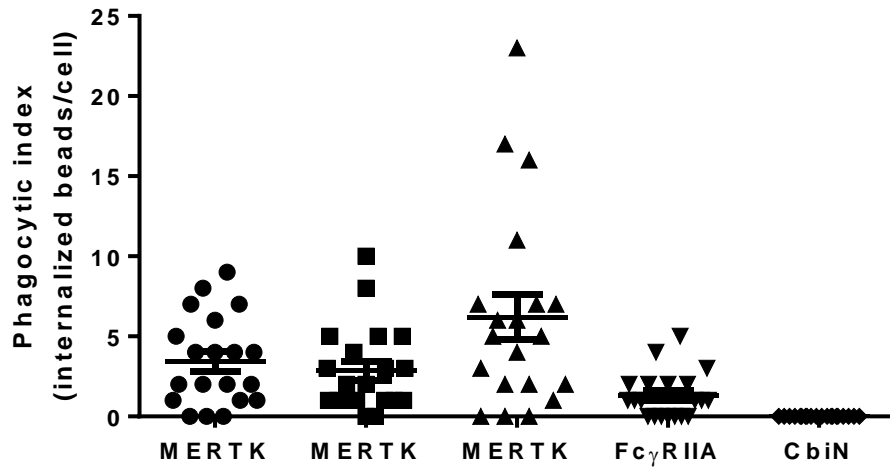
Figure 15: Mouse MERTK is heterologously expressed in COS-7 cells. COS-7 cells were transfected with a pEGFP-N1 vector containing *MerTK* and immunostained for surface expression using a goat anti-MERTK antibody (top row) or a goat isotype control antibody (bottom row) and subsequently fluorescently labelled using Cy3 anti-goat secondary antibody. Cells were counterstained with Hoechst 33342 to label nuclei. Arrow demarcates receptor accumulation at the membrane. Images are representative of three independent experiments. Scale bars represent 10 μm .

Figure 16: COS-7 *MerTK*-transfectants uptake antibody-coated beads. COS-7 cells were transfected with vectors containing *MerTK-GFP*, *FcyRIIA-GFP* or *CbiN-GFP* and fed polystyrene beads coated in 2 μ g of goat anti-MERTK, goat isotype control or human isotype control antibodies. **A)** Representative image of anti-MERTK coated bead internalization by *MerTK*-transfectants, arrows denote an internalized bead and scale bars represent 10 μ m **B)** Average number of internalized beads per cell from *MerTK*, *FcyRIIA* or *CbiN* transfected cells exposed to antibody coated beads (n=20). Data are presented as mean \pm SEM from one independent experiment.

A)



B)



Anti-MERTK	+	-	-	-	+
Isotype control	-	+	-	-	-
Human IgG	-	-	+	+	-

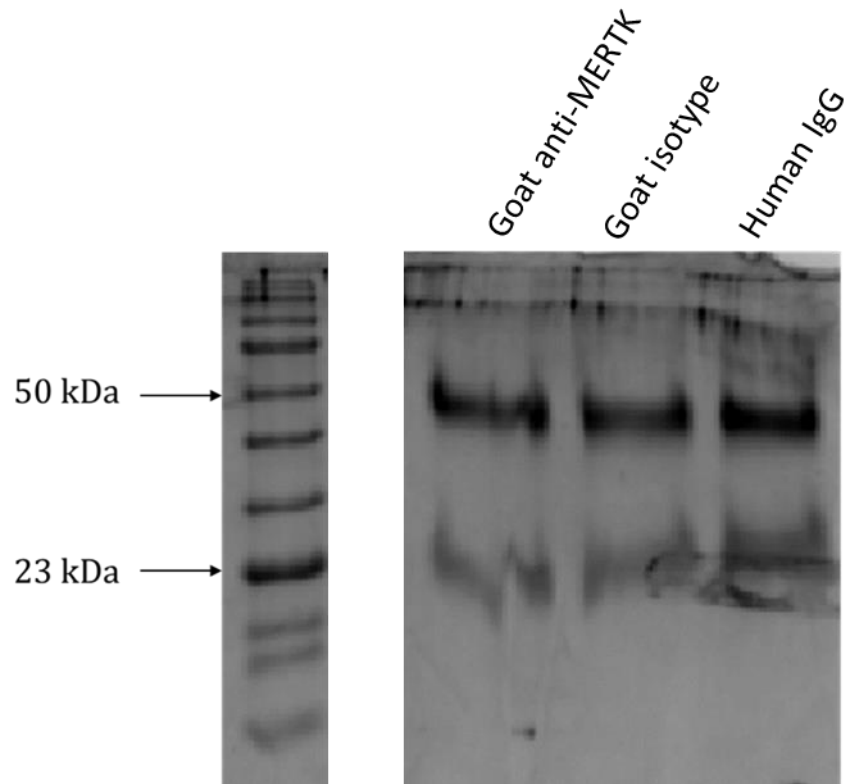


Figure 17: Coomassie blue stain of antibodies reveal no opsonin contamination. Purified goat anti-MERTK, goat isotype control and human IgG antibodies were run through an acrylamide gel under reducing conditions and stained using coomassie blue protein stain. Only bands corresponding to antibody heavy chain (50 kDa) and antibody light chain (23 kDa) were observed.

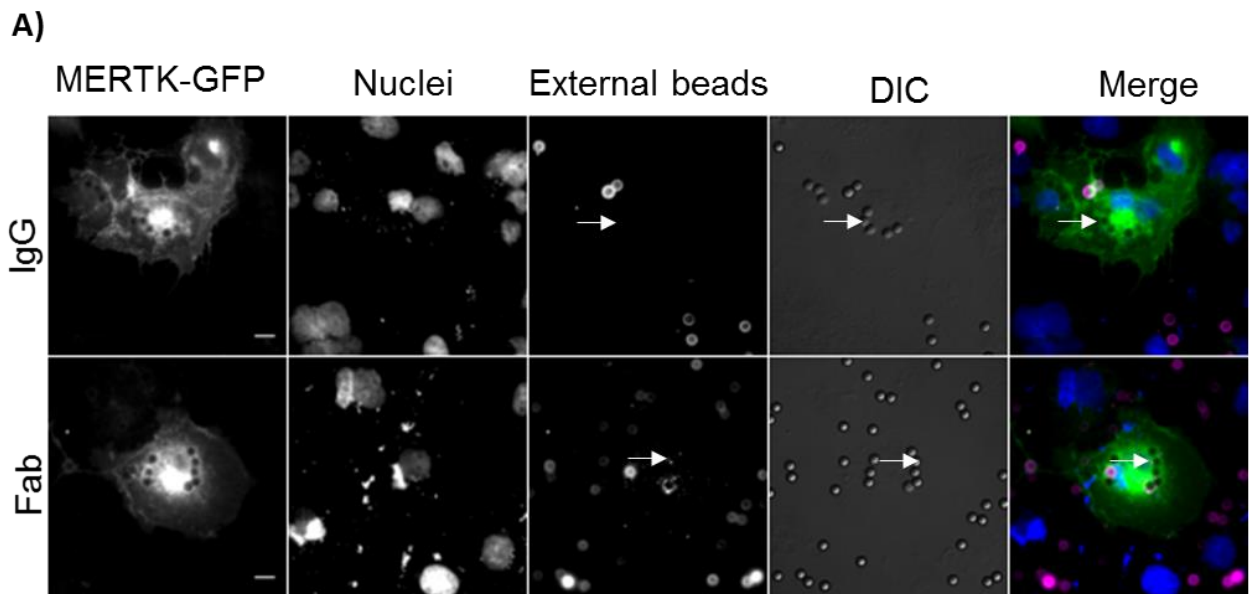


Figure 18: COS-7 *MerTK*-transfectants uptake Fab and full length IgG. COS-7 cells were transfected with vectors containing *MerTK-GFP* and fed polystyrene beads coated in full length goat IgG or fluorescent-tagged goat Fab fragments. External whole goat IgG was labelled using fluorescently-labelled secondary antibodies. Representative images are of goat IgG or goat Fab fragment coated bead internalization by *MerTK*-transfectants. Images are representative of one independent experiment. Scale bars represent 10 μ m and arrows note representative internalized beads.

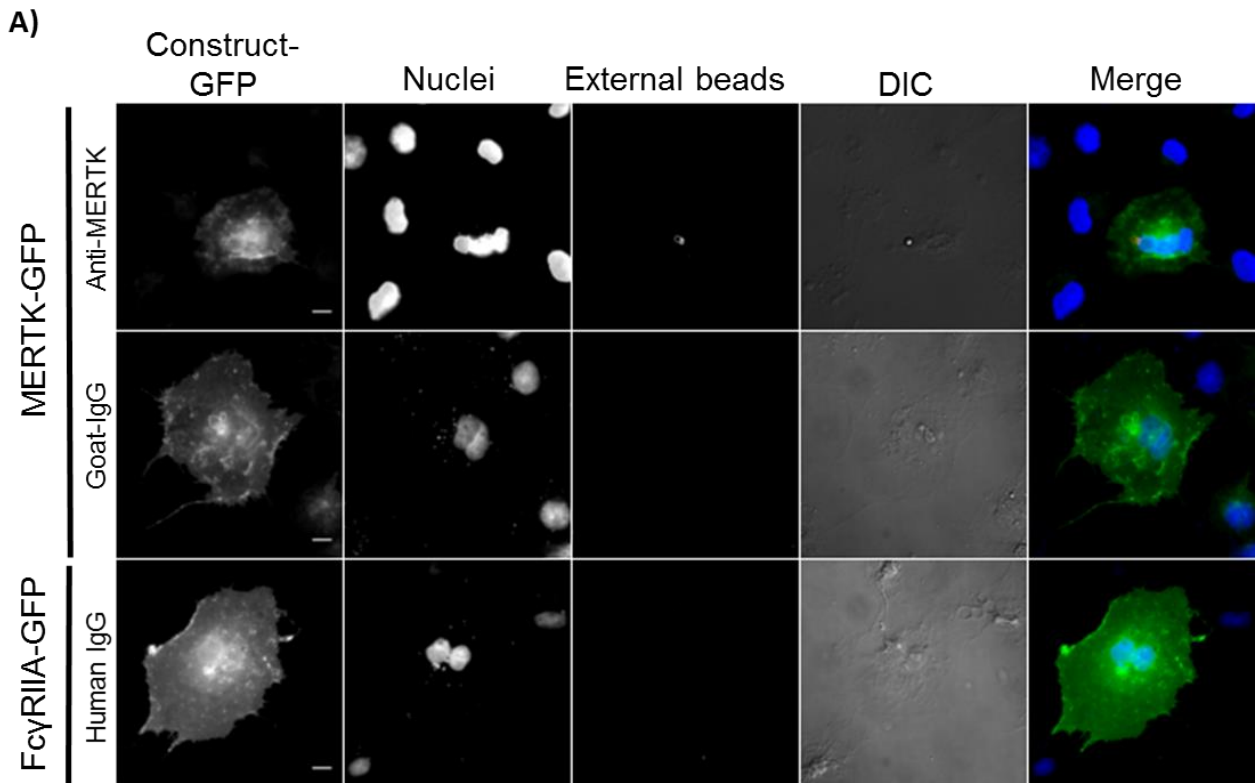


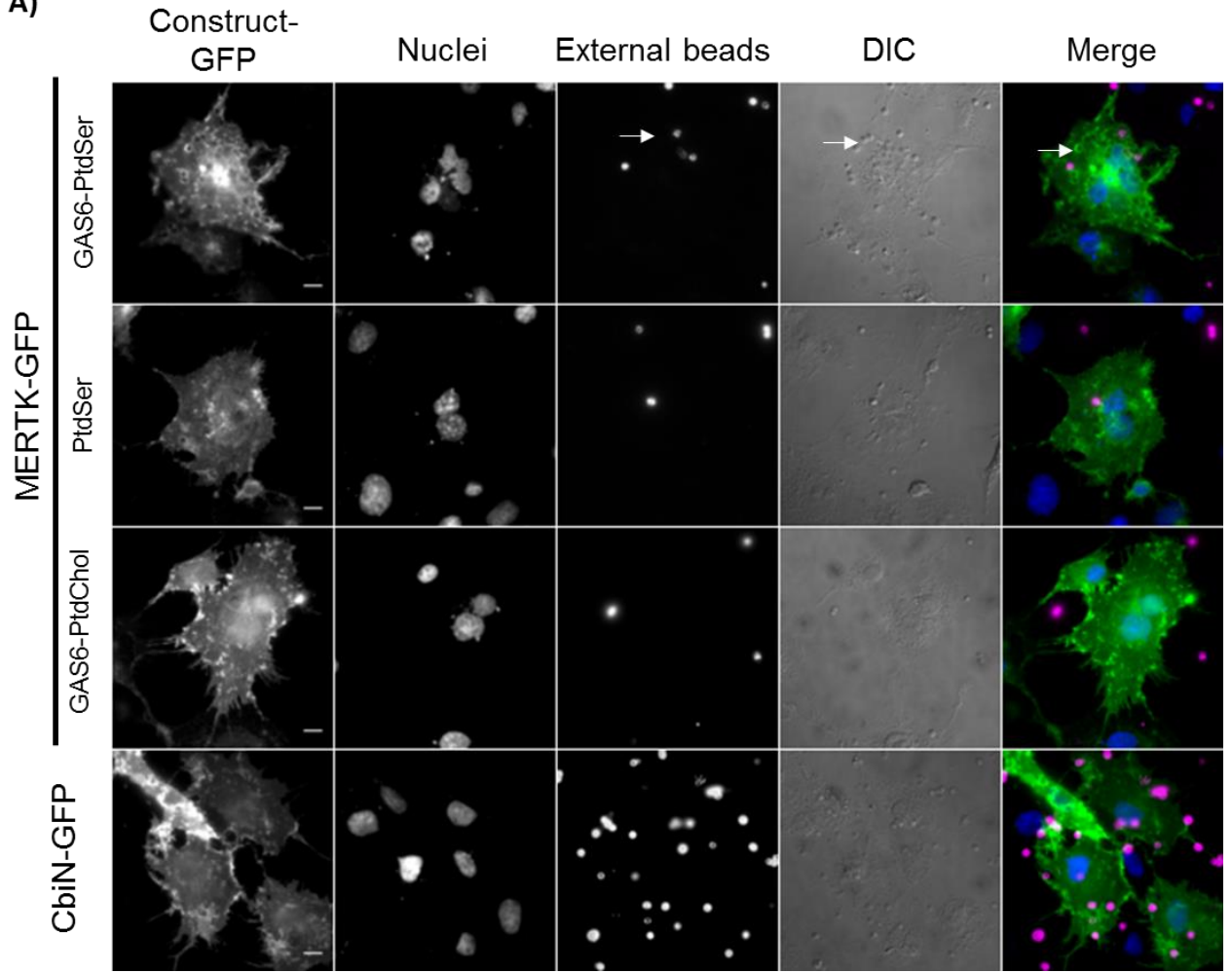
Figure 19: COS-7 *MerTK*-transfectants do not uptake IgG-coated protein A beads. COS-7 cells were transfected with vectors containing *MerTK-GFP* or *FcγIIA-GFP* and fed polystyrene beads coated in goat anti-MERTK, goat isotype control or human IgG. Representative images are of *MerTK-GFP* transfectants fed goat anti-MERTK or goat isotype control coated protein A beads and *FcγRIIA-GFP* fed human IgG coated protein A beads. External beads were labelled with appropriate secondary antibodies. Images are representative of one independent experiment. Scale bars represent 10 μ m.

In our second model, efferocytic targets comprised of 3 μm diameter glass beads coated in a mixture that mimics the plasma membrane of ACs (19.8% PtdSer, 80% PtdChol, and 0.2% biotin-PE) were generated, opsonized with GAS6, and their uptake by mouse *MerTK*-transfected COS-7 cells was quantified. Non-internalized beads were stained with streptavidin, which binds the exposed biotin-PE on non-internalized beads, and the cells were imaged. We found that *MerTK-GFP*-transfected COS-7 cells readily internalized PtdSer-beads opsonized with recombinant murine GAS6 (Figure 20). However, non-opsonized PtdSer-beads and GAS6 opsonized phosphatidylcholine beads (PC-beads) were rarely internalized by *MerTK-GFP* transfectants, demonstrating that this system is specific to MERTK and that both GAS6 and PtdSer are required for MERTK-dependent efferocytosis (Figure 20AB). We confirmed that this system is MerTK-specific by repeating these experiments using COS-7 cells expressing a different membrane protein (*CbiN*), which displayed background levels of internalization when fed GAS6 opsonized PtdSer-beads (Figure 20AB). The efferocytic index of all conditions were calculated and demonstrated a marked increase in efferocytosis for *MerTK-GFP* transfectants fed GAS6 opsonized PtdSer-beads (Figure 20B).

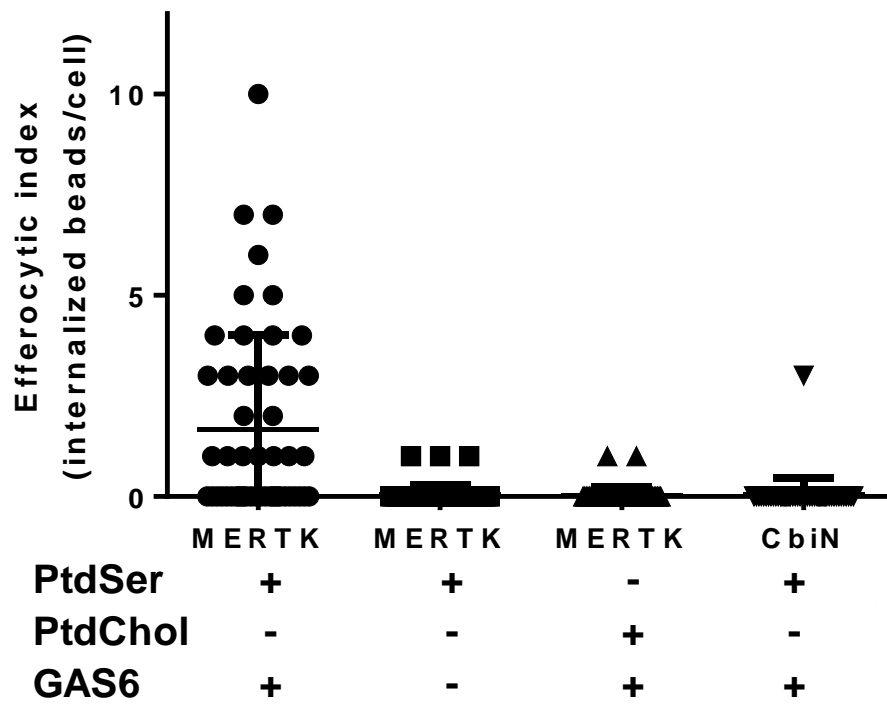
Shortly after developing the above method we discovered the high degree of divergence among *MERTK* primates (Figure 4C, 5D), and therefore decided that it would be critical for future experiments to recapitulate this model system using human MERTK in a human cell line (HEK293T cells). HEK293T cells were transfected with a codon-optimized *MERTK* in pcDNA3.1(+) and expression confirmed by immunostaining (Figure 21). For these assays, HEK293T cells were co-transfected with *CbiN-GFP* for visualization and fed PtdSer-beads coated in GAS6 with or without MFG-E8. Although MERTK more readily internalized beads coated in

Figure 20: COS-7 *MerTK*-transfectants uptake GAS6 opsonized PtdSer-silica beads. COS-7 cells were transfected with plasmids containing either *MerTK-GFP* or *CbiN-GFP* (negative control) and fed silica beads coated in either a mix of PtdSer, PtdChol and biotin-PE or PtdChol and biotin-PE. Following coating with lipids, beads were either opsonized in recombinant murine GAS6 or left non-opsonized. External beads were labelled with streptavidin-647 to differentiate them from internalized beads and nuclei stained with Hoechst. **A)** Images are representative of a minimum of 50 cells per condition. *MerTK-GFP* transfectants fed GAS6 opsonized PtdSer-beads readily internalized beads. White arrow demarcates exemplary internalized bead. As negative controls, *MerTK-GFP* transfected cells were fed non-opsonized PtdSer-beads or PtdChol-coated beads opsonized in GAS6. *CbiN-GFP* transfected cells were fed GAS6 opsonized PtdSer-beads as a negative control for MERTK. The average number of internalized beads per cell was determined for each condition **(B)**. Error bars represent \pm SEM from one independent experiment. Scale bars represent 10 μ m.

A)



B)



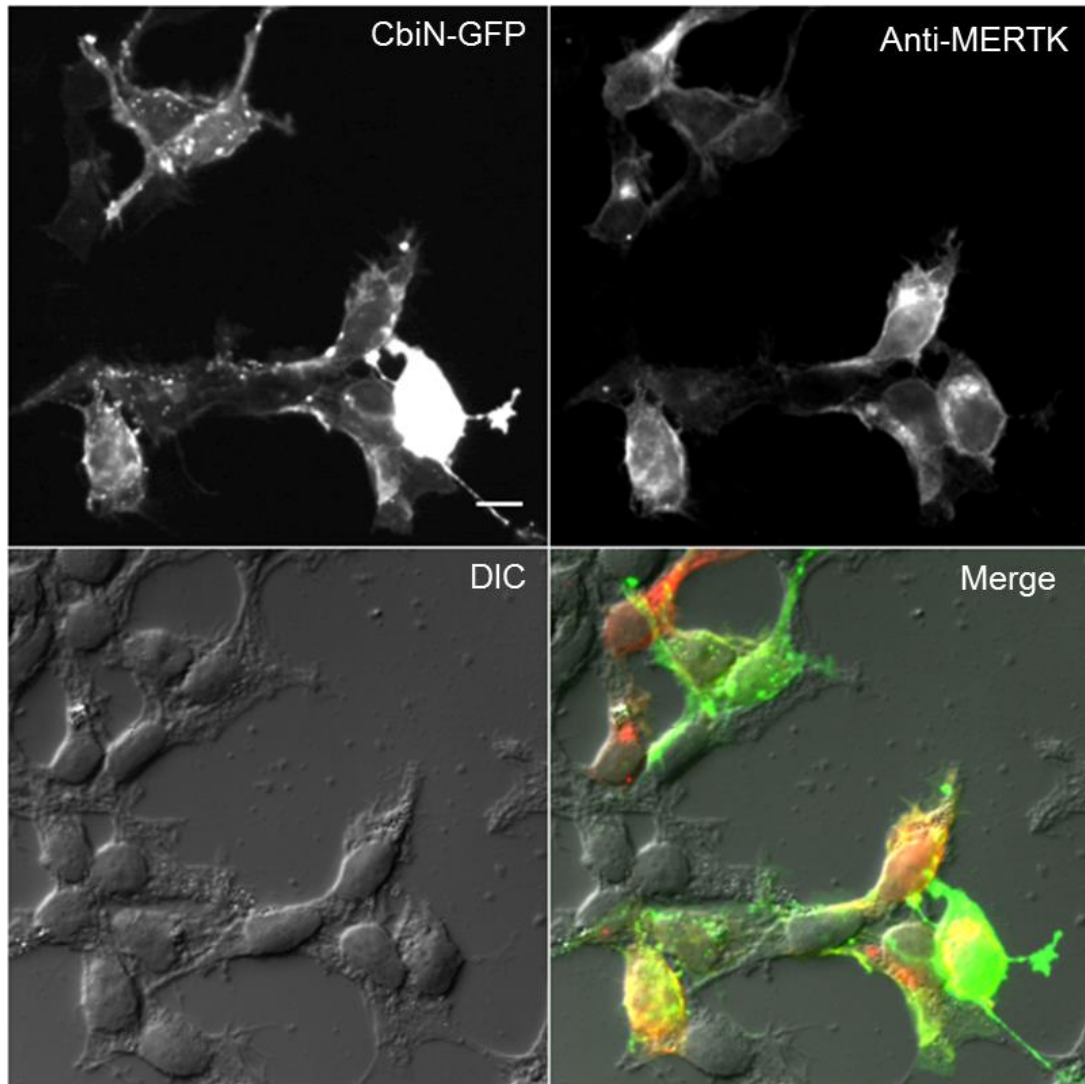
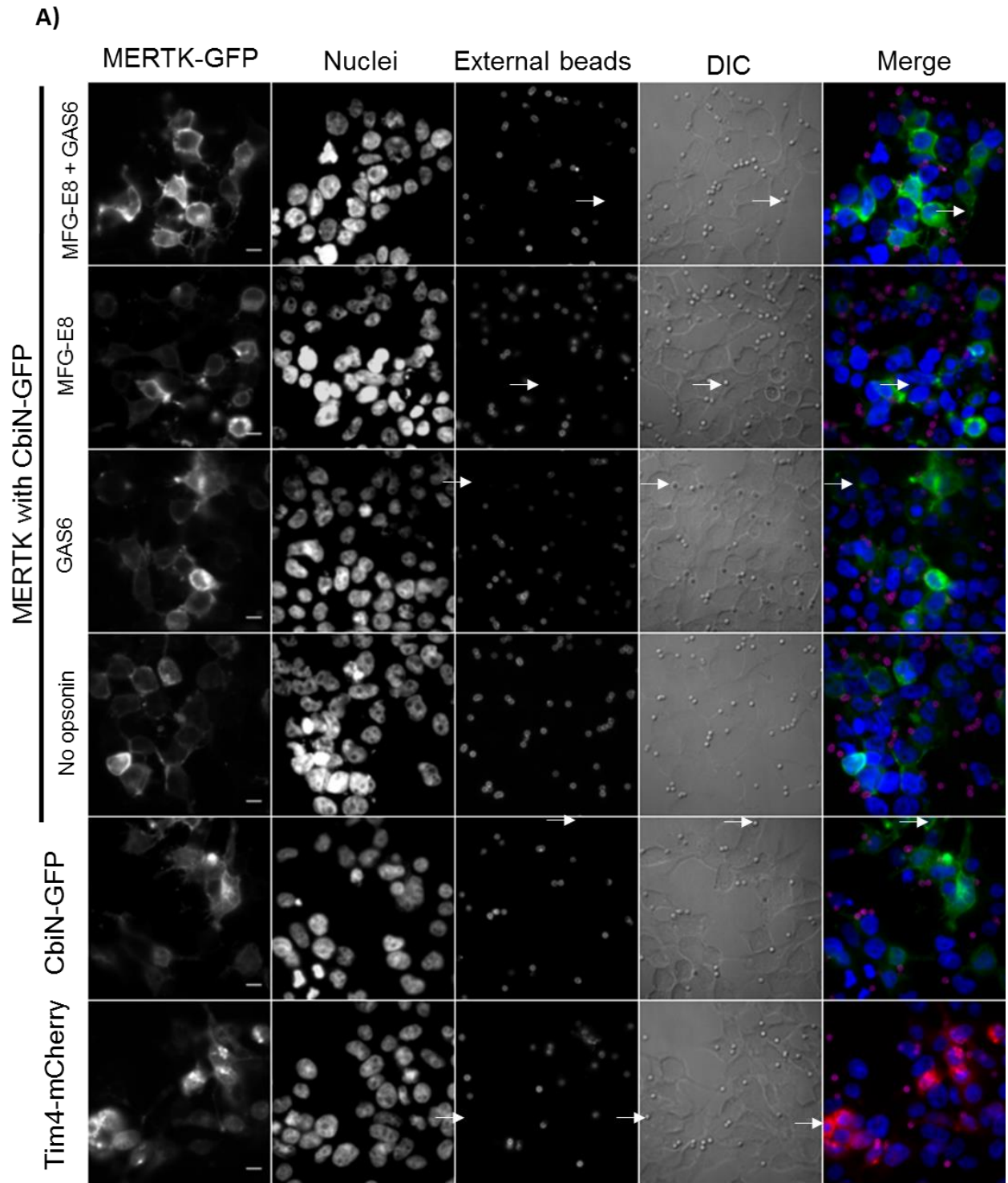


Figure 21: Human MERTK is heterologously expressed in HEK293T cells. HEK 293T cells were co-transfected with pCDNA3.1-*MERTK* and *CbiN-GFP* into and detected through immunostaining using an internally targeted anti-MERTK antibody and fluorescent secondary antibody. Images are representative of three independent experiments. Scale bar represents 10 μm .

GAS6 alone, the efferocytic index was unexpectedly low (Figure 22). Moreover, poor internalization was observed with our positive control (TIM-4), which normally would induce the uptake of 5-10 fold more beads than observed in these experiments, suggesting that there is an issue with our lot of HEK293T cells or the efferocytic targets (Figure 22)⁸⁰. Due to time constraints it was not possible to recapitulate this experiment with new HEK293T cells or efferocytic targets prior to thesis submission.

Although transfected cell lines provide an ideal system to study MERTK-dependent efferocytosis in isolation, it is important to verify key results in a more biologically relevant system such as primary human macrophages. To this end, we conducted a preliminary analysis by evaluating the efferocytic capacity of M0, M1, M2 and M2c polarized human PBMC-derived macrophages using human serum-coated PtdSer-beads. We found that M0 and M2c primary human macrophages displayed the highest level of efferocytosis capacity, which are both shown to highly express MERTK¹⁴ (Figure 23). While not tested in this thesis, siRNA, small molecule inhibitors, or blocking antibodies to MERTK and other TAM receptors could be used to assess their role in efferocytosis in the endogenous environment of primary human macrophages.

Figure 22: MERTK transfected HEK293T cells do not internalize opsonin-coated PtdSer-beads. HEK293T cells were transfected with plasmids containing either *MERTK* with *CbiN-GFP*, *CbiN-GFP* alone (negative control), or *Tim4-mCherry* (positive control) and fed silica beads coated in either a mix of PtdSer, PtdChol and biotin-PE or PtdChol and biotin-PE. Following coating with lipids, beads were either opsonized in recombinant GAS6 with or without MFG-E8. External beads were labelled with streptavidin-647 to differentiate them from internalized beads and nuclei stained with Hoechst. **A)** Representative images are displayed for each condition with arrows demonstrating representative internalized beads. Scale bars represent 10 μm . **B)** average efferocytic indexes calculated from two independent experiments with a minimum of 100 cells counted per condition. Error bars represent \pm SEM.



B)

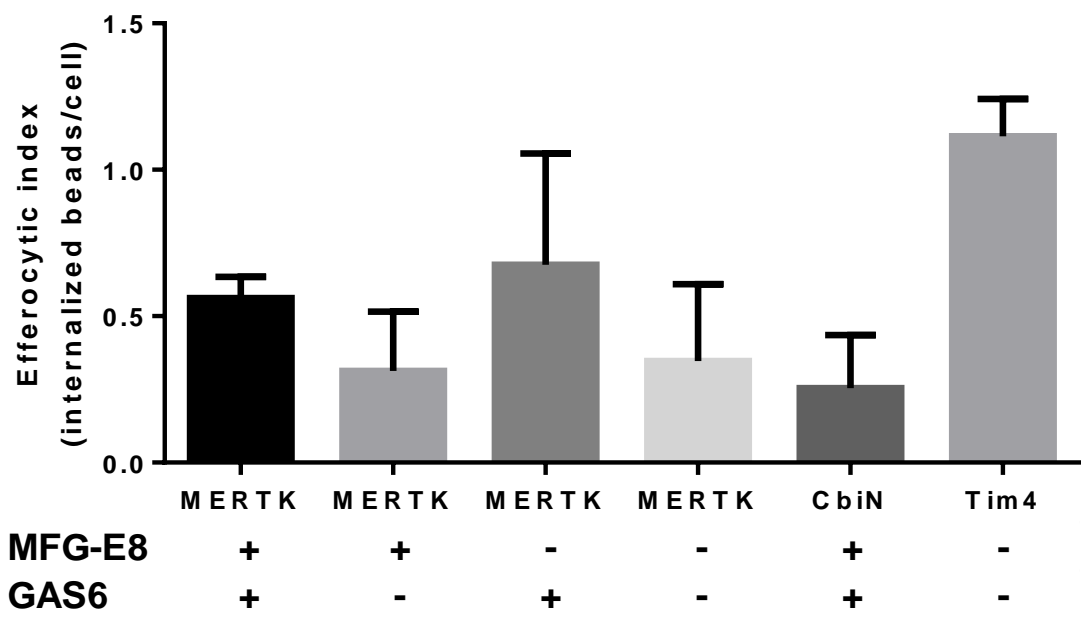
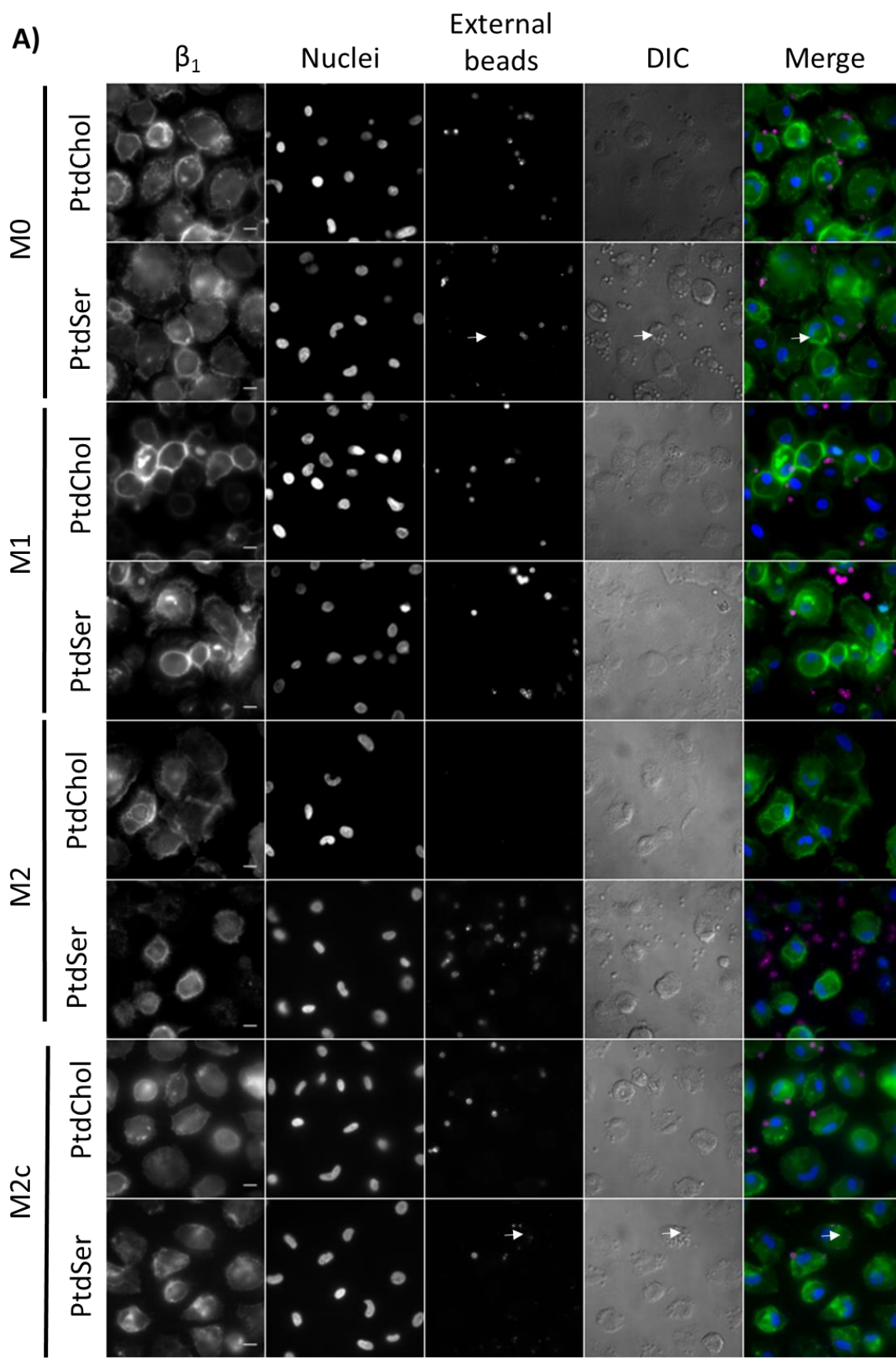
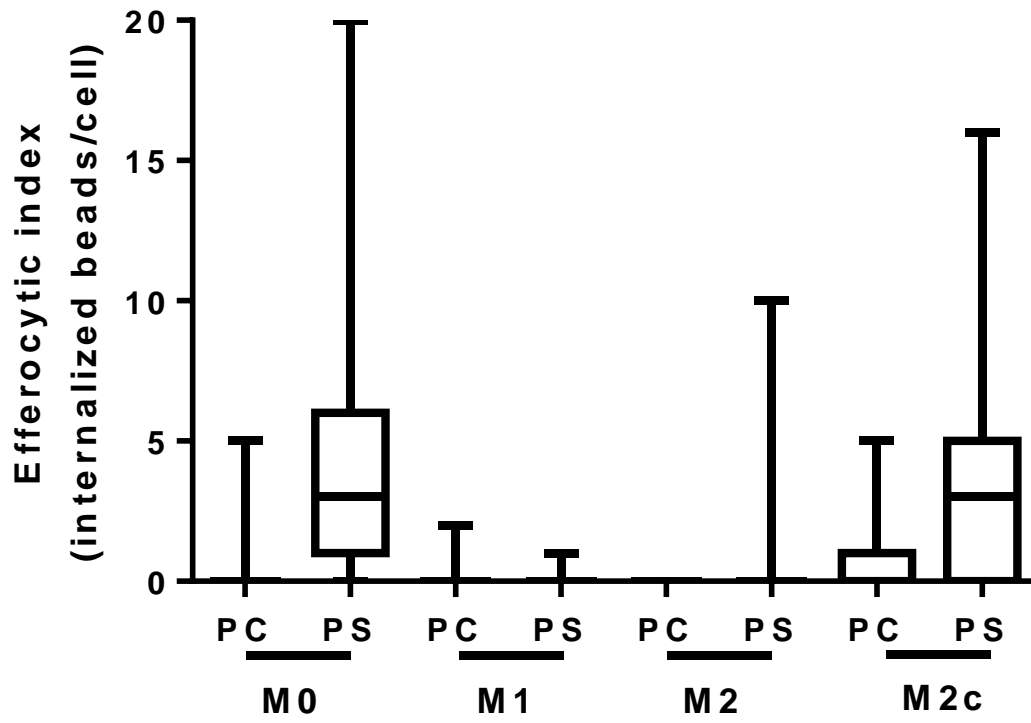


Figure 23: Efferocytosis of human serum opsonized PtdSer and PC beads by primary human macrophages. Representative images of M0, M1, M2 and M2c polarized macrophages fed silica beads containing 79.8% PtdChol, 20% PtdSer, 0.1% biotin-PE coated in human serum (A). Macrophages were immunostained for β_1 integrin, counterstained using Hoechst and external beads labelled using streptavidin-647. Arrows demarcate representative internalized beads. Scale bars represent 10 μm . B) Efferocytic index of M0, M1, M2 and M2c-polarized macrophages. Representative data from one independent experiment which is plotted as interquartile range \pm minimum/maximum, minimum of 60 cells/condition. PC = beads containing 99.9% PtdChol + 0.1% biotin-PE, PS = beads containing 79.9% PtdChol + 20% PtdSer + 0.1% biotin-PE.



B)



Chapter 4: Discussion

4.1 Rational for thesis

TAM receptors play a critical role in maintaining homeostasis, with MERTK playing the predominant role¹²⁰. The differential roles of TAM receptors is likely a product of their independent evolutionary histories, a characteristic of the TAM receptors which has not previously been investigated. Thus, using an evolutionary approach, we investigated the impact of recent evolution on the TAM family, and performed a detailed biochemical assessment of this evolution on MERTK function. We found numerous areas of conservation in *MERTK* as well as two areas of strong positive selection: the signal peptide and the transmembrane domain. Positive selection in humans is relatively rare, and the biological implications for these changes often remains unclear^{121,122}. As such, we set out to evaluate the functional relevance of the changes in *MERTK*'s signal peptide and transmembrane domain through use of *in vitro* studies using chimeric *MERTK* ancestral proteins with reconstructed primate- or hominid-ancestral signal peptides or transmembrane domains in place of human *MERTK*.

4.2 Hypothesis and aims

Our initial characterization of the TAM receptors determined that only MERTK had undergone significant adaptive evolution, with much of this evolution confined to the signal peptide and transmembrane domain. Given these observations, and previous observations that many enveloped viruses enhance infectivity or gain cell entry via TAM receptors⁹², **we hypothesized that the positive selection in *MERTK*'s signal peptide would lead to reduced surface expression, and this lower surface MERTK expression would be compensated for by the co-evolution of**

avidity-enhancing self-clustering. Our first aim was to reconstruct the primate- and hominid-ancestral signal peptide and transmembrane domains to identify specific nucleotide and residue changes in these regions. The second aim was to use create expression vectors containing chimeric human *MERTK* with either the reconstructed primate or hominid signal peptide or transmembrane domain for biological analysis. These chimeric proteins were to be used to test for expression level and protein trafficking differences in ancestral signal peptides, and the ability to self-cluster in the ancestral transmembrane domains. In our third aim, we wanted to create a reproducible *in vitro* assay in which to study MERTK-dependent efferocytosis, allowing for a comparison of how evolutionary changes in the transmembrane domain may have influenced efferocytosis capacity. Our data indicates that this hypothesis is partially correct – while we did not observe the decrease in MERTK expression we predicted, we did observe an increase in MERTK self-clustering, consistent with an increase in MERTK avidity and/or the formation of new MERTK/co-receptor interactions.

4.3 *MERTK* signal peptide evolution

Positive selection in humans is a relatively rare occurrence, and progress on understanding positive selection is mostly limited to the types of genes that are likely to undergo positive selection. In humans, positive selection is most often observed in immune-related genes, and genes involved in olfaction, sperm development and skin pigmentation^{107,123–125}. In addition, likely target genes are those where the protein is expressed at low levels and involved in a signalling cascade^{122,126}. These factors make TAM receptors likely targets for positive selection; however, *MERTK* is the only TAM receptor that demonstrated positive selection. This difference may highlight preferential

binding of MERTK over other TAM receptors by enveloped viruses, leading to antagonistic coevolution.

Signal peptides generally evolve at a slower rate than other coding regions, and moreover, tend to be under stabilizing selection^{106,127,128}. This relatively slow rate of change, which is otherwise neutral, is a product of the minimal biochemical attributes required of most signal peptides – ie. polar or neutral amino acids surrounding a somewhat hydrophobic core¹⁰⁶. As such, signal peptides are relatively free to evolve, so long as the amino acid substitutions maintain this overall biochemical characteristic, hence the slow but otherwise neutral evolution typically observed in signal peptides. A marked exception to this pattern is found in a number of immune-related genes, where signal peptides – and to a lesser degree, the mature protein – evolve faster than average and display modest-to-strong positive selection¹⁰⁶. Included among these positively-selected signal peptides is *MERTK*, as identified in this thesis, as well as IFN- γ ¹⁰⁵. However, like in this thesis, no biological effect of the evolution of the signal peptide of IFN- γ could be determined. They, and we, propose that the observed evolution of these signal peptides is likely due to antagonistic coevolution, wherein immune-related proteins are driven to rapidly evolve in response to a pathogen¹⁰⁵. Indeed, this would be consistent with the parasitism of TAM receptors by enveloped viruses, with mutations in *MERTK*'s signal peptide potentially acting to reduce cell-surface expression, thereby reducing viral binding sites. Regardless, the trend of accelerated evolution in immune-related signal peptides, in *MERTK* and other genes, warrants further investigation.

At this time, we have no clear indication of the role of this selection, other than excluding significant changes in expression level or protein trafficking efficiency. However, even this

conclusion must be taken with some reservation, as it is possible the non-B motif in MERTK's coding region may act in a cis- or trans-fashion to modify MERTK expression or splicing when under the control of the endogenous promoter^{129,130}. Our use of a CMV promoter and an intron-free transgene means that we cannot exclude the possibility that the formation of the non-B cruciform motif may regulate expression from the endogenous promoter or regulate other aspects of RNA processing. Alternatively, the presence of the non-B DNA and/or the associated amino acid substitutions may influence interactions between the RNA or polypeptide with intracellular RNA-binding or protein processing machinery – either endogenous – or pathogen-derived. Potential effects of these motifs on the promoter could be assessed using a luciferase-based promoter activity assay. Assessing the latter possibilities is more difficult, especially if a pathogen-derived factor drove this evolution, but it may be possible to assess changes in interactions with endogenous factors through conventional RNA interaction and protein interaction assays.

4.4 *MERTK* transmembrane evolution

In transmembrane evolution, the helical core is in general found to be highly conserved, with reduced conservation in the lipid-exposed regions and oligomerizing surfaces^{108,131}. In this study, we observed multiple amino acids under positive selection in primates, with a number of these changes adding leucines or isoleucines. Research has shown that TAM receptor homodimerize, but the specific interactions involved remain unclear. However, *MET* - a hepatocyte growth factor with high transmembrane similarity to TAM receptors⁸ – has been shown to dimerize through similar leucine motifs¹³². Furthermore, the RTK family member *DDR1*, which is involved in communication with the microenvironment and contains a transmembrane domain similar to that of TAM receptors, has been shown to require leucine zippering to dimerize and activate^{8,133}. As

additions of leucines and isoleucines can lead to zippering motifs, which are found in other RTKs, and areas of oligomerization have less conservation, we evaluated MERTK oligomerization. Our study demonstrated increased levels of protein oligomerization in human and hominid *MERTK* compared to primate *MERTK*.

In our investigations we observed a clear functional impact due to transmembrane evolution. Specifically, a dramatic and significant increase in MERTK self-clustering was observed, which is likely due to the evolution of a new hydrophobic interaction in the MERTK transmembrane domain during the divergence of hominids from primates. Indeed, *in silico* analysis conducted by our collaborators (Appendix 5) demonstrated that many of the leucine/isoleucine additions to MERTK occurred along a single facet, consistent with the formation of a leucine-zipper like motif. This increase in clustering could indicate one of two evolutionary processes – firstly, increased self-clustering is known to increase avidity, and therefore would act to enhance MERTK’s binding capacity¹³⁴. Secondly, the observed increase in clustering may not be due to self-clustering, and rather may indicate the presence of new inter-protein interactions. In this case, MERTK may engage in new signalling or biological functions through cooperation with new accessory molecules. It is important to note that these two possibilities are not mutually exclusive, and that this clustering may be indicative of both increased avidity and altered/expanded MERTK activity. In future experiments, specific protein interactions can be assessed directly by immunoprecipitating MERTK under conditions which preserve its interprotein interactions, followed by detection of any interacting proteins by immunoblotting or mass spectrometry¹¹³.

4.5 MERTK-dependent efferocytosis model development

To evaluate any functional differences from the evolutionary changes to the transmembrane domain, as well as evaluation of the effect of disease-related SNPs on efferocytosis and to fully elucidate *MERTK*'s efferocytosis signalling pathway, it was important to create a reproducible *in vitro* efferocytosis model. While many primary cell types and cell lines endogenously express TAM receptors, they tend to express multiple TAM receptors plus additional efferocytic and scavenger receptors, making studies of individual receptors in these cell difficult^{57,73,135}. As such, we chose to develop an ectopic expression based assay in cells that are not normally efferocytic. This would ensure all observations could be ascribed to the activity of the transfected receptors. While we were able to develop a functioning system using murine MERTK, our evolutionary results revealed that a high degree of divergence occurred in the primate/hominid/human lineage, with a concordant alteration of MERTK clustering and possibly MERTK signalling or function, thus making any human extrapolations from mouse *MerTK* models questionable.

Creating a model system to study human MERTK proved to be much more complicated, as human *MERTK* contains multiple motifs recognized by bacteria as recombination and phage sites, making cloning of the native sequence impossible. In fact, no studies have yet been published using ectopic expression of full-length human *MERTK*, with a recent study characterizing human *MERTK* as “refractory to cloning”¹². Indeed, the only studies using ectopically expressed human *MERTK* only expressed the extracellular or intracellular domains in a soluble form^{25,85,136}. Based on this, it is not surprising that most studies on MERTK have used rat or mouse *MerTK* knockout models, which must be interpreted with caution given the scale of recent *MERTK* evolution in the primate lineage. Due to time constraints we were unable to create a functioning efferocytosis model using

ectopic human MERTK expression, although, given the lack of efferocytosis observed with our positive control (TIM-4), it suggests that there was an issue either with the lipids used to prepare our target beads, or with the cell type used for the experiments. However, the same cell line used in our efferocytosis experiments are highly phagocytic when expressing the FcγRIIA phagocytic receptor (data not shown), and have been extensively used in other phagocytosis assays^{80,137,138}, indicating that the issue most likely lies in the lipids used in our model. Future work will use ACs or alternative lipid mixtures in place of the PtdChol/PtdSer-coated beads.

While an ectopic expression *in vitro* model system would be ideal, as it allows us to study MERTK in relative isolation from other efferocytic receptors, validation of any results from such a model would need to be verified using a more biologically relevant system. To this end, we started preliminary work on creating a model system using primary human macrophages. We isolated monocytes from human blood and differentiated the macrophages into M0, M1, M2 and M2c phenotypes. MERTK is most highly expressed on M0 and M2c phenotypes, which are nonpolarized and an anti-inflammatory phenotype respectively. We found that these phenotypes were also the most efferocytic cells when fed apoptotic mimics coated in human serum, consistent with a study by Zizzo *et al.* which demonstrated higher levels of efferocytosis when monocytes were differentiated with M-CSF (M0) and the highest rate of efferocytosis in M-CSF and IL-10 differentiated monocytes (M2c)⁸⁸. Although this assay is not specific for MERTK, it is interesting that MERTK high-expressing cells were the most efferocytic. In macrophages AXL is highly expressed on inflammatory M1 phenotypes³³ which exhibited background levels of efferocytosis in our assay. This may highlight MERTK as the essential efferocytic TAM receptor in macrophages, and moreover, raises questions about the efferocytic capacity of AXL compared to

MERTK. Future work using a macrophage model will require either overexpression of MERTK through transfection, or alternatively, pharmacological or siRNA inhibition of MERTK to ensure MERTK function is more specifically evaluated.

4.6 MERTK functional domains

TAM receptors bind to the SHBG domain on opsonins GAS6 and/or PROS through their Ig domains²⁵⁻²⁸. In our study, we found high levels of conservation in Ig1 and neutral selection in Ig2 of *MERTK*. In marked contrast, we observed high levels of conservation in Ig2 but neutral selection in Ig1 in *AXL*. *TYRO3* showed relative conservation in both Ig domains. These observations may explain the differential usage of GAS6, PROS and other TAM opsonins by TAM receptors, with binding to certain opsonins lost as the respective Ig domain underwent drift. Unexpectedly, Sasaki *et al.* demonstrated using human *AXL* Ig domains that Ig1 is more critical for GAS6 binding²⁵. However, this study used purified Ig domains rather than intact *AXL*, and thus binding experiments should be conducted using full-length *AXL* to account for this discrepancy. Apart from potential differences in opsonin binding to full length TAM receptors compared to their soluble counterparts, there may also be differences in binding patterns when the opsonins are bound to PtdSer. Indeed, this is the case with MERTK, which preferentially binds to PtdSer-engaged GAS6^{32,33}. Thus, future studies into TAM-opsonin interactions should use whole TAM receptors, and ligand-bound opsonins, to most accurately assess individual Ig domain preferences.

Interestingly, differential opsonin binding sites in the Ig domains of TAM receptors may permit heterodimerization. Although homodimerization of TAM receptors has been shown, the ability for TAM receptors to heterodimerize remains unexplored, but widely speculated^{1,57,60,64,139}. Other

RTKs, like the EGFR family members, have been shown to both homo- and heterodimerize, and in doing so increase the diversity of their ligand-binding and signalling capacities¹⁴⁰. Potential heterodimerization is supported by the fact that while *MerTK*^{-/-} mice show near abolishment in efferocytosis, *Axl*^{-/-}, *Tyro3*^{-/-}, and *Axl/Tyro3*^{-/-} mice show a 50% reduction, demonstrating probable interactions among the receptors⁵⁷. Furthermore, cooperation between AXL and TYRO3 has been demonstrated in the Rat2 cell line, where overexpression of TYRO3 – but not a kinase-dead TYRO3 – increased GAS6-mediated AXL phosphorylation⁶⁴. This close interaction is supported by the co-immunoprecipitation of TYRO3 and AXL in gonadotropin-releasing hormone neuronal cells¹⁴¹. Understanding these interactions will be critical to understanding TAM receptor biology, and will likely require crystal structures and *in silico* analysis with ligand-bound opsonins. Studies should use human TAM receptors for all heterodimerization studies, as recent divergence in *MERTK* may impact any inter-protein associations.

While the Fbg domains present on TAM receptor ectodomains are common among RTKs, they currently have no defined function¹⁴². However, we found that Fbg1 is highly conserved in both *AXL* and *MERTK*, and Fbg2 is highly conserved in *AXL*. These domains may have functional importance, as purifying selection is typically found in areas critical for protein function¹⁴³. Integrins have been shown to interact with Fbg domains on other proteins through the common-integrin binding site RGD¹⁴⁴, which is not present in *MERTK*. However, recent findings have shown integrin binding to Fbg domains in the absence of RGD¹⁴⁵. Thus, conservation in the Fbg domains of *AXL* and *MERTK* may be due to interactions with integrins, or potentially due to interactions with other unelucidated binding partners. This potential binding site should be

investigated through co-immunoprecipitation assays using human stimulated TAM receptors with or without mutated Fbg domains.

The most critical region in TAM receptors is their TKD, through which all TAM-derived cellular signals are believed to be generated^{1,120,146}. Thus, unsurprisingly, we found the TKD to be strongly conserved in all three TAM receptors, with stronger conservation observed in *AXL* and *MERTK*. The higher degree of conservation may be due to the greater importance of *MERTK* and *AXL* in maintaining homeostasis. Indeed, *Axl*^{-/-}*MerTK*^{-/-} mice accumulate the highest number of ACs, as well as the worst phenotypes among TAM KO mice¹⁴⁷.

4.8 Summary and future aims

In summary, I have identified two areas of positive selection unique to *MERTK* among TAM receptors. This positive selection is restricted to two key structural domains in *MERTK*: the signal peptide and transmembrane domain. Through reconstruction of the primate and hominid ancestral signal peptide and transmembrane domain, I have identified specific nucleotide and residue changes in *MERTK* and have used chimeric *MERTK* constructs containing the ancestral signal peptides or transmembrane domains to evaluate the biological implications of these changes. Evolutionary changes in the signal peptide were evaluated for possible changes in protein expression and trafficking, with no significant differences observed. We evaluated the ancestral transmembrane domains for changes in *MERTK* self-clustering and found that human and hominid *MERTK* clustered significantly more than primate-ancestral *MERTK*, despite all three constructs displaying roughly equal total and cell surface expression. This increase in clustering appears to be due to the evolution of a new hydrophobic interaction motif within the transmembrane domain,

although whether this motif mediates homodimerization or the formation of complexes with other co-receptors remains to be elucidated. This work indicates that recent evolution has altered MERTK function, which could relate to viral pressure or changes in immunological function. Progress was made on a mouse MERTK efferocytosis model, but, as evidenced by our evolutionary data, human *MERTK* has undergone significant evolutionary change, necessitating the development of a human MERTK model system for future studies.

In future experiments evolutionary analysis should be conducted on non-coding regions of *MERTK*. These regions have been associated with numerous disease-related SNPs, and may unveil other key regions that have undergone selection. Furthermore, as positive selection has been shown to occur in multiple proteins in the same signalling cascade¹²², proteins known to be involved in MERTK signalling should undergo selection analysis. This may identify which components of the MERTK-induced signalling cascade, if any, have undergone positive selection alongside MERTK. These analyses may provide further insight into the normal signalling of human MERTK, and moreover, may provide insight into the source of the selective pressure which mediated recent MERTK evolution. Lastly, the human MERTK *in vitro* efferocytosis model will enable the study of MERTK signalling, as well as functional impacts of recent evolutionary changes or disease-related SNPs on efferocytosis capacity. These analyses will provide insight into MERTK's cellular function, identifying critical signalling components and functional domains, thereby identifying potential therapeutic targets.

References

1. Lemke, G. & Rothlin, C. V. Immunobiology of the TAM receptors. *Nat. Rev. Immunol.* **8**, 327–36 (2008).
2. Wu, Y., Singh, S., Georgescu, M.-M. & Birge, R. B. A role for Mer tyrosine kinase in α v β 5 integrin-mediated phagocytosis of apoptotic cells. *J. Cell Sci.* **118**, 539–53 (2005).
3. Nagata, K. *et al.* Identification of the product of growth arrest-specific gene 6 as a common ligand for Axl, Sky, and Mer receptor tyrosine kinases. *J. Biol. Chem.* **271**, 30022–30027 (1996).
4. Stitt, T. N. *et al.* The anticoagulation factor protein S and its relative, Gas6, are ligands for the Tyro 3/Axl family of receptor tyrosine kinases. *Cell* **80**, 661–670 (1995).
5. Caberoy, N. B., Zhou, Y. & Li, W. Tubby and tubby-like protein 1 are new MerTK ligands for phagocytosis. *EMBO J.* **29**, 3898–3910 (2010).
6. Caberoy, N. & Alvarado, G. Galectin-3 is a new MerTK-specific eat-me signal. *J. Cell. Physiol.* **227**, 401–407 (2012).
7. Laitinen, I. *et al.* Evaluation of α v β 3 integrin-targeted positron emission tomography tracer ¹⁸F-galacto-RGD for imaging of vascular inflammation in atherosclerotic mice. *Circ. Cardiovasc. Imaging* **2**, 331–338 (2009).
8. Brunet, F. G., Volff, J.-N. & Schartl, M. Whole Genome Duplications Shaped the Receptor Tyrosine Kinase Repertoire of Jawed Vertebrates. *Genome Biol. Evol.* **8**, 1600–1613 (2016).
9. Lemke, G. The TAM Receptor Family Introduction to the TAM Receptor Tyrosine. 53–77 (2015). doi:10.1007/978-3-319-11888-8

10. Hurtado, B. *et al.* Association study between polymorphisms in GAS6-TAM genes and carotid atherosclerosis. *Thromb. Haemost.* **104**, 592–598 (2010).
11. Ma, G. Z. M., Stankovich, J., Kilpatrick, T. J., Binder, M. D. & Field, J. Polymorphisms in the receptor tyrosine kinase MERTK gene are associated with multiple sclerosis susceptibility. *PLoS One* **6**, e16964 (2011).
12. Binder, M. D. *et al.* Common and Low Frequency Variants in MERTK Are Independently Associated with Multiple Sclerosis Susceptibility with Discordant Association Dependent upon HLA-DRB1*15:01 Status. *PLoS Genet.* **12**, e1005853 (2016).
13. Brea-Fernández, A. J. *et al.* Novel splice donor site mutation in MERTK gene associated with retinitis pigmentosa. *Br. J. Ophthalmol.* **92**, 1419–1423 (2008).
14. Hsiao, F. C. *et al.* Effect of GAS6 and AXL gene polymorphisms on adiposity, systemic inflammation, and insulin resistance in adolescents. *Int. J. Endocrinol.* **2014**, doi:10.1155/2014/674069 (2014).
15. Lu, Q. & Lemke, G. Homeostatic Regulation of the Immune System by Receptor Tyrosine Kinase of the Tyro 3 Family. *Science* **293**, 306–311 (2001).
16. Scott, R. S. *et al.* Phagocytosis and clearance of apoptotic cells is mediated by MER. *Nature* **411**, 207–211 (2001).
17. Rothlin, C. V & Lemke, G. TAM receptor signaling and autoimmune disease. *Curr. Opin. Immunol.* **22**, 740–746 (2010).
18. Shao, W.-H. *et al.* Disrupted Mer receptor tyrosine kinase expression leads to enhanced MZ B-cell responses. *J. Autoimmun.* **35**, 368–74 (2010).
19. Wallet, M. A. *et al.* MerTK is required for apoptotic cell-induced T cell tolerance. *J. Exp. Med.* **205**, 219–232 (2008).

20. Radic, M. Z. *et al.* Heterogeneous nuclear ribonucleoprotein P2 is an autoantibody target in mice deficient for Mer, Axl, and Tyro3 receptor tyrosine kinases. *J. Immunol.* **176**, 68–74 (2006).
21. Linger, R., Keating, A., Earp, H. & Graham, D. TAM receptor tyrosine kinases: biologic functions, signaling, and potential therapeutic targeting in human cancer. *Adv. Cancer Res.* **100**, 35–83 (2008).
22. Graham, D. K., Dawson, T., Mullaney, D., Snodgrass, H. R. & Earp, H. S. Human and mRNA expression analysis of a novel human protooncogene, c-mer. **5**, 647–657 (1994).
23. Rothlin, C. V., Leighton, J. A., Ghosh, S. Tyro3, Axl, and Mertk Receptor signaling in inflammatory bowel disease and colitis-associated cancer. *Inflamm. bowel Dis.* **20**, 1472–1480 (2014).
24. Ling, L., Templeton, D., Chem, J. B. & Kung, H. Protein Chemistry and Structure : Identification of the Major Autophosphorylation Sites of Nyk / Mer , an NCAM-related Receptor Tyrosine Kinase Identification of the Major Autophosphorylation Sites of Nyk / Mer , an NCAM-related Receptor Tyrosine Kinase. **271**, 18355–18362 (1996).
25. Sasaki, T. *et al.* Structural basis for Gas6–Axl signalling. *EMBO J.* **25**, 80–87 (2006).
26. Sasaki, T. *et al.* Crystal structure of a C-terminal fragment of growth arrest-specific protein Gas6: Receptor tyrosine kinase activation by laminin G-like domains. *J. Biol. Chem.* **277**, 44164–44170 (2002).
27. Tanabe, K. *et al.* Roles of γ -carboxylation and a sex hormone-binding globulin-like domain in receptor-binding and in biological activities of Gas6. *FEBS Lett.* **408**, 306–310 (1997).
28. Nyberg, P., He, X., Härdig, Y., Dahlback, B. & García de Frutos, P. Stimulation of Sky

- tyrosine phosphorylation by bovine protein S--domains involved in the receptor-ligand interaction. *Eur. J. Biochem.* **246**, 147–154 (1997).
29. Manfioletti, G., Brancolini, C., Avanzi, G. & Schneider, C. The protein encoded by a growth arrest-specific gene (gas6) is a new member of the vitamin K-dependent proteins related to protein S, a negative coregulator in the blood coagulation cascade. *Mol. Cell. Biol.* **13**, 4976–4985 (1993).
 30. Burstyn-Cohen, T., Heeb, M. J. & Lemke, G. Lack of Protein S in mice causes embryonic lethal coagulopathy and vascular dysgenesis. *J. Clin. Invest.* **119**, 2942–2953 (2009).
 31. Angelillo-Scherrer, A. *et al.* Deficiency or inhibition of Gas6 causes platelet dysfunction and protects mice against thrombosis. *Nat. Med.* **7**, 215–221 (2001).
 32. Lew, E. D. *et al.* Differential TAM receptor-ligand-phospholipid interactions delimit differential TAM bioactivities. *Elife* **3**, 1–23 (2014).
 33. Zagórska, A., Través, P. G., Lew, E. D., Dransfield, I. & Lemke, G. Diversification of TAM receptor tyrosine kinase function. *Nat. Immunol.* **15**, 920–928 (2014).
 34. Rothlin, C. V., Ghosh, S., Zuniga, E. I., Oldstone, M. B. A. & Lemke, G. TAM Receptors Are Pleiotropic Inhibitors of the Innate Immune Response. *Cell* **131**, 1124–1136 (2007).
 35. Lu, Q. *et al.* Tyro-3 family receptors are essential regulators of mammalian spermatogenesis. *Nature* **398**, 723–728 (1999).
 36. Prasad, D. *et al.* TAM receptor function in the retinal pigment epithelium. *Mol. Cell. Neurosci.* **33**, 96–108 (2006).
 37. Caberoy, N. B., Alvarado, G. & Li, W. Tubby regulates microglial phagocytosis through MerTK. *J. Neuroimmunol.* **252**, 40–48 (2012).
 38. Santagata, S. G-Protein Signaling Through Tubby Proteins. *Science* **292**, 2041–2050

- (2001).
39. Ikeda, A., Nishina, P. M. & Naggert, J. K. The tubby-like proteins, a family with roles in neuronal development and function. *J. Cell Sci.* **115**, 9–14 (2002).
 40. Caberoy, N. B. & Li, W. Unconventional secretion of tubby and tubby-like protein 1. *FEBS Lett.* **583**, 3057–3062 (2009).
 41. Caberoy, N. B., Maignel, D., Kim, Y., Li, W. Identification of tubby and tubby-like protein 1 as eat-me signals by phage display. *Exp. Cell Res.* **4**, 245–257 (2011).
 42. Uehara, F., Ohba, N. & Ozawa, M. Isolation and characterization of galectins in the mammalian retina. *Investig. Ophthalmol. Vis. Sci.* **42**, 2164–2172 (2001).
 43. Grillo, M. A. & Colombatto, S. Advanced glycation end-products (AGEs): Involvement in aging and in neurodegenerative diseases. *Amino Acids* **35**, 29–36 (2008).
 44. Vlassara, H. *et al.* Identification of galectin-3 as a high-affinity binding protein for advanced glycation end products (AGE): a new member of the AGE-receptor complex. *Mol. Med.* **1**, 634–646 (1995).
 45. Hubbard, S. R. & Miller, W. T. Receptor tyrosine kinases: mechanisms of activation and signaling. *Curr. Opin. Cell Biol.* **19**, 117–123 (2007).
 46. Blomme, T. *et al.* The gain and loss of genes during 600 million years of vertebrate evolution. *Genome Biol.* **7**, R43 (2006).
 47. Kondrashov, F. a, Rogozin, I. B., Wolf, Y. I. & Koonin, E. V. Selection in the evolution of gene duplications. *Genome Biol.* **3**, 1–9 (2002).
 48. Jaillon, O., Aury, J. M. & Wincker, P. ‘Changing by doubling’, the impact of Whole Genome Duplications in the evolution of eukaryotes. *Comptes Rendus Biol.* **332**, 241–253 (2009).

49. Kulman, J. D. *et al.* Vitamin K-dependent proteins in *Ciona intestinalis*, a basal chordate lacking a blood coagulation cascade. *Proc. Natl. Acad. Sci. U. S. A.* **103**, 15794–15799 (2006).
50. Camenisch, T. D., Koller, B. H., Earp, H. S. & Matsushima, G. K. A novel receptor tyrosine kinase, Mer, inhibits TNF- α production and lipopolysaccharide-induced endotoxic shock. *J. Immunol.* **162**, 3498–3503 (1999).
51. Duncan, J. L. *et al.* An RCS-like retinal dystrophy phenotype in Mer knockout mice. *Investig. Ophthalmol. Vis. Sci.* **44**, 826–838 (2003).
52. Chen, Y. *et al.* Functions of TAM RTKs in regulating spermatogenesis and male fertility in mice. *Reproduction* **138**, 655–666 (2009).
53. Sun, B. *et al.* Sertoli cell-initiated testicular innate immune response through toll-like receptor-3 activation is negatively regulated by Tyro3, Axl, and mer receptors. *Endocrinology* **151**, 2886–2897 (2010).
54. Strauss, O. The Retinal Pigment Epithelium in Visual Function. *Physiol. Rev.* **85**, 845–881 (2005).
55. Kevany, B. M. & Palczewski, K. Phagocytosis of retinal rod and cone photoreceptors. *Physiology* **25**, 8–15 (2010).
56. Feng, W., Yasumura, D., Matthes, M. T., LaVail, M. M. & Vollrath, D. Mertk triggers uptake of photoreceptor outer segments during phagocytosis by cultured retinal pigment epithelial cells. *J. Biol. Chem.* **277**, 17016–17022 (2002).
57. Seitz, H. M., Camenisch, T. D., Lemke, G., Earp, H. S. & Matsushima, G. K. Macrophages and Dendritic Cells Use Different Axl/Mertk/Tyro3 Receptors in Clearance of Apoptotic Cells. *J. Immunol.* **178**, 5635–5642 (2007).

58. Braunger, J. *et al.* Intracellular signaling of the Ufo/Axl receptor tyrosine kinase is mediated mainly by a multi-substrate docking-site. *Oncogene* **14**, 2619–2631 (1997).
59. Lan, Z. *et al.* Transforming activity of receptor tyrosine kinase tyro3 is mediated, at least in part, by the PI3 kinase-signaling pathway. *Blood* **95**, 633–638 (2000).
60. Goruppi, S., Ruaro, E., Varnum, B. & Schneider, C. Requirement of phosphatidylinositol 3-kinase-dependent pathway and Src for Gas6-Axl mitogenic and survival activities in NIH 3T3 fibroblasts. *Mol. Cell. Biol.* **17**, 4442–4453 (1997).
61. Tibrewal, N. *et al.* Autophosphorylation docking site Tyr-867 in Mer receptor tyrosine kinase allows for dissociation of multiple signaling pathways for phagocytosis of apoptotic cells and down-modulation of lipopolysaccharide-inducible NF-kappaB transcriptional activation. *J. Biol. Chem.* **283**, 3618–3627 (2008).
62. Weinger, J. G. *et al.* In brain, Axl recruits Grb2 and the p85 regulatory subunit of PI3 kinase; in vitro mutagenesis defines the requisite binding sites for downstream Akt activation. *J. Neurochem.* **106**, 134–146 (2008).
63. Georgescu, M. M., Kirsch, K. H., Shishido, T., Zong, C. & Hanafusa, H. Biological effects of c-Mer receptor tyrosine kinase in hematopoietic cells depend on the Grb2 binding site in the receptor and activation of NF-kappaB. *Mol. Cell. Biol.* **19**, 1171–81 (1999).
64. Brown, J. E., Krodel, M., Pazos, M., Lai, C. & Prieto, A. L. Cross-phosphorylation, signaling and proliferative functions of the Tyro3 and Axl receptors in Rat2 cells. *PLoS One* **7**, 1–11 (2012).
65. Zong, C., Yan, R., August, A., EDarnell, J. & Hanafusa, H. Unique signal transduction of Eyk: constitutive stimulation of the JAK-STAT pathway by an oncogenic receptor-type

- tyrosine kinase. *EMBO J.* **15**, 4515–4525 (1996).
66. Darnell, J. E., Kerr, I. M. & Stark, G. R. Jak-STAT pathways and transcriptional activation in response to IFNs and other extracellular signaling proteins. *Science* **264**, 1415–1421 (1994).
 67. Lee, Y.-J. *et al.* Inhibiting Mer receptor tyrosine kinase suppresses STAT1, SOCS1/3, and NF- κ B activation and enhances inflammatory responses in lipopolysaccharide-induced acute lung injury. *J. Leukoc. Biol.* **91**, 921–932 (2012).
 68. Van Vré, E. A., Ait-Oufella, H., Tedgui, A. & Mallat, Z. Apoptotic cell death and efferocytosis in atherosclerosis. *Arterioscler. Thromb. Vasc. Biol.* **32**, 887–93 (2012).
 69. Segawa, K. *et al.* Caspase-mediated cleavage of phospholipid flippase for apoptotic phosphatidylserine exposure. *Science* **344**, 1164–1168 (2014).
 70. Suzuki, J. *et al.* Calcium-dependent phospholipid scramblase activity of TMEM16 protein family members. *J. Biol. Chem.* **288**, 13305–13316 (2013).
 71. van Meer, G., Voelker, D. R. & Feigenson, G. W. Membrane lipids: where they are and how they behave. *Nat. Rev. Mol. Cell Biol.* **9**, 112–124 (2008).
 72. Miyanishi, M. *et al.* Identification of Tim4 as a phosphatidylserine receptor. *Nature* **450**, 435–439 (2007).
 73. Kobayashi, N. *et al.* TIM-1 and TIM-4 Glycoproteins Bind Phosphatidylserine and Mediate Uptake of Apoptotic Cells. *Immunity* **27**, 927–940 (2007).
 74. DeKruyff, R. H. *et al.* T Cell/Transmembrane, Ig, and Mucin-3 Allelic Variants Differentially Recognize Phosphatidylserine and Mediate Phagocytosis of Apoptotic Cells. *J. Immunol.* **184**, 1918–1930 (2010).
 75. Albert, M. L. *et al.* Immature dendritic cells phagocytose apoptotic cells via α v β 5

- and CD36, and cross-present antigens to cytotoxic T lymphocytes. *J. Exp. Med.* **188**, 1359–68 (1998).
76. Rubartelli, A., Poggi, A. & Zocchi, M. R. The selective engulfment of apoptotic bodies by dendritic cells is mediated by the alphavbeta3 integrin and requires intracellular and extracellular calcium. *Eur. J. Immunol.* **27**, 1893–1900 (1997).
77. Platt, N., Suzuki, H., Kodama, T. & Gordon, S. Apoptotic thymocyte clearance in scavenger receptor class A-deficient mice is apparently normal. *J. Immunol.* **164**, 4861–4867 (2000).
78. Platt, N., Suzuki, H., Kurihara, Y., Kodama, T. & Gordon, S. Role for the class A macrophage scavenger receptor in the phagocytosis of apoptotic thymocytes in vitro. *Proc. Natl. Acad. Sci. U. S. A.* **93**, 12456–12460 (1996).
79. Finnemann, S. C. & Nandrot, E. F. MerTK activation during RPE phagocytosis in vivo requires alphaVbeta5 integrin. *Adv. Exp. Med. Biol.* **572**, 499–503 (2006).
80. Flannagan, R. S., Canton, J., Furuya, W., Glogauer, M. & Grinstein, S. The phosphatidylserine receptor TIM4 utilizes integrins as coreceptors to effect phagocytosis. *Mol. Biol. Cell* **25**, 1511–1522 (2014).
81. Todt, J. C., Hu, B. & Curtis, J. L. The scavenger receptor SR-A I/II (CD204) signals via the receptor tyrosine kinase Mertk during apoptotic cell uptake by murine macrophages. *J. Leukoc. Biol.* **84**, 510–518 (2008).
82. Nandrot, E. F. *et al.* Essential role for MFG-E8 as ligand for alphavbeta5 integrin in diurnal retinal phagocytosis. *Proc. Natl. Acad. Sci. U. S. A.* **104**, 12005–12010 (2007).
83. Dransfield, I., Zagórska, A., Lew, E. D., Michail, K. & Lemke, G. Mer receptor tyrosine kinase mediates both tethering and phagocytosis of apoptotic cells. *Cell Death Dis.* **6**,

- e1646 (2015).
84. Meer, J. H. M. Van Der, Poll, T. Van Der & Veer, C. Van. Review Article TAM receptors , Gas6 , and protein S : roles in in fl ammation and hemostasis. **123**, 2460–2469 (2014).
 85. Shelby, S. J., Colwill, K., Dhe-Paganon, S., Pawson, T. & Thompson, D. a. MERTK interactions with SH2-domain proteins in the retinal pigment epithelium. *PLoS One* **8**, e53964 (2013).
 86. Ravichandran, K. S. Beginnings of a good apoptotic meal: the find-me and eat-me signaling pathways. *Immunity* **35**, 445–55 (2011).
 87. Muñoz, L. E., Lauber, K., Schiller, M., Manfredi, A. a & Herrmann, M. The role of defective clearance of apoptotic cells in systemic autoimmunity. *Nat. Rev. Rheumatol.* **6**, 280–9 (2010).
 88. Zizzo, G., Hilliard, B. a, Monestier, M. & Cohen, P. L. Efficient clearance of early apoptotic cells by human macrophages requires M2c polarization and MerTK induction. *J. Immunol.* **189**, 3508–20 (2012).
 89. Thorp, E., Cui, D., Schrijvers, D. M., Kuriakose, G. & Tabas, I. Mertk receptor mutation reduces efferocytosis efficiency and promotes apoptotic cell accumulation and plaque necrosis in atherosclerotic lesions of apoe^{-/-} mice. *Arterioscler. Thromb. Vasc. Biol.* **28**, 1421–1428 (2008).
 90. Recarte-Pelz, P. *et al.* Vitamin K-dependent proteins GAS6 and Protein S and TAM receptors in patients of systemic lupus erythematosus: correlation with common genetic variants and disease activity. *Arthritis Res. Ther.* **15**, 1–9 (2013).
 91. Best, S. M. Viruses play dead to TAME interferon responses. *Cell Host Microbe* **14**, 117–118 (2013).

92. Morizono, K. & Chen, I. S. Y. Role of phosphatidylserine receptors in enveloped virus infection. *J. Virol.* **88**, 4275–4290 (2014).
93. Lew, E. D. *et al.* Enveloped Viruses Disable Innate Immune Responses in Dendritic Cells by Direct Activation of TAM Receptors. **14**, 136–147 (2013).
94. Read, S. A. *et al.* The Mechanism of Interferon Refractoriness During Hepatitis C Virus Infection and Its Reversal with a Peroxisome Proliferator-Activated Receptor α Agonist. *J. Interf. Cytokine Res.* **35**, 488–497 (2015).
95. Read, S. A. *et al.* Hepatitis C virus driven AXL expression suppresses the hepatic type I interferon response. *PLoS One* **10**, e0136227 (2015).
96. Verma, A., Warner, S. L., Vankayalapati, H., Bearss, D. J. & Sharma, S. Targeting Axl and Mer kinases in cancer. *Mol. Cancer Ther.* **10**, 1763–1773 (2011).
97. Nguyen, K.-Q., Tsou, W.-I., Kotenko, S. & Birge, R. B. TAM receptors in apoptotic cell clearance, autoimmunity, and cancer. *Autoimmunity* **46**, 294–297 (2013).
98. Jia, R. & Hanafusa, H. The proto-oncogene of v-eyk (v-ryk) is a novel receptor-type protein tyrosine kinase with extracellular Ig/FN-III Domains. *J. Biol. Chem.* **269**, 1839–1844 (1994).
99. Jia, R., Mayer, B. J., Hanafusa, T. & Hanafusa, H. A novel oncogene, v-ryk, encoding a truncated receptor tyrosine kinase is transduced into the RPL30 virus without loss of viral sequences. *J. Virol.* **66**, 5975–5987 (1992).
100. Holland, S. J. *et al.* R428, a selective small molecule inhibitor of Axl kinase, blocks tumor spread and prolongs survival in models of metastatic breast cancer. *Cancer Res.* **70**, 1544–1554 (2010).
101. Zhang, W. *et al.* UNC2025, a Potent and Orally Bioavailable MER/FLT3 Dual Inhibitor.

- J. Med. Chem.* **57**, 7031–4041 (2014).
102. Tworkoski, K. A. *et al.* MERTK controls melanoma cell migration and survival and differentially regulates cell behavior relative to AXL. *Pigment Cell Melanoma Res.* **26**, 527–541 (2013).
 103. Graham, D. K., DeRyckere, D., Davies, K. D. & Earp, H. S. The TAM family: phosphatidylserine-sensing receptor tyrosine kinases gone awry in cancer. *Nat. Rev. Cancer* **14**, 769–785 (2014).
 104. Axten, J. M. *et al.* Discovery of 7-Methyl-5-(1-([3-(trifluoromethyl)phenyl]acetyl)-2,3-dihydro-1H-indol-5-yl)-7H-pyrrolo[2,3-d]pyrimidin-4-amine (GSK2606414), a Potent and Selective First-in-Class Inhibitor of Protein Kinase R (PKR)-like Endoplasmic Reticulum Kinase (PERK). *J. Med. Chem.* **55**, 7193–7207 (2012).
 105. Wang, Z., Zhong, M., Fu, M., Dou, T. & Bian, Z. Evidence of positive selection at signal peptide region of interferon gamma. *Biosci. Biotechnol. Biochem.* **78**, 588–592 (2014).
 106. Williams, E. J. B., Pal, C. & Hurst, L. D. The molecular evolution of signal peptides. *Gene* **253**, 313–22 (2000).
 107. Anisimova, M. & Yang, Z. Multiple hypothesis testing to detect lineages under positive selection that affects only a few sites. *Mol. Biol. Evol.* **24**, 1219–1228 (2007).
 108. Stevens, T. & Arkin, I. Substitution rates in α helical transmembrane proteins. *Protein Sci.* **10**, 2507–2517 (2001).
 109. Tamura, K., Stecher, G., Peterson, D., Filipski, A. & Kumar, S. MEGA6: Molecular evolutionary genetics analysis version 6.0. *Mol. Biol. Evol.* **30**, 2725–2729 (2013).
 110. Edgar, R. C. MUSCLE: Multiple sequence alignment with high accuracy and high throughput. *Nucleic Acids Res.* **32**, 1792–1797 (2004).

111. Stern, A. *et al.* Selecton 2007: Advanced models for detecting positive and purifying selection using a Bayesian inference approach. *Nucleic Acids Res.* **35**, 506–511 (2007).
112. Caetano, F. A. *et al.* MliSR: Molecular Interactions in Super-Resolution Imaging Enables the Analysis of Protein Interactions, Dynamics and Formation of Multi-protein Structures. *PLoS Comput. Biol.* **11**, e1004634 (2015).
113. Heit, B. *et al.* Multimolecular signaling complexes enable syk-mediated signaling of CD36 internalization. *Dev. Cell* **24**, 372–383 (2013).
114. Evans, A. L. Blackburn, J. W. D. Yin, C. Heit, B. Quantitative Efferocytosis Assays. *Methods Mol. Biol.* In press. (2016).
115. Wang, G. & Vasquez, K. M. Non-B DNA structure-induced genetic instability. **598**, 103–119 (2006).
116. Benham, C. J. Analysis of the Structure of a Natural Alternating d (TA) n Sequence in Yeast Chromatin. **326**, 313–326 (1997).
117. Kyte, J. & Doolittle, R. F. A simple method for displaying the hydropathic character of a protein. *J. Mol. Biol.* **157**, 105–132 (1982).
118. Gibson, D. G. *et al.* Enzymatic assembly of DNA molecules up to several hundred kilobases. *Nat. Methods* **6**, 343–345 (2009).
119. Li, E., Wimley, W. C. & Hristova, K. Transmembrane helix dimerization: Beyond the search for sequence motifs. *Biochim. Biophys. Acta* **1818**, 183–193 (2012).
120. Rothlin, C. V, Carrera-Silva, E. A., Bosurgi, L. & Ghosh, S. TAM receptor signaling in immune homeostasis. *Annu. Rev. Immunol.* **33**, 355–391 (2015).
121. Arbiza, L., Dopazo, J. & Dopazo, H. Positive selection, relaxation, and acceleration in the evolution of the human and chimp genome. *PLoS Comput. Biol.* **2**, 288–300 (2006).

122. Kosiol, C. *et al.* Patterns of positive selection in six mammalian genomes. *PLoS Genet.* **4**, e1000144 (2008).
123. Vallender, E. J. & Lahn, B. T. Positive selection on the human genome. *Hum. Mol. Genet.* **13**, 245–254 (2004).
124. Williamson, S. H. *et al.* Localizing recent adaptive evolution in the human genome. *PLoS Genet.* **3**, 901–915 (2007).
125. Bakewell, M. a, Shi, P. & Zhang, J. More genes underwent positive selection in chimpanzee evolution than in human evolution. *Proc. Natl. Acad. Sci. U. S. A.* **104**, 7489–7494 (2007).
126. Drummond, D. A., Bloom, J. D., Adami, C., Wilke, C. O. & Arnold, F. H. Why highly expressed proteins evolve slowly. *Proc. Natl. Acad. Sci. U. S. A.* **102**, 14338–14343 (2005).
127. Hurst, L. D. & McVean, G. T. Do we understand the evolution of genomic imprinting? *Curr. Opin. Genet. Dev.* **8**, 701–708 (1998).
128. Li, W. -H., Wu, C. I., & Luo, C.-C. A new method for estimating synonymous and nonsynonymous rates of nucleotide substitution considering the relative likelihood of nucleotide and codon changes. *J. Chem. Inf. Model.* **53**, 1689–1699 (2013).
129. Kim, E. L., Peng, H., Esparza, F. M., Maltchenko, S. Z. & Stachowiak, M. K. Cruciform-extruding regulatory element controls cell-specific activity of the tyrosine hydroxylase gene promoter. *Nucleic Acids Res.* **26**, 1793–1800 (1998).
130. Mougin, A. *et al.* Secondary structure of the yeast *Saccharomyces cerevisiae* pre-U3A snoRNA and its implication for splicing efficiency. *RNA* **2**, 105–109 (1996).
131. Mokrab, Y., Stevens, T. J. & Mizuguchi, K. A structural dissection of amino acid

- substitutions in helical transmembrane proteins. *Proteins Struct. Funct. Bioinforma.* **78**, 2895–2907 (2010).
132. Rodrigues, G. A. & Park, M. Dimerization mediated through a leucine zipper activates the oncogenic potential of the met receptor tyrosine kinase. *Mol. Cellular Biol.* **13**, 6711–6722 (1993).
133. Noordeen, N. A., Carafoli, F., Hohenester, E., Horton, M. A. & Leitinger, B. A transmembrane leucine zipper is required for activation of the dimeric receptor tyrosine kinase DDR1. *J. Biol. Chem.* **281**, 22744–22751 (2006).
134. Stewart, M. & Hogg, N. Regulation of leukocyte integrin function: Affinity vs. avidity. *J. Cell. Biochem.* **61**, 554–561 (1996).
135. Areschoug, T. & Gordon, S. Scavenger receptors: Role in innate immunity and microbial pathogenesis. *Cell. Microbiol.* **11**, 1160–1169 (2009).
136. Tsou, W.-I. *et al.* Receptor tyrosine kinases, TYRO3, AXL, and MER, demonstrate distinct patterns and complex regulation of ligand-induced activation. *J. Biol. Chem.* **289**, 25750–25763 (2014).
137. Gu, B. J., Saunders, B. M., Petrou, S. & Wiley, J. S. P2X(7) is a scavenger receptor for apoptotic cells in the absence of its ligand, extracellular ATP. *J. Immunol.* **187**, 2365–2375 (2011).
138. Stuart, L. M. *et al.* Response to *Staphylococcus aureus* requires CD36-mediated phagocytosis triggered by the COOH-terminal cytoplasmic domain. *J. Cell Biol.* **170**, 477–485 (2005).
139. Lemke, G. Biology of the TAM Receptors. *Cold Spring Harb. Perspect. Biol.* **5**, 1–17 (2013).

140. Yarden, Y. The EGFR family and its ligands in human cancer. signalling mechanisms and therapeutic opportunities. *Eur. J. Cancer* **37**, S3–S8 (2001).
141. Pierce, A. *et al.* Axl and Tyro3 modulate female reproduction by influencing gonadotropin-releasing hormone neuron survival and migration. *Mol. Endocrinol.* **22**, 2481–2495 (2008).
142. Grassot, J., Gouy, M., Perrière, G. & Mouchiroud, G. Origin and molecular evolution of receptor tyrosine kinases with immunoglobulin-like domains. *Mol. Biol. Evol.* **23**, 1232–1241 (2006).
143. Yang, Z., Nielsen, R., Goldman, N., Pedersen, A. K. Codon-Substitution Models for Heterogeneous Selection Pressure at Amino Acid Sites. *Mol. Biol. Evol.* **19**, 49–57 (2000).
144. Richards, J. *et al.* Engineered fibronectin type III domain with a RGDWXE sequence binds with enhanced affinity and specificity to human alphavbeta3 integrin. *J. Mol. Biol.* **326**, 1475–1488 (2003).
145. Yokosaki, Y. *et al.* The integrin alpha 9 beta 1 mediates cell attachment to a non-RGD site in the third fibronectin type III repeat of tenascin. *J. Biol. Chem.* **269**, 26691–26696 (1994).
146. O’Neill, L. A. J. TAMpering with Toll-like Receptor Signaling. *Cell* **131**, 1039–1041 (2007).
147. Bosurgi, L. *et al.* Paradoxical role of the proto-oncogene Axl and Mer receptor tyrosine kinases in colon cancer. *Proc. Natl. Acad. Sci. U. S. A.* **110**, 13091–13096 (2013).

Appendix

10 20 30 40 50 60 70 80 90 100
MerTK ATGGGGCGGGCCCGCTGCCGCTGCTGCTGGGCTCTTCCTCCCGGGCTCTGGCGTAGAGTATCACTGAGGCAAGGAAGAAGCAAGCCTTACCCGC
Opt.A..C..A..A.....A.....A..G..T..G..T..T..G...A.AC.G.....T..C..A..T.....G..G..T.....A.....C..

110 120 130 140 150 160 170 180 190 200
MerTK TATTCGCCGGACCTTTTCCAGGGAGCCTGCAAACTGACCACACACCCGCTGTATCCCTTCCACAGCCAGTGGGTACCAGCCTGCCTTGATTTTTCCACC
Opt. .G..T..T..G..A..C..C..A.....G..C.....A...C.G..A..G..C..T.....C..C..T.....C..AC.....C..C..

210 220 230 240 250 260 270 280 290 300
MerTK AACCCAGCCTGGAAGACCACATACAGAAACGTAGCCATTCGCCAGGTGACCTCTGTCGAATCAAGCCCCTACCGCCTTGCCTTCAAACACACAGTT
Opt. T..T.....A..CC.G..C..C..C.....G.....C..T..A.....T..C.....T.....A..G..C.....G.....T.....C..G

310 320 330 340 350 360 370 380 390 400
MerTK GGACACATAACTTTCTGAACATAAAGGTGTCAAATTTAATGTCTCAATCAGTGTACCTAATATATACCAGGACACCACAATTTCTTGGTGGAAAGATG
Opt. ..G..T...C..T..G..C..G.....G..A.....G.....C...TC...G..C..C..C.....G.....

410 420 430 440 450 460 470 480 490 500
MerTK GGAAGGAATTTGCTGGGGACACATCATGCAATTACACAGTTTTATCCAGATGATGAAGTTACAGCAATAATCGCTTCTTCAGCATAACCAGTGTGCAGCG
Opt. .A..A..GC.....G..C..C..C.....T..C..T.....T..C.....C..C.....C..T..CAGT...TCA..C..ATCA.....A..

510 520 530 540 550 560 570 580 590 600
MerTK TTCAGACAATGGGTCGTATATCTGTAAGATGAAATAAACAATGAAGAGATCGTGTCTGATCCCATCTACATCGAAGTACAAGGACTTCCTCACTTTACT
Opt. AAGC..T.....C..C.....C.....T.....G..A.....CAGC..C..T.....T..T..G..G..G.....G.....A

610 620 630 640 650 660 670 680 690 700
MerTK AAGCAGCCTGAGAGCATGAATGTACCAGAAACACAGCCCTCAACCTCACCTGTCAGGCTGTGGGCCCGCTGAGCCCGTCAACATTTTCTGGGTTCAA
Opt.A..ATC.....C..G..T..G..T..C..T.....G..T.....G.....A..A..A..C.....T..G.....C..T.....C..G..

710 720 730 740 750 760 770 780 790 800
MerTK ACAGTAGCCGTGTTAACGAACAGCCGTGAAATAATCCCGCTCCGTGCTAATCTGTTCCAGGCCCTGACGGAGATGGCGGTCTTCAGTTGTGAGGCCCAATGA
Opt. T..CTC...C..G.....G.....GAG...A.....G..C..C.....A.....C..G.....C.....A..T.....

810 820 830 840 850 860 870 880 890 900
MerTK CAAAGGGCTGACCGTGTCCAGGGAGTGCAGATCAACATCAAAGCAATTCCTCCCACTGAAGTCAAGTCAAGTCAAGTCAAGTCAAGTCAAGTCAAGT
Opt. ...G..C.....A..G..C.....G..C.....T..T..T.....G..GTCT...A.G..T..T..C..T..TCA..C

910 920 930 940 950 960 970 980 990 1000
MerTK CTGATCTCCGGTTCCTGGTTTTGATGGATACTCCCGTTCAGGAATGTCAGCATTGAGGTCAAGGAGCTGATCCCGTGAATAGGCTCAGTCATGA
Opt.TAG.....G..C..C.....G...AG...T...C..C..C...TC...C.....G..C..C..T.....G.....

1010 1020 1030 1040 1050 1060 1070 1080 1090 1100
MerTK TTTTAAACACCTCTGCCTTACCACATCTGTACCAATCAAGCAGCTGCAAGCCCTGGCTAATTACAGCATTGGTGTTCCTGCATGAATGAAATAGGCTG
Opt. .C..C.....AGC.....C..G.....G.....G.....A.....T.....G..T.....A.....TTC...A..C..T..T.....C..G..C..A..

1110 1120 1130 1140 1150 1160 1170 1180 1190 1200
MerTK GTCTGACGTGAGCCCTTGGATTTAGCCAGCAGCACTGAAGGAGCCCATCAGTAGCACCTTTAAATGTCACCTGTGTTCTGAATGAATCTAGTGATAAT
Opt. .AGC..C...TC...C.....G...TTCT..T..C...C..T..CAGT..G.....C.G.....G..C..C..C.....G.....C..C..

1210 1220 1230 1240 1250 1260 1270 1280 1290 1300
MerTK GTGGACATCAGATGGATGAAGCCCTCCGACTAAGCAGCAGGATGGAGAACTGGTGGCTACCGGATATCCCACTGTGGCAGAGTGCAGGGATTCCAAAG
Opt.C.G.....C..T..A..A.....C.....C..G...A..A..T.....C..C..C..A..G..

1310 1320 1330 1340 1350 1360 1370 1380 1390 1400
MerTK AGCTCTTGGAGGAGTTGGCCAGAATGGCCAGCCGAGCTCGGATCTCTGTTCAAGTCCACAATGCTACGTGCACAGTGAAGGATGGAGCCGTCCAGCAGT
Opt.GC.....G..A.....TC.A.G..A..C..T.....G..G.....T..C..C..A...T...C..A..C...T.....C.G..

1410 1420 1430 1440 1450 1460 1470 1480 1490 1500
MerTK GGGAGTTGGCCCTTCACTGATCCAGTGAATAATTTATCCCTGCACAGCGTTGGGTAGATTATGCCCTTCACTCCGGCCCTGGCAACGCAGAT
Opt. C.....G..A.....C..C..C..G..T..C.....C.....A.....G.....T..AAGC..A..T..A..A..A.....T..C

1510 1520 1530 1540 1550 1560 1570 1580 1590 1600
MerTK CCTGTGCTCATCATCTTGGCTGCTTTTGGGATTTATTTGATGGGTGATTTTATACATCTCCTTGGCCATCAGAAAAGAGTCCAGGAGACAAAGT
Opt. .C.....G.....T..C..A.....C..C..CC.....CC...CC.G.....T..C.....C...GC.G..G.....A..

1610 1620 1630 1640 1650 1660 1670 1680 1690 1700
MerTK TTGGGAATGCATTACAGAGGAGGATTCTGAATTAGTGGTGAATTATAGCAAGAAATCCTTCTGTCGGCGAGCCATTGAAGTACCTTACATAGCTT
Opt.T.....T.....A..CAG...C.G.....C..C.....T..C.....A..T.....A...T..C.....G...C.G.....C..

1710 1720 1730 1740 1750 1760 1770 1780 1790 1800
MerTK GGGAGTCACTGAGGAACTACAAAATAAAGTGAAGATGTTGTGATGACAGGAATCTTCTAATCTTGGAAAATCTGGGTGAAGGAGAGTTGGGTCT
Opt. ...C..GTCC.....G..G.....G..G..G..C..G..C..C..T.....C..G..G..C..G.....G..G.....C.....

1810 1820 1830 1840 1850 1860 1870 1880 1890 1900
MerTK GTAATGGAAGAAATCTTAAGCAGGAAGATGGGACCTCTCTGAAAGTGGCAGTGAAGACCATGAAGTTGGACAACCTCTTACAGCGGGAGATCCGAGGAGT
Opt. ..G.....G.....G.....C..AAG.....C.....C.....T.....AC.....C..T.....C..T.....A..

1910 1920 1930 1940 1950 1960 1970 1980 1990 2000
MerTK TTCTCAGTGAGGCAGCTGCATGAAAGACTTCAGCCCAAAATGTCATTGCACTTCTAGGTGTGTATAGAAATGAGCTCTCAAGGCATCCCAAGGCC
Opt.GTCA..A.....C.....G..T.....C.....A.....G..G..C.....C..C.....T..A..G..G..T..C.....

2010 2020 2030 2040 2050 2060 2070 2080 2090 2100
MerTK CATGTAATTTTACCTTTCATGAATAACGGGGACCTGCATACTTACTTCTTATCCCGATTGGAGACAGGACCAAGCATATTCCTCTGCAGACACTA
Opt. T.....C..CC.G.....T.....C.....C.G..G.....T..CC.....C.....T.....A.....C..G

2110 2120 2130 2140 2150 2160 2170 2180 2190 2200
MerTK TTGAAGTTCATGGTGGATTTGCCCTGGGAATGGAGTATCTGAGCAACAGGAATTTCTTCTCATCGAGATTAGCTGCTCGAAACTGCATGTTGGAGATG
Opt. C.....C.....C.....G.....TC...C.....C..G..A.....CC.G.....AA.G..T.....C.....C..C..

2210 2220 2230 2240 2250 2260 2270 2280 2290 2300

```

MerTK ACATGACTGTCGTGTTGCGGACTTCGGCCTCTCTAAGAAGATTTACAGTGGCGATTATTACCGCCAAGGCCGATTGCTAAGATGCCTGTAAATGGAT
Opt.  .T....C..G..C..G..C....T..A..GAGC....A..C...TCA..A....C..TA..A..G...A.G..C..C.....C..C.....

      2310      2320      2330      2340      2350      2360      2370      2380      2390      2400
MerTK CGCCATAGAAAGTCTTGCAGACCGAGTCTACACAAGTAAAAGTGATGTGTGGGCATTGGCGTGACCATGTGGGAAATAGCTACGCGGGGAATGACTCCC
Opt.  ...A..T.....C..G..C.....G.....TC...G.....C....T..C.....T.....G..T..A..AA..A..G.....A

      2410      2420      2430      2440      2450      2460      2470      2480      2490      2500
MerTK TATCCTGGGGTCCAGAACCATGAGATGTATGACTATCTCTCCATGGCCACAGGTTGAAGCAGCCGAAGACTGCCTGGATGAACTGTATGAAATAATGT
Opt.  ....C..A..G.....C.....C..T....G..G..C..G..TC..C.....A.....G.....C.....C....

      2510      2520      2530      2540      2550      2560      2570      2580      2590      2600
MerTK ACTCTTGCTGGAGAACCGATCCCTTAGACCGCCACCTTTTCAGTATTGAGGCTGCAGCTAGAAAACTCTTAGAAAAGTTGCCTGACGTTCCGGAACCA
Opt.  .TAGC..T.....C..C..G..TA.G..T..A..CAGT..GC..C.....G..G.....GC.G...TCAC....C.....G..A..T..

      2610      2620      2630      2640      2650      2660      2670      2680      2690      2700
MerTK AGCAGACGTTATTTACGTCAATACACAGTTGCTGGAGAGCTCTGAGGGCCTGGCCAGGGCTCCACCTTGCTCCACTGGACTTGAACATCGACCCCTGAC
Opt.  G..C..T..G..C.....C..C..C.....AGC..A..G....A....AG.....G..C.....C....T..T....C...T

      2710      2720      2730      2740      2750      2760      2770      2780      2790      2800
MerTK TCTATAATTGCCTCCTGCATCCCGCGCTGCCATCAGTGTGGTCACAGCAGAAGTTCATGACAGCAAACCTCATGAAGGACGGTACATCCTGAATGGGG
Opt.  ....C.....AAGT.....A.G..C..T...TCC.....C..T..G..G..C..TTCT..G.....C..C..T.....C..A.

      2810      2820      2830      2840      2850      2860      2870      2880      2890      2900
MerTK GCAGTGGGAATGGGAAGATCTGACTTCTGCCCTCTGCTGCAGTACAGCTGAAAAGAACAGTGTTTTACCGGGGAGAGACTGTTAGGAATGGGGT
Opt.  ..TC.....G..C.....C....T..AAG...A..C.....A..G..A..T..C..GC.G..A..A..AC.C..G..GC.A..C.....

      2910      2920      2930      2940      2950      2960      2970      2980      2990
MerTK CTCTGGTCCCATTCGAGCATGCTGCCCTTGGGAAGCTCAT---TGCCCGATGAACTTTTGTTGCTGACGACTCCTCAGAAGGCTCAGAAGTCCGTGATG
Opt.  ...A...AG..C..T..T.....C..---.....AGCC...A..C.....GC.....T..T..AAGC..G..G..C..G..G.....

3000
MerTK TGA
Opt.  .A.

```

Appendix 1: Codon-optimized *MERTK* sequence. Alignment of the codon-optimized *MERTK* construct (Opt.) with the human *MERTK* mRNA coding region (*MERTK*). The amino acid sequence of the Opt construct is identical to the sequence encoded by the *MERTK* mRNA.

Principal Investigator: Prof. Bryan Heit
File Number: 104010
Review Level: Delegated
Protocol Title: Venipuncture for Immune Cell Purification
Department & Institution: Schulich School of Medicine and Dentistry/Microbiology & Immunology, Western University
Sponsor:
Ethics Approval Date: October 09, 2013 **Expiry Date:** July 31, 2016
Documents Reviewed & Approved & Documents Received for Information:

Document Name	Comments	Version Date
Protocol	Microscopy & analysis protocols	2013/07/02
Letter of Information & Consent	Consent Statement	2013/07/02
Protocol	Preparation of phagocytic/efferoctytic targets	2013/07/02
Protocol	Western blotting protocol	2013/07/02
Protocol	Mass spectrometry protocols	2013/07/02
Protocol	Macrophage & neutrophil isolation and differntiation methods.	2013/07/02
Western University Protocol		2013/07/03
Other	Reply to Reviewer Request #4 - attach data collection forms.	2013/08/13
Letter of Information & Consent	Consent form	2013/08/22
Advertisement	Advertisement poster	2013/08/22


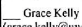
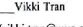
This is to notify you that The University of Western Ontario Research Ethics Board for Health Sciences Research Involving Human Subjects (HSREB) which is organized and operates according to the Tri-Council Policy Statement: Ethical Conduct of Research Involving Humans and the Health Canada/ICH Good Clinical Practice Practices: Consolidated Guidelines; and the applicable laws and regulations of Ontario has reviewed and granted approval to the above referenced revision(s) or amendment(s) on the approval date noted above. The membership of this REB also complies with the membership requirements for REB's as defined in Division 5 of the Food and Drug Regulations.

The ethics approval for this study shall remain valid until the expiry date noted above assuming timely and acceptable responses to the HSREB's periodic requests for surveillance and monitoring information. If you require an updated approval notice prior to that time you must request it using the University of Western Ontario Updated Approval Request Form.

Members of the HSREB who are named as investigators in research studies, or declare a conflict of interest, do not participate in discussion related to, nor vote on, such studies when they are presented to the HSREB.

The Chair of the HSREB is Dr. Joseph Gilbert. The HSREB is registered with the U.S. Department of Health & Human Services under the IRB registration number IRB 0000940.

Ethics Officer to Contact for Further Information

 Erika Basile (ebasile@uwo.ca)	 Grace Kelly (grace.kelly@uwo.ca)	 Vikki Tran (vikki.tran@uwo.ca)
---	--	---

This is an official document. Please retain the original in your files.

Western University, Research, Support Services Bldg., Rm. 5150
 London, ON, Canada N6A 3K7 t. 519.661.3036 f. 519.850.2466 www.uwo.ca/research/services/ethics

Appendix 2: Ethics approval for performing venipuncture on human participants.

Appendix 3: Fisher's Exact Test of Neutrality for Sequence Pairs for TAM receptors. All available primate sequences for *TYRO3* (A), *AXL* (B), and *MERTK* (C) were used to test the probability of rejecting the null hypothesis of strict neutrality in favour of a hypothesis of positive selection for each sequence pair. Data are represented as p-values, where p values less than 0.05 are significant.

A)

		TYRO3											
		1	2	3	4	5	6	7	8	9	10	11	12
<i>Homo sapiens</i>	1												
<i>Pan troglodytes</i>	2	0.672											
<i>Papio anubis</i>	3	1.000	1.000										
<i>Pan paniscus</i>	4	0.671	1.000	1.000									
<i>Callithrix jacchus</i>	5	1.000	1.000	1.000	1.000								
<i>Chlorocebus sabaesus</i>	6	1.000	1.000	1.000	1.000	1.000							
<i>Gorilla gorilla</i>	7	1.000	1.000	1.000	1.000	1.000	1.000						
<i>Saimiri boliviensis</i>	8	1.000	1.000	1.000	1.000	1.000	1.000	1.000					
<i>Pongo abelii</i>	9	0.465	0.583	1.000	0.413	0.339	1.000	0.364	0.339				
<i>Nomascus leucogenys</i>	10	1.000	1.000	1.000	1.000	1.000	1.000	1.000	1.000	0.267			
<i>Macaca mulatta</i>	11	1.000	1.000	1.000	1.000	1.000	1.000	1.000	1.000	1.000	1.000		
<i>Macaca fascicularis</i>	12	1.000	1.000	1.000	1.000	1.000	1.000	1.000	1.000	1.000	1.000	1.000	
<i>Tarsius syrichta</i>	13	1.000	1.000	1.000	1.000	1.000	1.000	1.000	1.000	0.321	1.000	1.000	1.000
<i>Otolemur garnettii</i>	14	1.000	1.000	1.000	1.000	1.000	1.000	1.000	1.000	1.000	1.000	1.000	1.000

B)

		AXL											
<i>Homo sapiens</i>	1												
<i>Gorilla gorilla</i>	2	1.000											
<i>Callithrix jacchus</i>	3	1.000	1.000										
<i>Pan paniscus</i>	4	0.567	1.000	1.000									
<i>Tarsius syrichta</i>	5	1.000	1.000	1.000	1.000								
<i>Chlorocebus sabaesus</i>	6	0.453	1.000	1.000	0.565	1.000							
<i>Otolemur garnettii</i>	7	1.000	1.000	1.000	1.000	1.000	1.000						
<i>Pongo abelii</i>	8	1.000	1.000	1.000	1.000	1.000	1.000	1.000					
<i>Papio anubis</i>	9	1.000	1.000	1.000	1.000	1.000	0.620	1.000	1.000				
<i>Saimiri boliviensis</i>	10	1.000	1.000	1.000	1.000	1.000	1.000	1.000	1.000	1.000			
<i>Pan troglodytes</i>	11	1.000	1.000	1.000	1.000	1.000	0.480	1.000	1.000	1.000	1.000		
<i>Nomascus leucogenys</i>	12	1.000	1.000	1.000	1.000	1.000	1.000	1.000	1.000	1.000	1.000	1.000	
<i>Macaca fascicularis</i>	13	1.000	1.000	1.000	1.000	1.000	1.000	1.000	1.000	1.000	1.000	1.000	1.000

C)

		MERTK											
<i>Homo sapiens</i>	1												
<i>Gorilla gorilla</i>	2	1.000											
<i>Pongo abelii</i>	3	1.000	1.000										
<i>Pan troglodytes</i>	4	1.000	1.000	1.000									
<i>Nomascus leucogenys</i>	5	1.000	1.000	1.000	1.000								
<i>Macaca mulatta</i>	6	1.000	1.000	1.000	1.000	1.000							
<i>Macaca fascicularis</i>	7	1.000	1.000	1.000	1.000	1.000	1.000						
<i>Papio anubis</i>	8	1.000	1.000	1.000	1.000	1.000	1.000	1.000					
<i>Tarsius syrichta</i>	9	1.000	1.000	1.000	1.000	1.000	1.000	1.000	1.000				
<i>Chlorocebus sabaesus</i>	10	1.000	1.000	1.000	1.000	1.000	1.000	1.000	1.000	1.000			
<i>Saimiri boliviensis</i>	11	1.000	1.000	1.000	1.000	1.000	1.000	1.000	1.000	1.000	1.000		
<i>Otolemur garnettii</i>	12	1.000	1.000	1.000	1.000	1.000	1.000	1.000	1.000	1.000	1.000	1.000	

Appendix 4: Z-Tests for TAM receptors. Whole gene evolutionary Z-tests were conducted using the Nei-Gojobori method in MEGA6 using all available primate sequences from TYRO3 (A), AXL (B), and MERTK (C). Tests show the probability of rejecting the null hypothesis of strict-neutrality, purifying or positive selection for each TAM receptor. Values of p are shown in the bottom left of each table and values less than 0.05 are considered significant. Test values are shown in the right diagonal section of each table; $K_a - K_s$ for neutral and positive selection, and $K_s - K_a$ for purifying selection.

A)

		Neutrality													
		1	2	3	4	5	6	7	8	9	10	11	12	13	14
<i>Homo sapiens</i>	1		0.0177	-1.3565	0.0179	-0.7406	-1.3592	-0.8380	-1.0027	0.4108	-0.7366	-1.6423	-1.6255	-2.9270	-4.0163
<i>Pan troglodytes</i>	2	0.9859		-1.2718	-0.8883	-0.5071	-1.2746	-1.0679	-1.1326	0.1130	-0.9322	-1.5588	-1.5388	-2.8352	-4.1119
<i>Papio anubis</i>	3	0.1775	0.2059		-0.7366	-0.6756	-0.9748	-1.1810	-0.5957	-0.8844	-1.5217	-0.3126	-0.1854	-2.3948	-4.0503
<i>Pan paniscus</i>	4	0.9858	0.3761	0.4628		-0.5064	-0.7395	-0.4685	-0.7884	0.5987	-0.4015	-1.0515	-1.0145	-2.8352	-3.9476
<i>Callithrix jacchus</i>	5	0.4604	0.6130	0.5006	0.6135		-1.0553	-0.5963	-1.5207	0.7954	-0.8615	-0.7506	-0.8653	-3.5887	-3.9973
<i>Chlorocebus sabaeus</i>	6	0.1766	0.2049	0.3316	0.4610	0.2934		-1.1844	-0.8084	-0.3772	-1.6735	-1.2633	-1.3934	-2.3948	-3.9825
<i>Gorilla gorilla</i>	7	0.4037	0.2877	0.2399	0.6402	0.5521	0.2386		-0.8107	1.0013	-1.1025	-1.4386	-1.4123	-3.1806	-4.0325
<i>Saimiri boliviensis</i>	8	0.3180	0.2596	0.5525	0.4320	0.1310	0.4205	0.4191		0.8062	-1.2234	-0.9406	-0.9072	-3.4236	-3.9609
<i>Pongo abelii</i>	9	0.6820	0.9102	0.3783	0.5505	0.4280	0.7067	0.3187	0.4217		1.0401	-0.7537	-0.6109	2.1350	-0.0950
<i>Nomascus leucogenys</i>	10	0.4628	0.3531	0.1307	0.6888	0.3907	0.0968	0.2724	0.2236	0.3004		-1.3362	-1.7470	-2.1560	-3.4313
<i>Macaca mulatta</i>	11	0.1031	0.1217	0.7551	0.2951	0.4543	0.2089	0.1529	0.3488	0.4525	0.1840		-1.0825	-2.2071	-4.2012
<i>Macaca fascicularis</i>	12	0.1067	0.1265	0.8533	0.3124	0.3886	0.1661	0.1604	0.3661	0.5424	0.0832	0.2812		-2.5764	-4.1151
<i>Tarsius syrichta</i>	13	0.0041	0.0054	0.0182	0.0054	0.0005	0.0182	0.0019	0.0008	0.0348	0.0331	0.0292	0.0112		-3.6473
<i>Otolemur garnettii</i>	14	0.0001	0.0001	0.0001	0.0001	0.0001	0.0001	0.0001	0.0001	0.9245	0.0008	0.0001	0.0001	0.0004	
		Purifying													
		1	2	3	4	5	6	7	8	9	10	11	12	13	14
<i>Homo sapiens</i>	1		-0.0177	1.3565	-0.0179	0.7406	1.3592	0.8380	1.0027	-0.4108	0.7366	1.6423	1.6255	2.9270	4.0163
<i>Pan troglodytes</i>	2	1.0000		1.2718	0.8883	0.5071	1.2746	1.0679	1.1326	-0.1130	0.9322	1.5588	1.5388	2.8352	4.1119
<i>Papio anubis</i>	3	0.0887	0.1029		0.7366	0.6756	0.9748	1.1810	0.5957	0.8844	1.5217	0.3126	0.1854	2.3948	4.0503
<i>Pan paniscus</i>	4	1.0000	0.1881	0.2314		0.5064	0.7395	0.4685	0.7884	-0.5987	0.4015	1.0515	1.0145	2.8352	3.9476
<i>Callithrix jacchus</i>	5	0.2302	0.3065	0.2503	0.3067		1.0553	0.5963	1.5207	-0.7954	0.8615	0.7506	0.8653	3.5887	3.9973
<i>Chlorocebus sabaeus</i>	6	0.0883	0.1025	0.1658	0.2305	0.1467		1.1844	0.8084	0.3772	1.6735	1.2633	1.3934	2.3948	3.9825
<i>Gorilla gorilla</i>	7	0.2018	0.1439	0.1200	0.3201	0.2761	0.1193		0.8107	-1.0013	1.1025	1.4386	1.4123	3.1806	4.0325
<i>Saimiri boliviensis</i>	8	0.1590	0.1298	0.2763	0.2160	0.0655	0.2102	0.2096		-0.8062	1.2234	0.9406	0.9072	3.4236	3.9609
<i>Pongo abelii</i>	9	1.0000	1.0000	0.1891	1.0000	1.0000	0.3534	1.0000	1.0000		-1.0401	0.7537	0.6109	-2.1350	0.0950
<i>Nomascus leucogenys</i>	10	0.2314	0.1765	0.0654	0.3444	0.1953	0.0484	0.1362	0.1118	1.0000		1.3362	1.7470	2.1560	3.4313
<i>Macaca mulatta</i>	11	0.0516	0.0608	0.3776	0.1476	0.2272	0.1045	0.0764	0.1744	0.2262	0.0920		1.0825	2.2071	4.2012
<i>Macaca fascicularis</i>	12	0.0533	0.0632	0.4266	0.1562	0.1943	0.0830	0.0802	0.1831	0.2712	0.0416	0.1406		2.5764	4.1151
<i>Tarsius syrichta</i>	13	0.0020	0.0027	0.0091	0.0027	0.0002	0.0091	0.0009	0.0004	1.0000	0.0165	0.0146	0.0056		3.6473
<i>Otolemur garnettii</i>	14	0.0001	0.0000	0.0000	0.0001	0.0001	0.0001	0.0000	0.0001	0.4622	0.0004	0.0000	0.0000	0.0000	0.0002
		Positive													
		1	2	3	4	5	6	7	8	9	10	11	12	13	14
<i>Homo sapiens</i>	1		0.0177	-1.3565	0.0179	-0.7406	-1.3592	-0.8380	-1.0027	0.4108	-0.7366	-1.6423	-1.6255	-2.9270	-4.0163
<i>Pan troglodytes</i>	2	0.4930		-1.2718	-0.8883	-0.5071	-1.2746	-1.0679	-1.1326	0.1130	-0.9322	-1.5588	-1.5388	-2.8352	-4.1119
<i>Papio anubis</i>	3	1.0000	1.0000		-0.7366	-0.6756	-0.9748	-1.1810	-0.5957	-0.8844	-1.5217	-0.3126	-0.1854	-2.3948	-4.0503
<i>Pan paniscus</i>	4	0.4929	1.0000	1.0000		-0.5064	-0.7395	-0.4685	-0.7884	0.5987	-0.4015	-1.0515	-1.0145	-2.8352	-3.9476
<i>Callithrix jacchus</i>	5	1.0000	1.0000	1.0000	1.0000		-1.0553	-0.5963	-1.5207	0.7954	-0.8615	-0.7506	-0.8653	-3.5887	-3.9973
<i>Chlorocebus sabaeus</i>	6	1.0000	1.0000	1.0000	1.0000	1.0000		-1.1844	-0.8084	-0.3772	-1.6735	-1.2633	-1.3934	-2.3948	-3.9825
<i>Gorilla gorilla</i>	7	1.0000	1.0000	1.0000	1.0000	1.0000	1.0000		-0.8107	1.0013	-1.1025	-1.4386	-1.4123	-3.1806	-4.0325
<i>Saimiri boliviensis</i>	8	1.0000	1.0000	1.0000	1.0000	1.0000	1.0000	1.0000		0.8062	-1.2234	-0.9406	-0.9072	-3.4236	-3.9609
<i>Pongo abelii</i>	9	0.3410	0.4551	1.0000	0.2752	0.2140	1.0000	0.1594	0.2109		1.0401	-0.7537	-0.6109	2.1350	-0.0950
<i>Nomascus leucogenys</i>	10	1.0000	1.0000	1.0000	1.0000	1.0000	1.0000	1.0000	1.0000	0.1502		-1.3362	-1.7470	-2.1560	-3.4313
<i>Macaca mulatta</i>	11	1.0000	1.0000	1.0000	1.0000	1.0000	1.0000	1.0000	1.0000	1.0000	1.0000		-1.0825	-2.2071	-4.2012
<i>Macaca fascicularis</i>	12	1.0000	1.0000	1.0000	1.0000	1.0000	1.0000	1.0000	1.0000	1.0000	1.0000	1.0000		-2.5764	-4.1151
<i>Tarsius syrichta</i>	13	1.0000	1.0000	1.0000	1.0000	1.0000	1.0000	1.0000	1.0000	0.0174	1.0000	1.0000	1.0000		-3.6473
<i>Otolemur garnettii</i>	14	1.0000	1.0000	1.0000	1.0000	1.0000	1.0000	1.0000	1.0000	1.0000	1.0000	1.0000	1.0000	1.0000	

B)

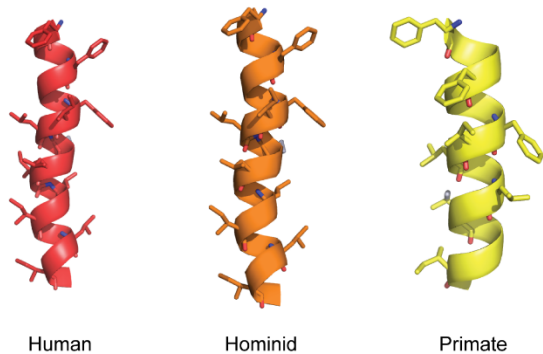
		Neutrality												
		1	2	3	4	5	6	7	8	9	10	11	12	13
<i>Homo sapiens</i>	1		-0.5088	-1.3002	0.2058	-0.3979	0.4604	-2.6713	-0.2105	-0.1618	-0.4004	-0.2553	-1.3457	-0.6455
<i>Gorilla gorilla</i>	2	0.6118		-1.2288	-0.3377	-0.8055	-0.2089	-2.9325	-0.4659	-0.8667	-0.4538	-0.6060	-2.0506	-1.3273
<i>Callithrix jacchus</i>	3	0.1960	0.2215		-1.7917	-1.1276	-1.0535	-2.2854	-2.3187	-1.3474	-1.6635	-1.6784	-1.5932	-1.8724
<i>Pan paniscus</i>	4	0.8373	0.7362	0.0757		-0.6757	0.1449	-2.8721	-0.4735	-0.4339	-0.9241	-0.2841	-0.6666	-0.6146
<i>Tarsius syrichta</i>	5	0.6914	0.4221	0.2617	0.5006		-0.5798	-2.4211	-1.7638	-1.1104	-0.7436	-0.7059	-0.6508	-1.9622
<i>Chlorocebus sabaeus</i>	6	0.6460	0.8349	0.2942	0.8850	0.5631		-2.5182	-0.4053	0.0239	-0.4158	0.3779	-0.2788	-1.4093
<i>Otolemur garnettii</i>	7	0.0086	0.0040	0.0240	0.0048	0.0170	0.0131		-2.9827	-2.8906	-1.9953	-2.8406	-3.0002	-3.6608
<i>Pongo abelii</i>	8	0.8336	0.6421	0.0221	0.6367	0.0803	0.6860	0.0035		-0.7987	-1.6918	-0.4740	-1.4580	-0.7696
<i>Papio anubis</i>	9	0.8718	0.3879	0.1804	0.6651	0.2690	0.9810	0.0046	0.4261		-0.5296	-0.2232	-0.8064	-1.2528
<i>Saimiri boliviensis</i>	10	0.6896	0.6508	0.0988	0.3573	0.4586	0.6783	0.0483	0.0933	0.5974		-1.0122	-1.4288	-1.9635
<i>Pan troglodytes</i>	11	0.7989	0.5456	0.0959	0.7768	0.4816	0.7061	0.0053	0.6364	0.8237	0.3135		-0.9043	-0.3740
<i>Nomascus leucogenys</i>	12	0.1809	0.0425	0.1138	0.5063	0.5164	0.7808	0.0033	0.1474	0.4216	0.1557	0.3676		-1.5037
<i>Macaca fascicularis</i>	13	0.5199	0.1869	0.0636	0.5400	0.0521	0.1613	0.0004	0.4431	0.2127	0.0519	0.7091	0.1353	
		Purifying												
		1	2	3	4	5	6	7	8	9	10	11	12	13
<i>Homo sapiens</i>	1		0.5088	1.3002	-0.2058	0.3979	-0.4604	2.6713	0.2105	0.1618	0.4004	0.2553	1.3457	0.6455
<i>Gorilla gorilla</i>	2	0.3059		1.2288	0.3377	0.8055	0.2089	2.9325	0.4659	0.8667	0.4538	0.6060	2.0506	1.3273
<i>Callithrix jacchus</i>	3	0.0980	0.1108		1.7917	1.1276	1.0535	2.2854	2.3187	1.3474	1.6635	1.6784	1.5932	1.8724
<i>Pan paniscus</i>	4	1.0000	0.3681	0.0378		0.6757	-0.1449	2.8721	0.4735	0.4339	0.9241	0.2841	0.6666	0.6146
<i>Tarsius syrichta</i>	5	0.3457	0.2111	0.1309	0.2503		0.5798	2.4211	1.7638	1.1104	0.7436	0.7059	0.6508	1.9622
<i>Chlorocebus sabaeus</i>	6	1.0000	0.4174	0.1471	1.0000	0.2816		2.5182	0.4053	-0.0239	0.4158	-0.3779	0.2788	1.4093
<i>Otolemur garnettii</i>	7	0.0043	0.0020	0.0120	0.0024	0.0085	0.0066		2.9827	2.8906	1.9953	2.8406	3.0002	3.6608
<i>Pongo abelii</i>	8	0.4168	0.3211	0.0111	0.3184	0.0402	0.3430	0.0017		0.7987	1.6918	0.4740	1.4580	0.7696
<i>Papio anubis</i>	9	0.4359	0.1939	0.0902	0.3326	0.1345	1.0000	0.0023	0.2130		0.5296	0.2232	0.8064	1.2528
<i>Saimiri boliviensis</i>	10	0.3448	0.3254	0.0494	0.1786	0.2293	0.3391	0.0241	0.0466	0.2987		1.0122	1.4288	1.9635
<i>Pan troglodytes</i>	11	0.3995	0.2728	0.0479	0.3884	0.2408	1.0000	0.0026	0.3182	0.4119	0.1567		0.9043	0.3740
<i>Nomascus leucogenys</i>	12	0.0905	0.0212	0.0569	0.2532	0.2582	0.3904	0.0016	0.0737	0.2108	0.0778	0.1838		1.5037
<i>Macaca fascicularis</i>	13	0.2599	0.0935	0.0318	0.2700	0.0260	0.0807	0.0002	0.2215	0.1064	0.0259	0.3545	0.0676	
		Positive												
		1	2	3	4	5	6	7	8	9	10	11	12	13
<i>Homo sapiens</i>	1		-0.5088	-1.3002	0.2058	-0.3979	0.4604	-2.6713	-0.2105	-0.1618	-0.4004	-0.2553	-1.3457	-0.6455
<i>Gorilla gorilla</i>	2	1.0000		-1.2288	-0.3377	-0.8055	-0.2089	-2.9325	-0.4659	-0.8667	-0.4538	-0.6060	-2.0506	-1.3273
<i>Callithrix jacchus</i>	3	1.0000	1.0000		-1.7917	-1.1276	-1.0535	-2.2854	-2.3187	-1.3474	-1.6635	-1.6784	-1.5932	-1.8724
<i>Pan paniscus</i>	4	0.4187	1.0000	1.0000		-0.6757	0.1449	-2.8721	-0.4735	-0.4339	-0.9241	-0.2841	-0.6666	-0.6146
<i>Tarsius syrichta</i>	5	1.0000	1.0000	1.0000	1.0000		-0.5798	-2.4211	-1.7638	-1.1104	-0.7436	-0.7059	-0.6508	-1.9622
<i>Chlorocebus sabaeus</i>	6	0.3230	1.0000	1.0000	0.4425	1.0000		-2.5182	-0.4053	0.0239	-0.4158	0.3779	-0.2788	-1.4093
<i>Otolemur garnettii</i>	7	1.0000	1.0000	1.0000	1.0000	1.0000	1.0000		-2.9827	-2.8906	-1.9953	-2.8406	-3.0002	-3.6608
<i>Pongo abelii</i>	8	1.0000	1.0000	1.0000	1.0000	1.0000	1.0000	1.0000		-0.7987	-1.6918	-0.4740	-1.4580	-0.7696
<i>Papio anubis</i>	9	1.0000	1.0000	1.0000	1.0000	1.0000	0.4905	1.0000	1.0000		-0.5296	-0.2232	-0.8064	-1.2528
<i>Saimiri boliviensis</i>	10	1.0000	1.0000	1.0000	1.0000	1.0000	1.0000	1.0000	1.0000	1.0000		-1.0122	-1.4288	-1.9635
<i>Pan troglodytes</i>	11	1.0000	1.0000	1.0000	1.0000	1.0000	0.3531	1.0000	1.0000	1.0000	1.0000		-0.9043	-0.3740
<i>Nomascus leucogenys</i>	12	1.0000	1.0000	1.0000	1.0000	1.0000	1.0000	1.0000	1.0000	1.0000	1.0000	1.0000		-1.5037
<i>Macaca fascicularis</i>	13	1.0000	1.0000	1.0000	1.0000	1.0000	1.0000	1.0000	1.0000	1.0000	1.0000	1.0000	1.0000	

C)

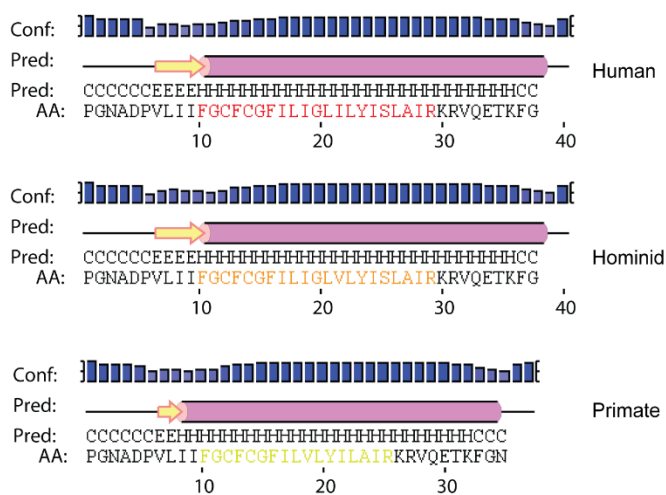
		Neutrality											
		1	2	3	4	5	6	7	8	9	10	11	12
<i>Homo sapiens</i>	1		-1.3274	-4.2472	-1.8871	-3.2994	-5.5268	-5.8634	-6.2358	-11.4481	-5.8279	-7.2380	-11.1601
<i>Gorilla gorilla</i>	2	0.1869		-4.2148	-1.8369	-3.5671	-5.4446	-5.7682	-6.2115	-10.7631	-5.9708	-7.3304	-10.7901
<i>Pongo abelii</i>	3	0.0000	0.0000		-4.8435	-3.7643	-5.8965	-6.0396	-6.5839	-11.2897	-5.9812	-7.5660	-11.1269
<i>Pan troglodytes</i>	4	0.0616	0.0687	0.0000		-4.1074	-6.1913	-6.5073	-6.8595	-11.7498	-6.3998	-7.7204	-11.2448
<i>Nomascus leucogenys</i>	5	0.0013	0.0005	0.0003	0.0001		-5.0211	-5.2298	-5.7693	-10.8395	-5.2982	-7.1070	-10.8292
<i>Macaca mulatta</i>	6	0.0000	0.0000	0.0000	0.0000	0.0000		-1.1536	-3.6155	-11.1767	-3.6094	-6.9410	-11.0363
<i>Macaca fascicularis</i>	7	0.0000	0.0000	0.0000	0.0000	0.0000	0.2510		-3.8413	-11.4172	-3.8620	-7.2260	-11.1459
<i>Papio anubis</i>	8	0.0000	0.0000	0.0000	0.0000	0.0000	0.0004	0.0002		-11.6141	-3.8907	-7.3265	-11.4114
<i>Tarsius syrichta</i>	9	0.0000	0.0000	0.0000	0.0000	0.0000	0.0000	0.0000	0.0000		-11.0365	-10.9746	-11.9989
<i>Chlorocebus sabaues</i>	10	0.0000	0.0000	0.0000	0.0000	0.0000	0.0004	0.0002	0.0002	0.0000		-6.9330	-11.0954
<i>Saimiri boliviensis</i>	11	0.0000	0.0000	0.0000	0.0000	0.0000	0.0000	0.0000	0.0000	0.0000	0.0000		-10.9440
<i>Otolemur garnettii</i>	12	0.0000	0.0000	0.0000	0.0000	0.0000	0.0000	0.0000	0.0000	0.0000	0.0000	0.0000	
		Purifying											
		1	2	3	4	5	6	7	8	9	10	11	12
<i>Homo sapiens</i>	1		1.3274	4.2472	1.8871	3.2994	5.5268	5.8634	6.2358	11.4481	5.8279	7.2380	11.1601
<i>Gorilla gorilla</i>	2	0.0935		4.2148	1.8369	3.5671	5.4446	5.7682	6.2115	10.7631	5.9708	7.3304	10.7901
<i>Pongo abelii</i>	3	0.0000	0.0000		4.8435	3.7643	5.8965	6.0396	6.5839	11.2897	5.9812	7.5660	11.1269
<i>Pan troglodytes</i>	4	0.0308	0.0343	0.0000		4.1074	6.1913	6.5073	6.8595	11.7498	6.3998	7.7204	11.2448
<i>Nomascus leucogenys</i>	5	0.0006	0.0003	0.0001	0.0000		5.0211	5.2298	5.7693	10.8395	5.2982	7.1070	10.8292
<i>Macaca mulatta</i>	6	0.0000	0.0000	0.0000	0.0000	0.0000		1.1536	3.6155	11.1767	3.6094	6.9410	11.0363
<i>Macaca fascicularis</i>	7	0.0000	0.0000	0.0000	0.0000	0.0000	0.1255		3.8413	11.4172	3.8620	7.2260	11.1459
<i>Papio anubis</i>	8	0.0000	0.0000	0.0000	0.0000	0.0000	0.0002	0.0001		11.6141	3.8907	7.3265	11.4114
<i>Tarsius syrichta</i>	9	0.0000	0.0000	0.0000	0.0000	0.0000	0.0000	0.0000	0.0000		11.0365	10.9746	11.9989
<i>Chlorocebus sabaues</i>	10	0.0000	0.0000	0.0000	0.0000	0.0000	0.0002	0.0001	0.0001	0.0000		6.9330	11.0954
<i>Saimiri boliviensis</i>	11	0.0000	0.0000	0.0000	0.0000	0.0000	0.0000	0.0000	0.0000	0.0000	0.0000		10.9440
<i>Otolemur garnettii</i>	12	0.0000	0.0000	0.0000	0.0000	0.0000	0.0000	0.0000	0.0000	0.0000	0.0000	0.0000	
		Positive											
		1	2	3	4	5	6	7	8	9	10	11	12
<i>Homo sapiens</i>	1		-1.3274	-4.2472	-1.8871	-3.2994	-5.5268	-5.8634	-6.2358	-11.4481	-5.8279	-7.2380	-11.1601
<i>Gorilla gorilla</i>	2	1.0000		-4.2148	-1.8369	-3.5671	-5.4446	-5.7682	-6.2115	-10.7631	-5.9708	-7.3304	-10.7901
<i>Pongo abelii</i>	3	1.0000	1.0000		-4.8435	-3.7643	-5.8965	-6.0396	-6.5839	-11.2897	-5.9812	-7.5660	-11.1269
<i>Pan troglodytes</i>	4	1.0000	1.0000	1.0000		-4.1074	-6.1913	-6.5073	-6.8595	-11.7498	-6.3998	-7.7204	-11.2448
<i>Nomascus leucogenys</i>	5	1.0000	1.0000	1.0000	1.0000		-5.0211	-5.2298	-5.7693	-10.8395	-5.2982	-7.1070	-10.8292
<i>Macaca mulatta</i>	6	1.0000	1.0000	1.0000	1.0000	1.0000		-1.1536	-3.6155	-11.1767	-3.6094	-6.9410	-11.0363
<i>Macaca fascicularis</i>	7	1.0000	1.0000	1.0000	1.0000	1.0000	1.0000		-3.8413	-11.4172	-3.8620	-7.2260	-11.1459
<i>Papio anubis</i>	8	1.0000	1.0000	1.0000	1.0000	1.0000	1.0000	1.0000		-11.6141	-3.8907	-7.3265	-11.4114
<i>Tarsius syrichta</i>	9	1.0000	1.0000	1.0000	1.0000	1.0000	1.0000	1.0000	1.0000		-11.0365	-10.9746	-11.9989
<i>Chlorocebus sabaues</i>	10	1.0000	1.0000	1.0000	1.0000	1.0000	1.0000	1.0000	1.0000	1.0000		-6.9330	-11.0954
<i>Saimiri boliviensis</i>	11	1.0000	1.0000	1.0000	1.0000	1.0000	1.0000	1.0000	1.0000	1.0000	1.0000		-10.9440
<i>Otolemur garnettii</i>	12	1.0000	1.0000	1.0000	1.0000	1.0000	1.0000	1.0000	1.0000	1.0000	1.0000	1.0000	

Appendix 5: *In silico* analysis of human and primate- and hominid-ancestral MERTK transmembrane domains. **A)** Predicted transmembrane domains of human (red), hominid (orange) and primate (yellow) MERTK were modeled using Phyre2. Hydrophobic residues are represented as sticks. **B)** Transmembrane secondary structure predictions for human, hominid and primate MERTK sequences. All sequences were analyzed using PSPRED. The relative confidence of secondary structure prediction is shown in blue bars. Highlighted residues correspond to the modelled helices in (A). **C)** A hydrophobic cluster analysis was conducted for the MERTK transmembrane domains. Hydrophobic residues are boxed, and non-hydrophobics are shown as diamonds and squares.

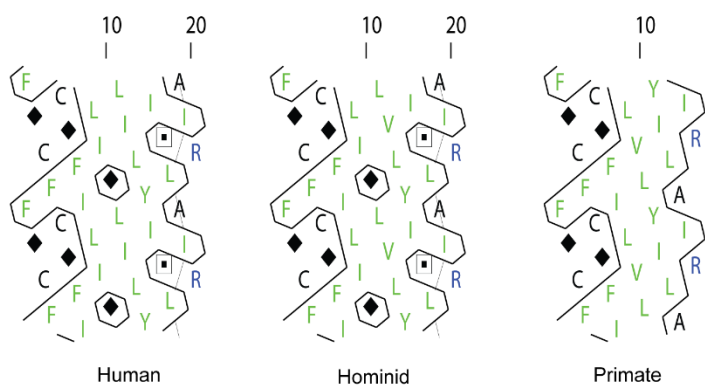
A.



B.



C.



Dear Amanda,

It is my pleasure to provide you with the *in silico* modeling data of the MerTK trans-membrane domain. I give you full permission to incorporate the data from the analysis in your Master's thesis for the Department of Microbiology and Immunology at Western University.

All the Best,



Brennan Dirk

Ph.D. Candidate
Department of Microbiology and Immunology
Western University

Appendix 6: Letter of permission for inclusion of appendix 5 in thesis.

Curriculum Vitae

Name: Amanda L. Evans

Post-secondary Education: University of Western Ontario, London, ON, Canada
2010-2014 BMSc (Hons: Microbiology and Immunology)

Honours and Awards: Microbiology and Immunology Travel Award, 2015, 2016.
Deans Honours List, 2011-2013.
Western Scholarship of Excellence, 2010.
Queen Elizabeth II Aiming for the Top Scholarship, 2010.

Related Work Experience:

Teaching Assistant, Univ. of Western Ontario, 2015.
Private Tutor, 2014.
Undergraduate Research Assistant, Univ. of Western Ontario,
2011-2013.
Research Assistant – Co-op placement, London Regional
Cancer Program, 2010.

Publications:

[1] Evans, A.L., Blackburn, J.W.D., Yin, C., and Heit, B. Quantitative efferocytosis assays.
Methods Mol. Biol. In press (2016).

Oral Presentation:

Amanda Evans, Ronald Flannagan, and Bryan Heit (May 2013). Regulation of phagocytosis by human CD16A and CD16B.
Ontario-Quebec Undergraduate Immunology Conference, University of Toronto, Toronto, Ontario

Poster Presentations:

Amanda Evans, Jack Blackburn, and Bryan Heit (April 2016). MERTK, but not other TAM receptors, has undergone recent positive selection in its signal peptide and transmembrane domain.
Canadian Society for Immunology, Ottawa, Ontario

Amanda Evans, Jack Blackburn, and Bryan Heit (March 2016). MERTK, but not other TAM receptors, has undergone recent positive selection in its signal peptide and transmembrane domain.

London Health Research Day, London, Ontario

Amanda Evans, Jack Blackburn, Ronald Flannagan and Bryan Heit (November 2015). Elucidating the efferocytic signalling pathway of MerTK and its contribution to inflammation and autoimmunity.

Infection and Immunity Research Forum, the University of Western Ontario, London, Ontario

Amanda Evans, Jack Blackburn, Ronald Flannagan and Bryan Heit (April 2015). Elucidating the efferocytic signalling pathway of MerTK receptor tyrosine kinase.

London Health Research Day, London, Ontario

Amanda Evans, Jack Blackburn, Ronald Flannagan and Bryan Heit (March 2015). Elucidating the efferocytic signalling pathway of MerTK receptor tyrosine kinase.

Annual McGill Biomedical Graduate Conference, McGill University, Montréal, Québec

Amanda Evans, Jack Blackburn, Ronald Flannagan and Bryan Heit (November 2014).

Elucidating the efferocytic signalling pathway of MerTK receptor tyrosine kinase.

Infection and Immunity Research Forum, the University of Western Ontario, London, Ontario

Amanda Evans, Ronald Flannagan and Bryan Heit (March 2014). Regulation of phagocytosis by human CD16A.

London Health Research Day, London, Ontario

Amanda Evans, Ronald Flannagan and Bryan Heit (November 2013). Regulation of phagocytosis by human CD16A and CD16B.

Infection and Immunity Research Forum, the University of Western Ontario, London, Ontario

Amanda Evans, Amber Ablack and John Lewis (June 2010). The building of a puromycin complex with green fluorescent protein.

Research Education Day, London, Ontario